

# DISPERSION & EXPLOSION CHARACTERISTICS OF LARGE VAPOUR CLOUDS

Volume 1: Summary Report





# **DISPERSION & EXPLOSION CHARACTERISTICS OF LARGE VAPOUR CLOUDS**

## **Volume 1: Summary Report**

Joint industry project sponsored by:

**BP**

**Health and Safety Executive (UK)**

**Petróleo Brasileiro S.A. - Petrobras**

**Shell Research Ltd.**

**Statoil**

**Total S.A.**

**Le Ministère de L'écologie, du Développement Durable et des Transports  
(France)**

**RIVM (National Institute for Public Health and The Environment,  
Netherlands)**





# **Dispersion and Explosion Characteristics of Large Vapour Clouds**

## **Volume 1 – Summary Report**

**B. A. Burgan, BSc, MSc, DIC, LLM, PhD FCI Arb, MI StructE, CEng**

© 2014 The Steel Construction Institute

Apart from any fair dealing for the purposes of research or private study or criticism or review, as permitted under the Copyright Designs and Patents Act, 1988, this publication may not be reproduced, stored or transmitted, in any form or by any means, without the prior permission in writing of the publishers, or in the case of reprographic reproduction only in accordance with the terms of the licences issued by the UK Copyright Licensing Agency, or in accordance with the terms of licences issued by the appropriate Reproduction Rights Organisation outside the UK.

Enquiries concerning reproduction outside the terms stated here should be sent to the publishers, The Steel Construction Institute, at the address given on the title page.

Although care has been taken to ensure, to the best of our knowledge, that all data and information contained herein are accurate to the extent that they relate to either matters of fact or accepted practice or matters of opinion at the time of publication, The Steel Construction Institute, the authors, the sponsors and the reviewers assume no responsibility for any errors in or misinterpretations of such data and/or information or any loss or damage arising from or related to their use.

Document Number: SCI ED024

## FOREWORD

This is the final report of the “Dispersion and Explosion Characteristics of Large Vapour Clouds” project. The project’s ultimate objectives were to understand vapour cloud development following large losses of primary containment, the characteristics of explosions involving large flat flammable vapour clouds and the explosion mechanisms that can give rise to very high overpressures over a large area as observed in the Buncefield incident. This has been done through large and medium scale experimental studies supplemented by numerical analysis.

The project was jointly funded by:

- BP
- Health and Safety Executive (UK)
- Petróleo Brasileiro S.A. – Petrobras
- Shell Research Limited
- Statoil
- Total S.A.
- Le Ministère de L’écologie, du Développement Durable et des Transports (France)
- RIVM (National Institute for Public Health and The Environment, Netherlands)

Their financial support is gratefully acknowledged.

The work was conducted under the guidance of a Technical Group comprising the following experts from or on behalf of the sponsoring organisations:

Dr Jens Holen	Statoil
Dr Jonathan Puttock	Shell Projects and Technology
Dr Paul Uijt de Haag	RIVM (National Institute for Public Health and the Environment)
Dr Pol Hoorelbeke	Total S.A.
Mr Rémy Bouet	Institut National de l'Environnement Industriel et des Risques
Mr Renato Mendes	Petróleo Brasileiro S.A. – Petrobras
Mr Robert Simpson	Health and Safety Executive
Professor Vincent Tam	BP

The project was managed by Dr B A Burgan of the Steel Construction Institute.

The project report is divided into two volumes. This, Volume 1, provides an overview and a summary of the work undertaken, the results and the main findings. It draws from the content of Volume 2, which is published as a separate document and contains the following final reports of the individual studies performed as part of the project:

Vapour cloud formation  
Health and Safety Executive  
*G. Atkinson and S. Coldrick*

Experimental investigation of the effect of flexible obstructions on flame propagation in vapour cloud explosions  
Gexcon  
*M. van Wingerden and B. Wilkins*

Medium-scale tests to investigate the influence of vegetation on flame propagation within semi-confined enclosures  
Gexcon  
*M. van Wingerden, and B. Wilkins*

Modelling of medium-scale vegetation tests  
Gexcon  
*H. H. Pedersen and R. W. Brewerton*

Large scale tests to investigate the influence of vegetation on vapour cloud explosions  
DNV GL  
*D. Allason and D. M. Johnson*

Modelling of large-scale vegetation tests (three reports)  
Gexcon  
*H. H. Pedersen*

Modelling of propane/air cloud detonations  
Fluid Gravity  
*S. B. Cargill*

Large scale tests to investigate the detonation characteristics of flammable vapour clouds  
DNV GL  
*D. Allason and D. M. Johnson*

Large scale tests to investigate the likelihood of alternative explosion mechanisms in large flammable vapour clouds  
DNV GL  
*D. Allason and D. M. Johnson*

Further analysis of Northgate Building cladding panels  
Steel Construction Institute  
*B. A. Burgan*

## EXECUTIVE SUMMARY

The Buncefield incident in December 2005 involved a large spill of petrol followed by a severe vapour cloud explosion that caused substantial damage to property and further loss of containment from nearby storage tanks. It also resulted in a major fire that took several days to extinguish. In October 2009, two similar incidents occurred, one in Puerto Rico and the other in Jaipur, India. A common feature of these incidents is a very large ( $> 100,000 \text{ m}^2$ ) relatively shallow (2 – 3 m) gas cloud and a very severe explosion causing damage over an area extending several kilometres.

The Major Incident Investigation Board (MIIB) which was responsible for looking into the Buncefield incident invited explosion experts to advise on the work that would be required to explain the severity of the Buncefield explosion. The Advisory Group carried out a preliminary assessment of forensic evidence and of results of supporting tests carried out by the Health and Safety Laboratory (HSL) but was not able in the time available to identify a single scenario that explained all aspects of the Buncefield explosion. It therefore recommended that a joint industry project be initiated with the objective of completing the assessment started by the Advisory Group and of defining the requirements for further research.

A joint industry project was therefore undertaken (May 2008 to May 2009) which examined in greater detail the forensic evidence and performed further tests and analysis. It concluded that the most likely scenario was that an initial deflagration of the gas cloud (caused by a spark in the pump house) transitioned into a detonation when the flame travelled through dense vegetation adjoining the site. The project also recommended that further work should be undertaken to gain a better understanding of the dispersion and explosion characteristics of large vapour clouds, the influence of dense vegetation on the explosion development and whether an alternative mechanism to detonation might have played a part in the explosion.

This further work commenced in July 2010 and was completed in December 2013. It involved several test programmes and analytical studies to understand how vapour clouds develop following large losses of primary containment, the characteristics of explosions involving large flat flammable vapour clouds and the key explosion mechanisms that can give rise to very high overpressures over a large area as observed in Buncefield and similar incidents. This summary report (Volume 1) provides an overview of the project and the key findings. A separate report (Volume 2) is a compilation of the final reports of individual experimental and analytical studies undertaken.

## Key Findings and their Practical Implications

### Flammable cloud formation

1. An atmospheric storage tank overfill incident in still conditions can lead to the development of a large shallow vapour cloud if unchecked. For a gasoline tank like that involved at Buncefield the cloud radius reaches 100 m after about 5 minutes and 200 m after about 20 minutes. An unconfined explosion involving such a large shallow vapour cloud can result in a severe explosion and very high overpressures.

2. A vapour cloud assessment method has been validated and extended to provide a scientific basis for estimating cloud size and how this depends on flow rate and duration of loss of containment. It can be used, for example, to determine whether a cloud will reach a vulnerable target (e.g. a control room) before the leak can be detected and whether additional mitigation measures should be considered. If the site is on a significant slope more sophisticated analysis (e.g. CFD) may be required to determine the true level of risk.

### **Effect of vegetation on explosion overpressure**

1. In the explosion tests conducted, the flame accelerated within a short distance of travel through vegetation (10 – 20 m) and, depending on the characteristics of the vegetation, either settled to a steady limiting speed or a transition to detonation occurred.
2. Two tests in which a 4.5 m wide row of vegetation were used resulted in detonations.
3. A test using 2 m wide very dense vegetation produced a flame speed of around 150 m/s and no transition to detonation.
4. The conditions that can give rise to a transition to detonation could not be determined within the limited number of tests performed and the high variability of vegetation. The presence of foliage and small twigs in the vegetation always resulted in increased flame speed.
5. The vegetation used in the tests was the result of cutting trees and assembling them in the test rig to form a hedge. The branch distribution in a naturally growing hedge is likely to differ from one that is “constructed” in the way described. It was not possible within the scope of the project to quantify this difference.

### **Detonation characteristics of large flammable vapour clouds**

1. Explosions involving large shallow unconfined vapour clouds can cause very high overpressures. A detonation can propagate through relatively thin ( $< 200$  mm) detonable layers and paths in a large propane/air vapour cloud.
2. Small variation from stoichiometric concentration and the location of the ignition point had little effect on overpressure outside the cloud.
3. The overpressure outside the cloud diminishes rapidly with distance from the edge of the cloud.
4. A simple expression has been derived which enables the maximum external overpressure to be estimated and is applicable to clouds with a radius  $\geq 50$  m. For smaller clouds, either the Multi-Energy Method or TNT Equivalence can be used. This approach appears robust within the limits of the tests and simulations performed.
5. Overpressures in excess of 3 bar were found to cause significant damage to cars and instrument boxes. Only minor damage occurred when the pressure was  $\leq 1$  bar. Oil drums were found to sustain damage at an overpressure  $> 2$  bar and the damage was pronounced at 3 bar.
6. A 20 ft ISO container sustained minor creasing to its wall facing the detonation at an overpressure of 420 mbar. It sustained significant damage

to its wall and roof when at an overpressure of 2 bar and was also shifted along the ground by around 3 m by the explosion.

7. The net impulse on objects well within a vapour cloud acts in the opposite direction to the direction of propagation of a detonation. Close to the cloud boundary, where the reverse flow will be shorter in duration, net impulse may act in the direction of propagation of the detonation.

### **Structural response of simple objects**

1. Simple objects such as instrument boxes, drums, containers, posts, *etc.* located on an incident site provide a very good indicator of explosion overpressure and direction after an incident.
2. The instrument boxes used in the tests were analysed and charts were developed for estimating explosion characteristics from an inspection of damage levels to such boxes.

## **Summary of experimental and analytical work**

### **Flammable cloud formation**

Seven full-scale over-spill tests were performed by the Health and Safety Laboratory (HSL) using a 10.4 m high model tank. In four of these, commercial hexane was used and the tests focused on vapour dispersion. The cascade impact zone was surrounded by bunds (either vertical or inclined). Vapour currents were deflected upwards by the bunds leading to recirculation and accumulation of vapour within the bund which subsequently spilled out entraining additional air. A further three tests (with no bunds) focused on the heat and mass transfer processes in the cascade and the early stages of the primary vapour current. Measurements were made of the vapour temperature outside the cascade, liquid temperature in the cascade, liquid temperature across the floor impact area, vapour concentration and relative humidity. All tests were also recorded using both normal and infra-red video.

It was found that conditions within the impact zone closely approach equilibrium. Simple methods (based on momentum conservation and equilibrium thermodynamics) for predicting the volume of air drawn into the cascade and the concentration of solvent in the outflow give remarkably reliable results. A small amount of liquid was ejected from the splash zone as a fine spray. As additional fresh air was entrained into the vapour current, the spray provided a small extra amount of vaporisation that amounted to 10-20% of the total vaporisation rate.

Comparisons made between the measurements and CFD predictions in the liquid cascade and for the vapour accumulation and outflow from the bund showed good agreement. A simplified method for calculating the rate at which the volume of a vapour cloud increases during an overfilling incident which had been developed by HSL prior to this project was tested against the data generated in this project and found to give reliable results. To allow wider application of this method, thermodynamic analysis was performed of a group of solvents and petrochemical mixtures that are commonly found in chemical and petrochemical processing facilities and the parameters necessary to extend the method to these substances were derived.

### **Effect of mixed diameter objects on explosion characteristics**

Seven explosion tests were performed by Gexcon in an explosion vessel measuring 1210 x 1220 x 6100 mm vented through one of its short ends. A propane air mixture with a concentration of 4.2-4.3% by volume was used in these tests. Congestion was provided by 4 rows of pipes having diameters of 4 mm, 20 mm and 104 mm. Measurements were made of overpressure generated inside and outside the vessel and high speed video records were used to track flame progression and assess flame speed. The pipe obstacles were used in single diameter arrangements and in different combinations to assess whether small-diameter obstacles are less effective in generating explosion overpressure than larger diameter obstacles, and the extent to which combinations of different diameter obstacles have the potential to generate greater overpressures than uniform arrays of obstacles.

The flame velocity profiles were very similar for all scenarios using single diameter pipes. In the test with combined 4 mm and 20 mm diameter pipes, the pressure increased by approximately 11%. This is a minor increase within the experimental error band in such tests. In all other cases, however, the increase in peak pressure was somewhat greater, with pressure increases of 15% and 16% in the tests that used two diameter pipes and 21% for the test with a mix of three diameter pipes. Since the area blockage is similar for these tests and the flame velocities were also higher in these tests, the enhanced explosion propagation, whilst moderate, is most likely caused by the mixing of different diameter pipes.

The tests provide well controlled data which can be used in CFD model development and validation, particularly for handling combinations of on-grid and sub-grid obstacles.

### **Medium-scale tests to investigate the influence of vegetation on flame propagation in semi-confined enclosures**

Sixteen explosion tests were performed by Gexcon in a 50 m<sup>3</sup> explosion test rig (8.0 m long, 2.5 m high and 2.5 m wide), vented only through one of its short ends with ignition near the opposite end. A range of vegetation types were used as congestion – three were performed with spruce trees, seven with birch trees, two with smooth pipes and two with hedges of Thuja trees. Tree samples were cut-up and measured in order to determine the characteristics of the congestion. Two tests were performed with an empty module as reference tests.

The congestion (trees or pipes) were installed at either 11 or 4 positions within the rig depending on whether a high or medium level of congestion was required in the test. In some tests, the birch trees were trimmed to remove leaves and branches of certain diameters. This congestion thinning was performed systematically in three stages to study the effect of the smaller diameter elements of the vegetation. All tests except one of the spruce tree tests were performed with a homogeneous nominally 4.2 %v/v propane-air mixture filling the entire module. Measurements were made of overpressures inside and outside the test rig and high speed video was used to track flame progression and assess flame speed. Medium and normal speed video records were also taken.

Tests using either 4 spruce trees or 4 birch trees and gas mixture of 4.2 %v/v generated similar overpressures; these were 5-9 times higher (1500 – 2500 mbar) than for the empty reference test (200 – 300 mbar). Removing foliage by



trimming the birch trees reduced the peak overpressures significantly. The largest decrease in explosion pressures occurred when the smallest twigs, <2 – 3 mm (and most leaves) were removed. A pressure reduction by a factor of approximately 2 – 3 (500 – 600 mbar) resulted compared to that for the untrimmed trees. Further trimming of twigs with diameter <8 mm produced overpressures in the range of 400 – 600 mbar. Removal of all branches to leave only the trunks produced overpressures approximately 30-40% higher than the reference tests.

No difference was observed in the strength of the explosions using smooth pipes compared with tree trunks of similar diameter and numbers. For a given congestion layout, no difference was found between the explosion pressure results obtained using spruce trees or birch trees, despite the slightly lower volume blockage ratio of the birch trees used compared to that for the spruce trees. When the vegetation congestion was changed to a hedge comprising a single-width row of Thuja bushes (approx. 0.5 m wide and 1.5 m high) along the centre of the test rig, peak overpressures approximately 2-3 times higher than the reference test scenario were obtained. Increasing the hedge width to 1.0 m by using a double row of Thuja bushes, increased the peak overpressures by a factor of approximately 5-12 times compared to the reference test scenario. This indicates that the density and width of the vegetation and foliage has a very significant effect on the explosion characteristics.

The volume blockage found to cause high flame speeds using vegetation as congestion was considerably lower than what would be required using piping/equipment. A reason for this may be the contribution by the many repeated small obstacles in the form of leaves, pine needles and small twigs and branches.

The tests generated an important source of data for explosion predictions using CFD models for the study of the influence of congestion caused by vegetation on gas explosions.

### **Large scale tests to investigate the influence of vegetation on vapour cloud explosions**

Eight explosion tests were performed by DNV GL in a test facility that allowed rows of trees of varying length (up to 100 m) and width (up to 4.5 m) to be used as congestion. In all tests, a nominally stoichiometric propane/air mixture was used and the ignition point was located within the row of trees, 1 m from the end, on the longitudinal centreline just above ground level. The density and width of vegetation were the key variables studied in this test. However, the nature of vegetation is such that unintended variability is always present between tests as no two trees are identical.

Vegetation was characterised by sampling a number of trees, cutting them up and measuring the diameters and lengths of the constituents of each tree sampled. Nominal congestion was varied using a number of trees/m<sup>2</sup> in the test rig. In the first test, spruce trees were used. Alders were used in the subsequent 6 tests and a combination of alders and silver birch trees were used in the final test. The width was varied from a minimum of 1 m to a maximum of 4.5 m. Measurements were made of overpressure and flame speed inside the test rig. Both high and normal speed video records of all tests were also made.

A deflagration to detonation transition occurred in two of the eight tests. These had 1.5 and 3 trees/m<sup>2</sup> and both had 4.5 m wide vegetation. In the 1.5 trees/m<sup>2</sup> test, the trees were arranged in a chequerboard pattern (repeated areas of 1 and 2 trees/m<sup>2</sup> to give 1.5 trees/m<sup>2</sup> average). This is a factor which may have contributed to flame acceleration. Transition to detonation was found to occur within 15 – 20 m of flame propagation. In the remaining six tests (with widths of 1 – 4.5 m and density of 1.5 – 6.5 trees/m<sup>2</sup>), maximum flame speeds ranged from 60 – 200 m/s and again, were reached within short distances of flame travel (circa 15 m).

There was reasonably consistent evidence from the tests that the presence of foliage contributed to higher flame speeds. The spruce trees for example, which had a large amount of foliage in the form of needles, produced relatively high flame speeds (140 m/s) but had by far the lowest volume blockage ratio of all tests (between 1/5<sup>th</sup> and 1/11<sup>th</sup>). This was evident in other tests where leaves were burnt in a first test (with no other damage to the trees) and the same trees were re-used in a subsequent test.

The highest vegetation density test (6.5 trees/m<sup>2</sup>) had a 2 m width of vegetation. This test produced a flame speed of around 150 m/s and no transition to detonation.

The experiments showed significant sensitivity to the exact experimental conditions. This is likely to be a characteristic of flame acceleration in high aspect ratio congested regions and variability in the nature of vegetation.

### **Analytical study of the detonation characteristics of large flammable vapour clouds**

A range of propane/air vapour cloud geometries and ignition locations were studied numerically by Fluid Gravity to provide a better understanding of the pressure/impulse and radial velocity both within and outside a circular shallow cloud ignited at different positions within the cloud.

Geometries studied included centre ignition of a 200 m radius cloud with heights of 3 m, 1 m and of tapering height from 3 m at the centre to 1 m at the cloud edge. Other centre ignition geometries studied included a 100 m radius 1 m high cloud and a 50 m radius 2 m high cloud. Pressure and impulse drop rapidly with distance from the cloud edge. They also drop rapidly with height above the cloud. Close to the edge of the cloud, the different cloud aspect ratios result in significant differences in the decay in peak pressure; clouds with larger radii maintain higher pressures with increased distance from the centre of the cloud. In the far field, the total energy released by the detonation (which is a function of cloud volume) becomes the dominant factor and the peak pressures from each of the different geometries converge. The precise geometry of the cloud becomes less important.

Lean mixes (3.2%) produced 10% lower overpressures at a distance of 100 m from a 200 m radius 3 m high cloud. Rich mixes (6.8% and 5.5%) produced similar overpressures to stoichiometric clouds, but greater impulse due to additional after burning in the rich mixes.

Off-centre ignition was found to have little effect on peak pressure outside the cloud but resulted in a significant increase in impulse on the side of the cloud

closest to the ignition point. Calculations were also performed to estimate the reflected overpressure on a range of objects located within and at different distances outside the cloud. These gave an indication of how both reflected pressure and impulse vary with distance from the cloud.

### **Large scale tests to investigate the detonation characteristics of flammable vapour clouds**

Six tests (all with a rectangular geometry on plan) using nominally stoichiometric propane/air mixtures were performed by DNV GL. Detonation of the vapour cloud was initiated using a small explosive charge. The first test demonstrated the effect of a gas cloud detonation on objects (cars, boxes, drums) within the cloud and provided information on the decay of pressure with distance from the cloud. A further three tests considered the effects of the aspect ratio of the vapour cloud on the pressure field generated away from the cloud and the effect on objects (cars, boxes, drums) placed outside the vapour cloud. The final two tests studied the effects of the height above ground of the vapour cloud on detonation propagation and in particular the minimum height of cloud required to sustain a detonation. In these tests, the height of the cloud was tapered from an initial height of 2 m at one end down to under 200 mm at the other end. The test set up allowed the cloud geometry to be changed with maximum length of 30 m, maximum width of 10 m and maximum height of 4 m.

Measurements were made of overpressure and flame speed inside the test rig and overpressure in different directions outside the rig. Both high and normal speed video records of all tests were also made.

Overpressures in the near field outside the cloud were found to be lower on the minor axis and on a 45° line between major and minor axis than on the major axis of the cloud, but these differences disappeared in the far field. Aspect ratio was found not to have an effect on pressure decay on the major axis, but differences were present on the minor axis with pressures being highest for the greatest aspect ratio test.

The far field pressures in the tests were under predicted by the TNO Multi-Energy and TNT Equivalence methods by up to 44%.

The tapering tests showed that a detonation can continue to propagate into clouds as thin as 200 mm. The implication of this is that a detonation would be able to propagate through relatively thin detonable layers and paths in a large cloud. This makes a detonation much less susceptible to concentrations variations than a deflagration; once a detonation has been initiated, it will propagate through the remainder of the cloud, bypassing any zones where concentrations are outside the detonable range.

The tests showed that overpressures over approximately 1 bar are required for significant damage to cars. Drums placed outside the vapour cloud indicate that creasing of the surfaces of the drum requires incident shock waves in excess of 2 bar overpressure. Instrument boxes placed outside the vapour cloud indicate that distortion of the door and sides occurs for incident shock waves in excess of 3 bar overpressure. No damage to instrument boxes occurs for incident shock waves less than 1 bar overpressure.

### **Structural response of instrument boxes**

The instrument boxes placed outside the cloud in the detonation tests were analysed by SCI using different finite element techniques varying in complexity and level of sophistication. Coupled Eulerian-Lagrangian analysis (to allow for the interaction between the incident pressure wave and the structure of the box as it deforms in response to the pressure load) was found to predict the deformation of the boxes very well, particularly where the deformation was severe (following exposure to  $> 3$  bar overpressure). Uncoupled analysis and pure Lagrangian analysis over-estimated the deformations. Therefore, if such analysis is used to estimate overpressure from observations of deformed boxes, the overpressure is likely to be underpredicted.

Very good agreement was found between the coupled analysis and the measured deformation. For some boxes, which were not located near pressure transducers, an overpressure was estimated. The overpressure values used in the analysis were generally at the upper end of the estimated range. Consequently, the calculated deformations in the analysis tended to be higher than those measured.

Pressure-impulse diagrams were constructed for the instrument boxes using the validated finite element model and visual representations of deformed shapes under a range of detonation loads were generated. These can be used for a rapid assessment of overpressures in incident investigation.

### **Large scale tests to investigate the likelihood of alternative explosion mechanisms in large flammable vapour clouds**

Three tests were performed by DNV GL to demonstrate at a realistic scale the feasibility or otherwise of the episodic deflagration mechanism. This mechanism was suggested in the previous joint industry project as a possible alternative to the deflagration to detonation transition. The vapour cloud in these tests was 30 m x 10 m and 3 m high. The explosion was initiated in an explosion chamber to create a large flame surface that would promote particle ignition ahead of the flame. Carbon black particles and leaves were spread on the floor of the test rig and on elevated trays within the rig. Two tests were performed with stoichiometric propane/air mixtures and one with a rich mix. Measurements were made of overpressure, flame radiation and flame speed inside the test rig. Both high and normal speed video records of all tests were also made. The tests did not provide evidence that supports the episodic deflagration mechanism.

# Contents

	Page No
FOREWORD	iv
EXECUTIVE SUMMARY	vi
1 BACKGROUND	1
1.1 Buncefield and Similar Incidents	1
1.2 The Buncefield Explosion Mechanism Project	2
2 OBJECTIVES, SCOPE AND ORGANISATION OF THE PROJECT	3
3 FLAMMABLE CLOUD FORMATION	5
3.1 Objectives	5
3.2 Key Findings	5
3.3 Description of the Test Programme	6
3.4 Summary of Experimental Observations	9
3.5 Modelling of Vapour Cloud Development using CFD	17
3.6 Simplified Method for Estimating Vapour Cloud Characteristics	18
4 EFFECT OF MIXED DIAMETER OBJECTS ON EXPLOSION CHARACTERISTICS	21
4.1 Objectives	21
4.2 Key Findings	21
4.3 Description of the Test Programme	21
4.4 Summary of Experimental Observations	24
5 EFFECT OF VEGETATION CONGESTION ON EXPLOSION CHARACTERISTICS	29
5.1 Objectives	29
5.2 Key Findings	29
5.3 Description of the Medium Scale Test Programme	30
5.4 Description of the Large Scale Test Programme	38
6 CHARACTERISTICS OF LARGE FLAT VAPOUR CLOUD DETONATIONS	47
6.1 Objectives	47
6.2 Key Findings	47
6.3 Analytical Study	48
6.4 Description of the Large Scale Detonation Test Programme	53
7 EXPLOSION RESPONSE OF INSTRUMENT BOXES	75
7.1 Objectives	75
7.2 Key Findings	75
7.3 Analytical Techniques and Numerical Models	75
7.4 Analysis Results	78
7.5 Pressure-Impulse and Explosion Damage Diagrams	83
8 INVESTIGATION OF ALTERNATIVE EXPLOSION MECHANISMS	85
8.1 Objectives	85
8.2 Key Findings	85
8.3 Description of the Test Programme	85
8.4 Summary of Findings	87
9 REFERENCES	89



# 1 BACKGROUND

## 1.1 Buncefield and Similar Incidents

On 11 December 2005, a series of explosions and subsequent fire destroyed large parts of the Buncefield oil storage depot. The main explosion was of massive proportions (reported to measure 2.4 on the Richter Scale). It was followed by a fire that engulfed 23 large fuel storage tanks and burned for five days. An estimated 185 tonnes of petrol had over-spilt from one of the tanks during filling operations. Petrol cascaded down the side of the tank and a large vapour cloud formed by the mixture of petrol and air.

The Buncefield incident was not unique. A study published in 2006 identified 242 storage tank incidents in the previous 40 years<sup>1</sup>. Of these, 74% occurred in petroleum refineries, oil terminals or storage depots. Fires and explosions occurred in 85% of these incidents. One third was found to have been caused by human error, a further third by lightning and a third by other causes such as equipment failure, sabotage, leak and line rupture, static electricity or open flames. Most could have been avoided by good engineering.

In October 2009, two large incidents occurred that bear several resemblances to the Buncefield incident. The first was at a fuel depot of the Caribbean Petroleum Corporation near San Juan, Puerto Rico on 23 October 2009. The explosion shortly after midnight shattered windows and sent tremors across San Juan. It was reported to measure 2.8 on the Richter scale by the Puerto Rico Seismic Network<sup>2</sup>. Immediately before the blast, a tanker ship had delivered 228,000 gallons of fuel into the tanks, which caused an overflow from one of the newest tanks at the site. An unidentified spark ignited the vapours. The fire which followed destroyed half of the depot's 40 fuel storage tanks and burned for more than 2 days. Hundreds of people had to be evacuated.

The second occurred at a fuel storage depot of the Indian Oil Company (IOC) in Jaipur, India on 29 October 2009<sup>3,4</sup>. The depot has a capacity of 9 million litres of fuel. It started with a massive spillage (caused by a valve failure rather than tank overfilling) when petrol was being transferred from a tank at the IOC terminal to Bharat Petroleum's storage nearby. An estimated 1300 tonnes of petrol was released over a period of around one hour and 20 minutes. A powerful explosion was followed by a fire that spread to the site's 11 storage tanks. The Meteorology Department recorded a tremor measuring 2.3 on the Richter scale around the time the explosion was heard at 7.36 pm. The impact of the explosion damaged windows and walls of buildings 3 km away from the site. There were five more blasts after the first one. The incident resulted in 12 fatalities (some offsite) and over 100 injuries.

A common feature of these three incidents is a very large ( $> 100,000 \text{ m}^2$ ) relatively shallow (2 – 3 m) gas cloud and a very severe explosion causing damage over an area extending several kilometres.

The Major Incident Investigation Board (MIIB) which was responsible for looking into the Buncefield incident invited explosion experts from academia and industry to form an Advisory Group to advise on the work that would be required to explain the severity of the Buncefield explosion<sup>5</sup>. This Advisory



Group carried out a preliminary assessment of the forensic evidence obtained following the incident and of the results of supporting tests carried out by the Health and Safety Laboratory (HSL). It attempted to explain the explosion event at Buncefield on the basis of deflagration, detonation or a combination of both explosion mechanisms. It also examined other possible means of flame acceleration. However, within the time available to it, the Advisory Group was not able to identify a single scenario that could explain all aspects of the Buncefield explosion. It therefore recommended that a joint industry project be initiated with the objective of completing the assessment started by the Advisory Group and, on the basis of this, of defining the requirements for further research.

## **1.2 The Buncefield Explosion Mechanism Project**

This joint industry project (May 2008 and May 2009) was a direct result of the recommendation of the MIIB Advisory Group. It was funded by HSE, UKPIA, the Dutch Ministry of Housing, Environment and Spatial Planning, Statoil and the Energy Institute. Its main objectives were (i) to provide an understanding of the explosion mechanism in the Buncefield incident and (ii) to define the scope of further work that may be necessary.

A vast amount of data in the form of witness statements (using extracts from anonymised witness statements), photographs, CCTV and video footage were studied and catalogued. Careful examination of this data supported by a considerable amount of analytical work and a limited number of tests enabled the explosion source terms and characteristics to be inferred.

It was concluded that the overpressure within the area covered by the cloud (irrespective of the nature of the terrain and whether congested or not) was generally greater than 200 kPa (2 bar) and that the maximum overpressure was probably much higher. Overpressure were found to diminish rapidly with distance from the edge of the cloud; evidence suggested overpressures in the region of 5-10 kPa (50 – 100 mbar) within ~150 m. Another distinctive feature was the direction of net impulse; within the cloud this acted in the opposite direction to the direction of propagation of the explosion whereas outside the cloud it acted in the direction of propagation of the explosion. The report concluded that an initial deflagration of the gas cloud (caused by a spark in the pump house) transitioned into a detonation when the flame travelled through dense vegetation adjoining the site. Whilst this conclusion was supported by most of the evidence, it seemed at odds with the level of damage caused to two buildings at the edge of the gas cloud (Northgate and Fuji). This led to the suggestion that another mechanism (episodic deflagration) may provide an alternative explanation; however, as little was known about this mechanism, this line of investigation could not be pursued further within the project.

The project reported its findings at a public meeting in June 2009<sup>6</sup> which coincided with publication of the project report<sup>7</sup>. It also provided an outline of the further work necessary to improve the understanding of the dispersion and explosion characteristics of large vapour clouds and recommended that this be carried forward as a joint industry project.



## 2 OBJECTIVES, SCOPE AND ORGANISATION OF THE PROJECT

The main objective of this project was to understand:

- (a) how vapour clouds develop following large losses of primary containment;
- (b) the characteristics of explosions involving large flat flammable vapour clouds; and
- (c) the key explosion mechanisms identified in the previous JIP<sup>7</sup> that can give rise to very high overpressures over a large area as observed in Buncefield and similar incidents.

To achieve these objectives experimental studies supported by some analytical work were undertaken to identify and quantify the important parameters that influence vapour cloud development and the characteristics of the explosion which results when such a vapour cloud is ignited.

The detailed scope of work was developed in close consultation with the project Technical Group, made up of 8 expert representatives from the sponsor organisations. This led to the preparation of bidding documents in a first stage of the project which were used to invite proposals from specialist contractors. Proposals received were evaluated technically and financially and the following organisations were selected to undertake the technical work:

### **Vapour cloud development (large scale tests)**

Health and Safety Executive (UK)

### **Effect of mixed diameter obstacles (medium scale tests)**

Gexcon (Norway)

### **Effect of vegetation on explosion development (medium scale tests)**

Gexcon (Norway)

### **Effect of vegetation on explosion development (large scale tests)**

DNV GL

### **Characteristics of large flat vapour cloud detonations (analytical studies)**

Fluid Gravity

### **Characteristics of large flat vapour cloud detonations (large scale tests)**

DNV GL

In addition, structural response modelling of obstacles used in the vapour cloud detonation tests was undertaken by SCI.

The project Technical Group was responsible for the technical direction of the project including selection of test configurations and reviewing of technical outputs.



## 3 FLAMMABLE CLOUD FORMATION

### 3.1 Objectives

The objectives of the flammable cloud formation tests are to:

- (a) Examine at full scale the effect of the following parameters on the development and characteristics of vapour clouds:
  - i. fuel/substance type
  - ii. bund filling
  - iii. height of cascade

and to understand the underlying phenomena affecting the dispersion mechanism.

- (b) Document the experimental data such that it can be used by others to validate existing (or develop new) techniques for modelling vapour cloud dispersion.
- (c) Understand the implications of dispersion of vapour clouds of different substances in low wind conditions (where numerical models currently have the greatest predictive difficulty) for safety assessment and zoning requirements.

### 3.2 Key Findings

1. An atmospheric storage tank overfill incident in still conditions can lead to the development of a large shallow vapour cloud if unchecked. For a gasoline tank like that involved at Buncefield, the cloud radius reaches 100 m after about 5 minutes and 200 m after about 20 minutes. An unconfined explosion involving such a large shallow vapour cloud can result in a severe explosion and very high overpressures.
2. For practical risk assessment, it is reasonable to assume that the extent of liquid vaporisation during an overfilling incident is that which would be achieved if the falling liquid and entrained air reached equilibrium. This provides a reliable means of estimating the degree of overall vaporization in the combined cascade and impact process.
3. Test results have been used to validate and further extend a simple method (VCA method) for calculating the rate at which the volume of a vapour cloud increases during an overfilling incident, the concentration of hydrocarbons in the cloud and the extent of cloud spread in relatively flat sites.
4. The VCA method takes into account the liquid heat capacity and vapour pressure, overfill rate, temperature of the liquid, ambient temperature and tank dimensions. The main entrainment processes into the vapour current occur close to the tank and the overall development of the cloud is not very sensitive to bund layout.
5. The VCA method provides a scientific basis for the assessment of cloud size and how this depends on flow rate and duration of loss of containment. It

can be used, for example, to determine whether a cloud will reach a vulnerable target (e.g. a control room) before the leak can be detected and whether additional mitigation measures should be considered. If the site is on a significant slope, more sophisticated analysis (e.g. CFD) may be required to determine the true level of risk.

### **3.3 Description of the Test Programme**

Previous tests of a similar nature to the tests in this programme were carried out by HSE<sup>8</sup>. This earlier work led to the development of a simple vapour cloud assessment (VCA) method which enables the cloud volume and concentration to be calculated for a given tank overfill scenario. However, these tests and the VCA method were limited to petrol (gasoline) spillages.

The present tests generated additional data using a wider range of instrumentation, extended the experimental range by investigating the interaction between vapour currents and bunds of various designs and studied the effects of a range of volatile liquids and mixtures. The tests also provide an opportunity for detailed comparison between predictions of the VCA method and full-scale tests with a range of fluids, flow rates, release temperatures and bund confinements. Full details of these tests were reported by HSL<sup>9</sup> and are reproduced in Volume 2 of this report<sup>10</sup>.

#### **3.3.1 Test programme**

The programme consisted of 7 tests (in two groups), summarised in Table 3.1. In 1, 2, 5 and 6 the fuel used was commercial hexane. These tests focused on vapour dispersion. The cascade impact zone was surrounded by bunds (either vertical or inclined) located at either 5 or 10 m from the tank wall. Vapour currents were deflected upwards by the bunds, leading to recirculation and accumulation of vapour within the bund which subsequently spilled out entraining additional air.

In 3, 4 and 7 no side bunds were used in the cascade impact zone. As a result, the primary vapour current drifted away from the rig without significant recirculation. Focus in these tests was on the heat and mass transfer processes in the cascade and the early stages of the primary vapour current. The toluene and cyclohexane used in tests 3 and 4 respectively were commercial grades with purity >98% and no contaminants in sufficient quantity to significantly affect the vaporisation process. In test 7, decene with dissolved butane was used. The bulk of the released fluid (88.2% w/w) was Neodene 10 (supplied by Shell). The material is about 95% mol/mol 1-decene with small quantities of branched C10 alkenes. Technical grade (95%) n-butane (BOC Special Gases 210150-BE) was dissolved in the Neodene to a level of 11.8% w/w.

**Table 3.1 Liquid spill tests and release conditions**

No.	Fluid	Type	Bund		Liquid temp. (°C)	Liquid flow rate (kg/s)	Air Temp. (°C)	Relative humidity (%)
			Distance to front bund (m)	Height of side bund (m)				
1	Hexane	Vertical	10	2	13.6	15.0	12.7	55
2	Hexane	Vertical	5	2	19.1	17.6	18	18
3	Toluene	N/A	—	—	7.9	17.0	7.5	7.5
4	Cyclohexane	N/A	—	—	9	16.1	11	11
5	Hexane	Sloping	5	2	9	12.8	-1	-1
6	Hexane	Sloping	10	2	15.7	11.8	10.4	10.4
7	Decene / butane	Sloping	10	—	16.2	12.5	20	20

### 3.3.2 Test facility and procedures

The test facility comprises a model tank wall with a 10.4 m high central section (where the cascade emanates), reducing to approximately 8.4 m towards the edges. The overall width of the wall is 7.5 m. Liquid spills impact on a 10 × 10 m concrete pad. The concreted impact area was provided with a 10 m<sup>3</sup> sump which was covered during tests and used to recover residual liquids and for cleaning after each test.

In an overflow scenario the tank volume provides for near complete stilling of any momentum introduced by the feed pipe. The discharge is consequently very steady, with minimal dispersal of liquid by inlet turbulence. This is important since the cascade trajectory and dispersal of liquid in the cascade is very sensitive to turbulence in the liquid flow to the discharge point. Therefore, in order to achieve similar discharge conditions in the tests, liquids were pumped slowly into a storage tank close to the discharge height. The tank was baffled to allow discharge of the liquid with (low pressure) compressed air. In this way, stable discharges were achieved with liquid being very uniformly distributed across the width of the discharge slot. The blower pressure characteristic allowed a substantial fixed pressure drop at the control valve so that changes in backpressure associated with emptying of the tank had a minimal effect on discharge rate.

The edge of the discharge chute (Figure 3.1) is 400 mm beyond the tank wall and 10.49 m above the ground. The total volume discharged was obtained by subtracting the (small) volume of liquid remaining at the end of the test from the measured fill volume. This was generally in the range 2000-2200 litres. The start and end of the discharge were clearly defined allowing the discharge duration and flow rate to be determined to within ±3%.

The test layout around the impact area varied between tests as shown in Table 3.1. The setup for Test 1 (vertical bund at 10 m) is shown in Figure 3.1. In all tests, the width of the discharge (measured along the wall) was 1500 mm. A 150 × 150 × 8 mm angle bolted to the tank at half height represents a stiffening (wind) girder, as is common in many large atmospheric storage tanks. However, as all the tests in this programme involved free liquid cascades, which were projected clear of the tank wall, the wind girder had little effect on liquid or gas flow. Such cascades are typical of overflow from tanks without firewater

deflectors and are more suitable for fundamental experimental and theoretical studies than bifurcated cascades (e.g. of the type at Buncefield). The relationship between the entrainment and mass transfer rates in the two type of cascade and the way in which the current results could be applied to bifurcated cascades are discussed in the HSE report<sup>8</sup>.



**Figure 3.1** Liquid spills facility at HSL (Buxton) showing Test 1 in progress (left) and the 1500 mm wide chute projecting 400 mm from the tank wall (right)

### **3.3.3 Instrumentation and measurements**

#### **Vapour temperature outside the cascade**

The vapour temperature outside the cascade was measured using 6-7 vertical arrays (8 thermocouples per array) of 1.5 mm stainless steel sheathed K-type thermocouples at distances between 4 and 22 m from the tank wall. Each array was at a fixed elevation from 200 mm to 1950 mm in 250 mm intervals. The elevations were common to all tests but the horizontal positions of the arrays differed between tests to suit bund design. In addition, a single 3 metre long, 15 thermocouple horizontal array at 150 mm elevation was used to measure temperatures closer to the wall (typically 2500 to 5500 mm from the wall).

#### **Liquid temperature in the cascade**

Liquid temperature in the cascade was measured using thermocouples located in small upward facing Perspex pots to maintain liquid cover to the thermocouples. Profiles of final liquid temperature in the cascade were obtained using a 16 point array of thermocouples at an elevation of 400 mm (*i.e.* just above the cascade splash zone).

#### **Liquid temperature across the impact surface**

Liquid temperatures in the flow on the floor were measured by an 8 point thermocouple array around the impact point. Junctions were located 2-3 mm from the surface. The depth of the draining flow varied with the distance from impact point but was typically in excess of 10 mm over the area covered by the array.

In addition, the liquid at the discharge point from the tank was also measured.

The comparison of liquid temperature in the cascade immediately before it enters the splash zone with the temperature of liquid across the impact surface reveals the extent of heat and mass transfer (vaporisation) associated with the splashing process. In all of the experiments a significant proportion (approximately 25%) of the total vaporization process occurred within the splash zone, which corresponds to less than 4% of the total height of the cascade.

### **Vapour concentration**

The measurement system used activated charcoal sample tubes (SKC Anasorb CTC) located in the flow and aspirated to draw the air loaded with hydrocarbons through the carbon bed. The tubes are in two sections that are analysed separately to prove that there is no breakthrough. A commissioning test in which the same atmosphere was simultaneously measured with 7 tubes (using the flow multiplexer and sample piping in the test configuration) gave individual tube loadings that varied by less than 5%.

### **Relative humidity**

The relative humidity was measured prior to each test.

### **Video records**

Both normal and infra-red video records were made of all tests.

## **3.4 Summary of Experimental Observations**

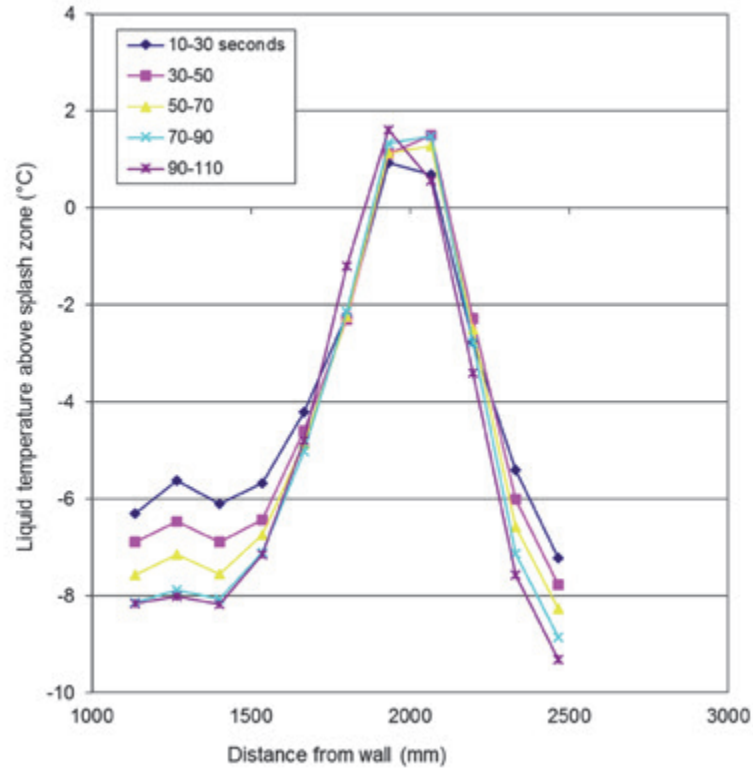
### **3.4.1 Observations relating to the free cascade**

The maximum width of the free cascade measured perpendicular to the wall can be judged from photographs and videos of the flow. In stable conditions the cascade is extremely narrow. Photographs of the cascade, from the side, show that almost all of the liquid is confined to an area that is less than 200 mm either side of the cascade centre. Measurements of liquid temperature confirm the narrowness of the liquid distribution. This is illustrated in Figure 3.2 which shows time averaged liquid temperature above the splash zone. It is clear that the highest liquid flux densities are found in an even narrower area at the core of the cascade.

Temperatures are highest in the core of the cascade where the liquid mass flux is highest. This occurs because the fuel to air ratio is highest in the cascade core. Droplets on the fringes of the cascade are relatively scarce and each droplet can vaporise (and cool) further before the co-flow of air approaches saturation and the vaporization is suppressed.

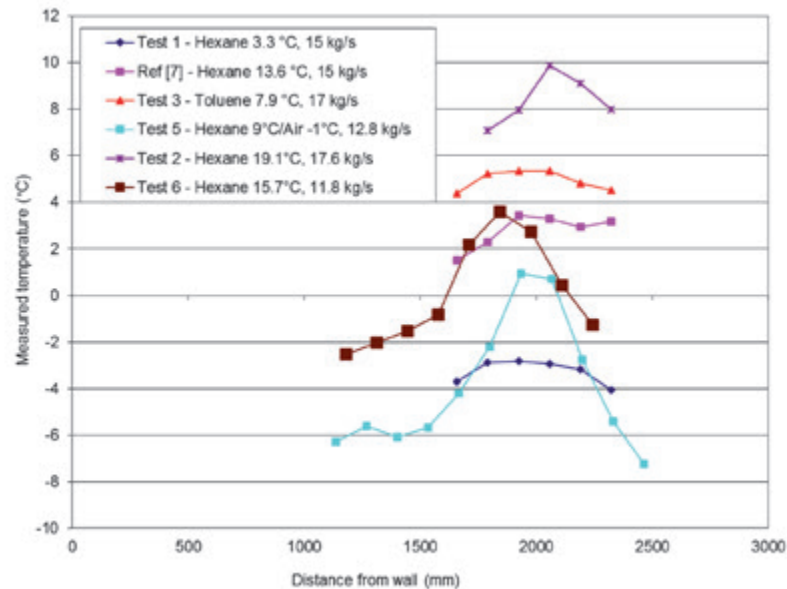
It should be noted that data from thermocouples at locations further than about 200 mm from the cascade core do not represent meaningful liquid temperature measurements. These peripheral thermocouples are splashed for a second or so as the flow starts and then simply dry out, with evaporative cooling, during the test. There is no significant liquid flow outside this area in the established cascade, so liquid temperature cannot be measured.





**Figure 3.2** Liquid temperature profiles across the cascade at 400 mm elevation (immediately above the splash zone) in Test 5 (sample points spaced at 133 mm horizontally)

Equivalent average liquid temperature profiles for all of the hexane tests (including one from reference [8]) and the toluene test (being of similarly high volatility) are shown in Figure 3.3.



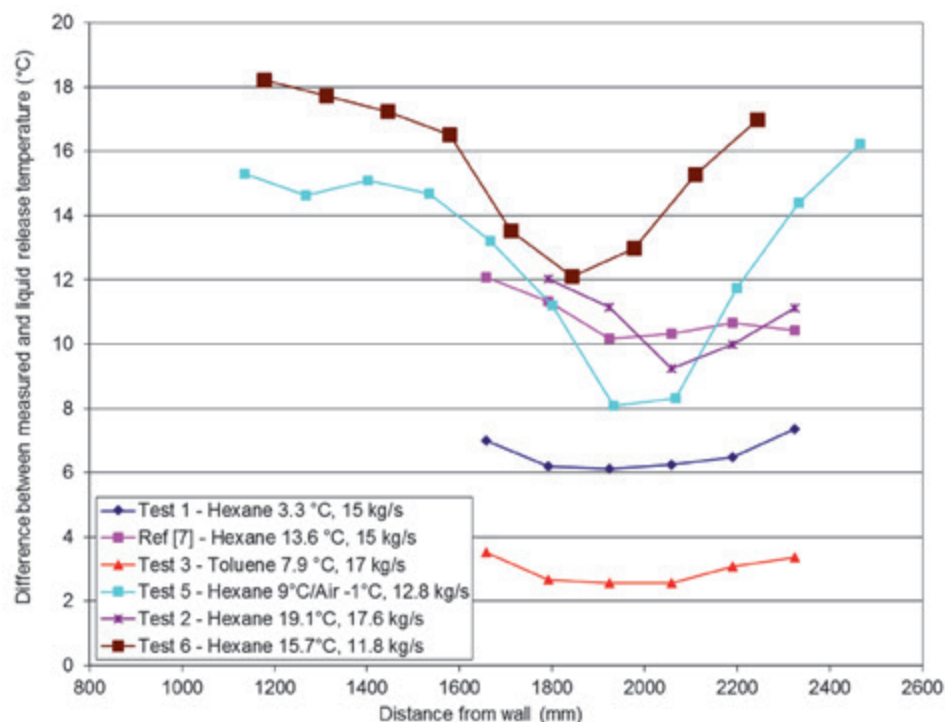
**Figure 3.3** Liquid temperature measurements in the cascade above the splash zone

The wide range of liquid release temperatures naturally leads to a range of measured temperatures in the cascade; a higher release temperature leads to a higher rate of vaporization. If, on the other hand, the well-defined drop in liquid



temperature in the cascade is used as the temperature scale, more consistent trends emerge as can be seen in Figure 3.4. Large drops in temperature in the core of the cascade are associated with:

- More volatile liquids (*i.e.* greater drop in hexane than toluene)
- High initial temperature (which increases the effective volatility)
- Low liquid mass fluxes (high air to fuel ratios)

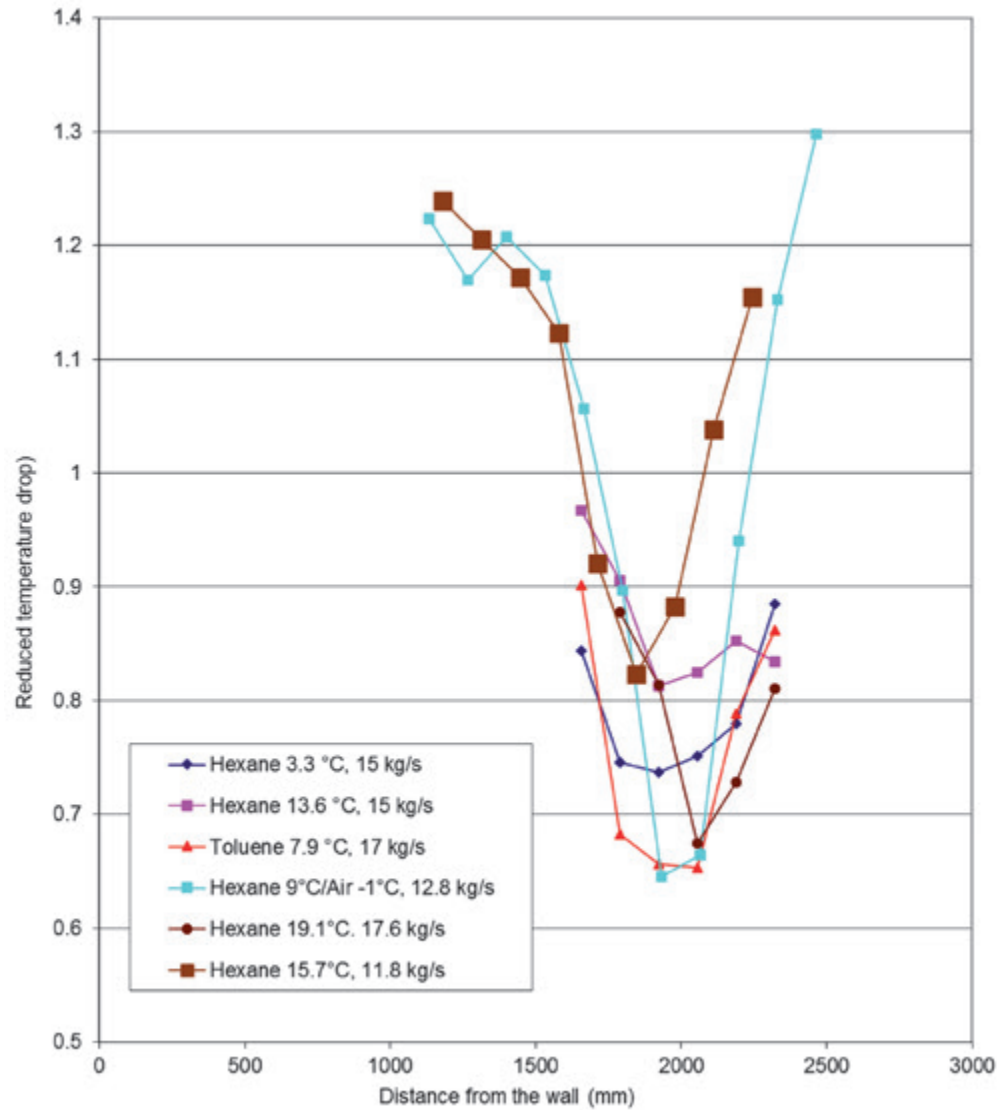


**Figure 3.4 Liquid temperature drops in the cascade above the splash zone**

It is possible to determine the air entrainment rate for the release as a whole<sup>8</sup> and this enables the thermodynamic equilibrium state for the combination of fuel and air to be calculated. The common temperature at which the liquid and co-flow of entrained air reach equilibrium provides a good scaling variable for comparing tests with different chemicals, release temperatures, air temperature, humidity *etc.* This has been done in Figure 3.5 which suggests that, at the top of the splash zone, the extent of hexane vaporisation is around 65-80% of the level that could be reached at equilibrium.

In the butane (11.8% w/w)/decene test (Test 7) where only a small proportion of the liquid was (extremely) volatile, the degree of cooling (vaporization) in the cascade centre increases during impact as was the case for the hexane and toluene tests.

In the cyclohexane test (Test 4), cyclohexane was released a few degrees above its freezing point. Evaporative cooling lowered the liquid temperature to the point where significant freezing occurred. In contrast to all of the other release experiments it is notable that the temperatures recorded above the splash zone and in the liquid/solid run-off are very similar.



**Figure 3.5** Reduced temperature drop (defined as the measured liquid temperature drop divided by the temperature drop to be expected if the air and fuel reached an equilibrium state)

### 3.4.2 Observations relating to the liquid run-off

Profiles of run-off liquid temperature across the flow in the impact zone are shown in Figure 3.6. Equivalent average liquid run-off temperature profiles for all of the hexane tests (including one from reference [8]) are shown in Figure 3.7 and the scaled reduced temperature drop (derived as explained in Section 3.4.1) are shown in Figure 3.8.

The ground level temperature measurements in the liquid run-off from all of the tests can be analysed in the same way as liquid temperatures above the impact zone. The liquid temperature falls significantly during the impact process as can be seen from a comparison of Figure 3.5 and Figure 3.8. The liquid temperature drop (related to the degree of vaporization) increases during the impact process reaching a level of 85-95% of that to be expected at equilibrium (Figure 3.8).

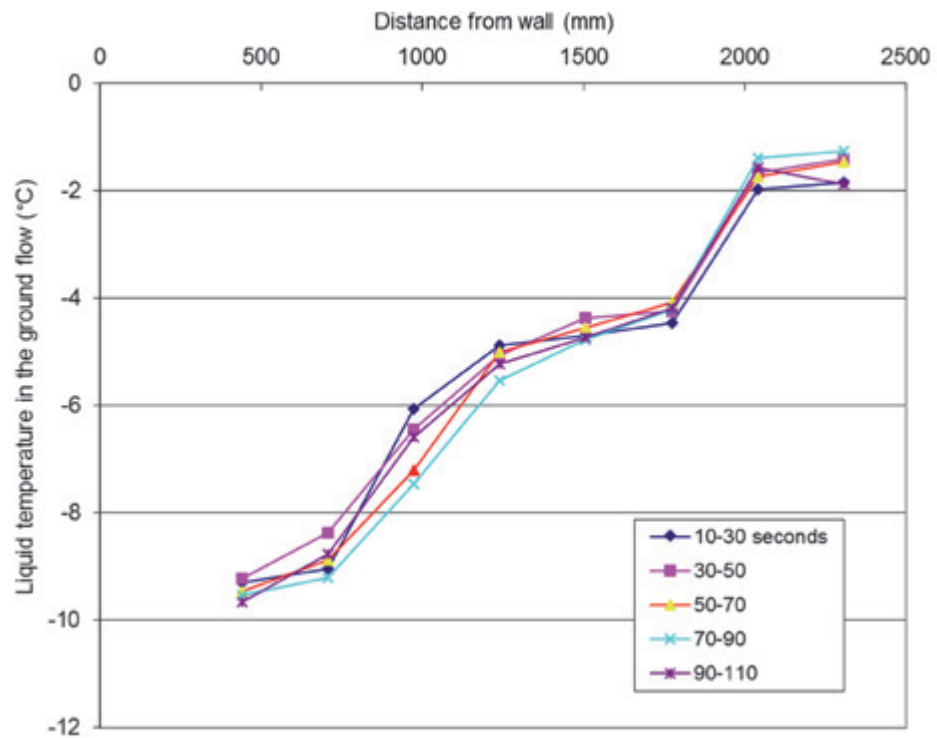


Figure 3.6 Run-off liquid temperature profiles across the impact area (ground level thermocouples at 266 mm spacing)

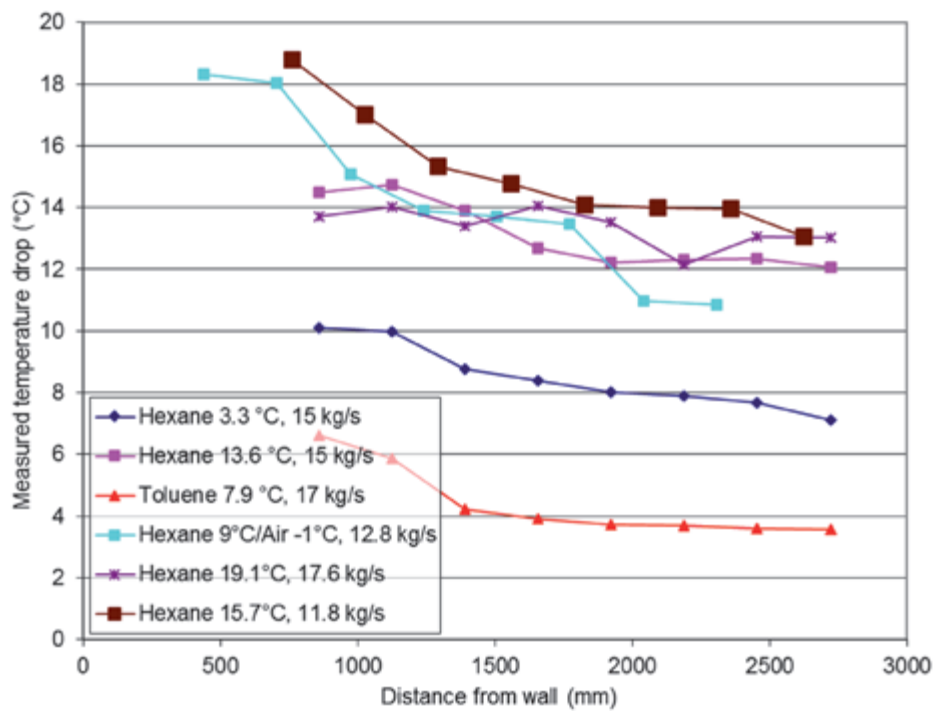
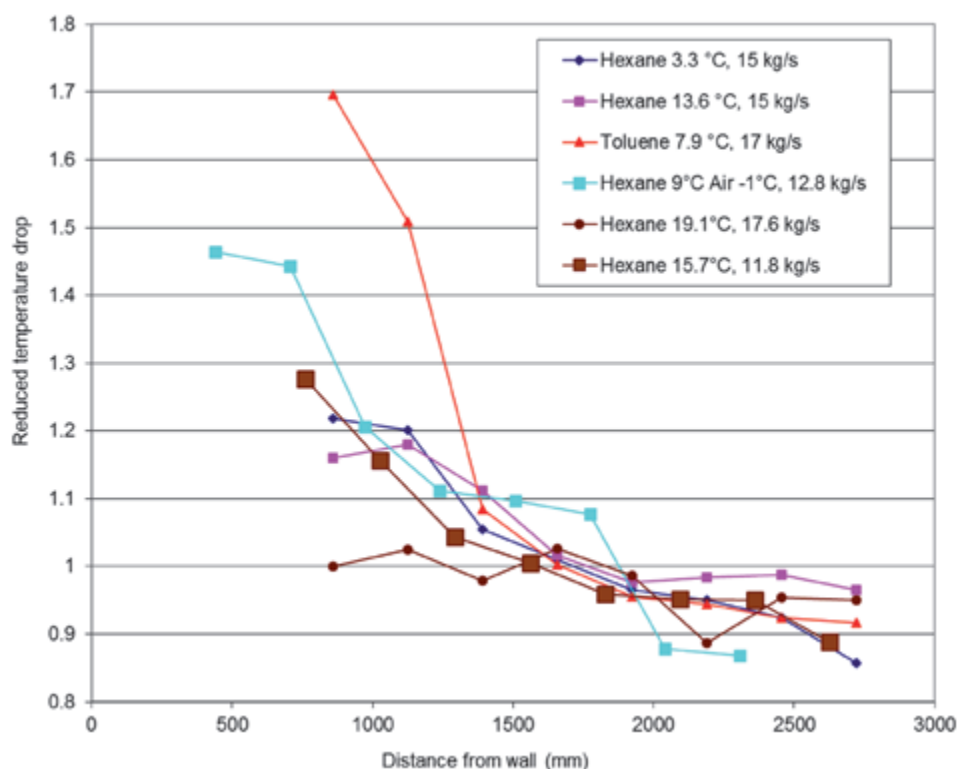


Figure 3.7 Liquid temperature drop in the ground level run-off flow



**Figure 3.8** Reduced temperature drop (defined as the measured liquid temperature drop divided by the temperature drop to be expected if the air and fuel reached an equilibrium state)

In the butane/decene test, loss of butane is relatively incomplete as the cascade nears the ground but enhanced heat and mass transfer in the impact process drive the system closer to the equilibrium state.

In the case of cyclohexane, there will be many smaller droplets in the cascade and larger droplets on the fringes that freeze may not splash on impact and consequently may be less likely to move quickly into thermal equilibrium with the rest of the flow. Nevertheless it is likely that the equilibrium assumption will give a reasonable estimate of the degree of vaporisation. The overall rate of air entrainment is likely to be unchanged but more sophisticated thermodynamic analysis of the equilibrium state is required for materials that freeze during a release e.g. cyclohexane and benzene.

### 3.4.3 Near-field vapour cloud characteristics

Three of the tests involving hexane or toluene (Test 1, 5 and 6) generated sufficient information to estimate the extent of additional vaporization that occurs in the early stages of the vapour current because of a fine spray generated in the impact zone. The remaining two tests (Tests 2 and 3) were not suitable because the liquid mass flow rates were higher and the spray extended beyond the instrumentation. Analysis of the results of Tests 1, 5 and 6 suggests that the ratio of spray vaporization to total liquid mass release was in the range of 1-1.6% of the total liquid release rate.

It is likely that the tests at higher liquid release rates, that produced more persistent sprays, also led to higher rates of spray vaporization. Without more data it would be appropriate to assume somewhat higher rates of spray vaporisation for a risk assessment involving a volatile material: a figure of 2%

of total mass release rate was assumed in the Vapour Cloud Assessment method (see Section 3.6) and this is consistent with the data collected.

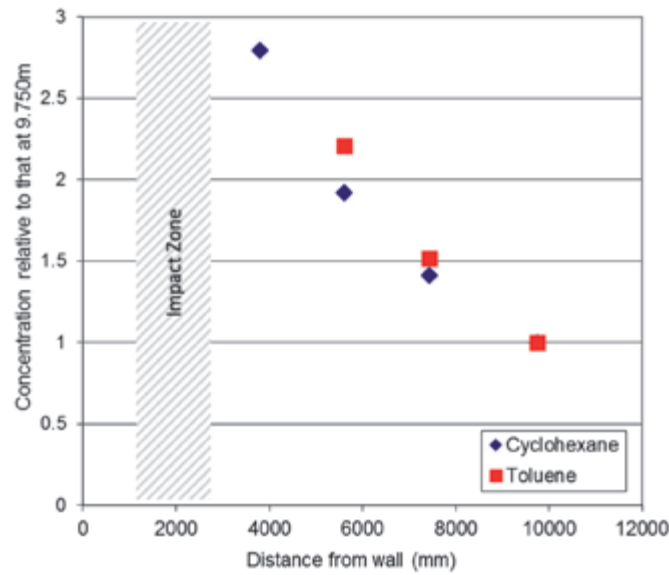
### 3.4.4 Concentration in the hexane, cyclohexane and toluene tests

Sampling for concentration measurement was in the last 10 to 20 seconds of the release at a stage when the primary vapour current most closely approached a steady state (except in Test 1 where sampling was following the end of the release). In banded tests (Tests 1, 2, 5 and 6) there was obvious accumulation of cold contaminated material in the bund which fed back into the composition of the primary current. For the unbanded tests (Tests 3 and 4) there was little accumulation and the composition of the primary current would not have changed much after the first few tens of seconds. The concentration measurements (C) are summarised in Table 3.2. All distance measurements (D) are from the tank wall on the centreline of the cascade at an elevation of 150 mm above ground except where noted otherwise in the Table.

**Table 3.2 Concentration measurements (% v/v)**

Test 1		Test 2		Test 3		Test 4		Test 5		Test 6	
D (mm)	C (%v/v)	D (mm)	C (%v/v)	D (mm)	C (%v/v)	D (mm)	C (%v/v)	D (mm)	C (%v/v)	D (mm)	C (%v/v)
3900	2.6	2900	DNR <sup>4</sup>	380	DNR	3800	2.2	3400	1.75	4600	2.21
4700	2.1	3900	4.7	4630	DNR	4630	DNR	4260	1.67	5500	2.51
5500	2.1	4900	5.3	5600	0.72	5600	1.4	5210	1.8	7430	2.44
6400 <sup>1</sup>	1.9	4400 <sup>2</sup>	3.4	5800 <sup>1</sup>	0.51	5800 <sup>1</sup>	1.5	3900 <sup>1</sup>	DNR	9740	1.99
7300	2	7430 <sup>3</sup>	1.4	7430	0.49	7430	1.0	8560 <sup>5</sup>	1.69	13460 <sup>5</sup>	1.58
9750	1.6	9750 <sup>3</sup>	1.4	9750	0.32	9750	0.72	13500	1.16	17080	1.47
Notes											
1. Measurement taken 800 mm from centreline											
2. Measurement taken 1000 mm from centreline											
3. Measurement outside the bund											
4. Did Not Record											
5. Measurement taken at apex of bund + 40 mm											

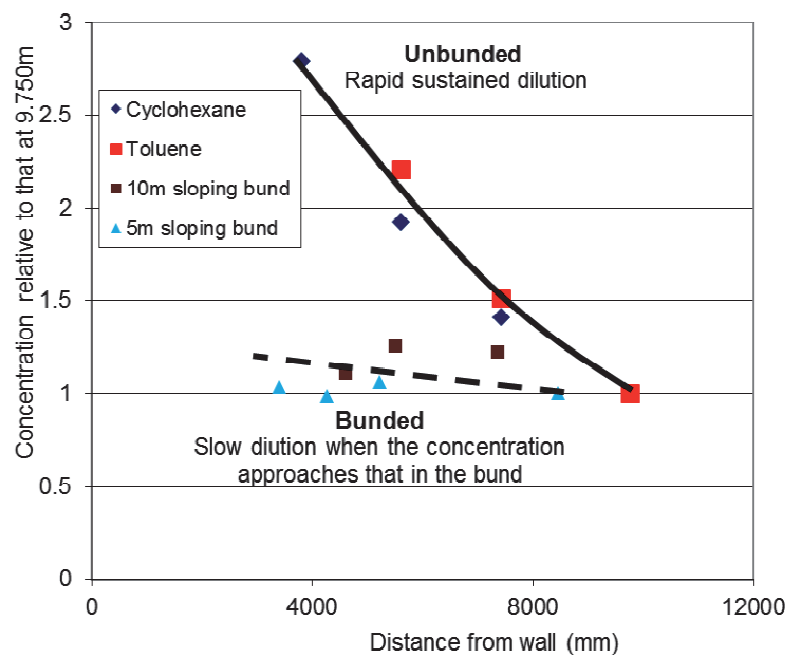
The difference in the absolute values of concentration between toluene and cyclohexane (Tests 3 and 4 with no bunds) is due to the higher volatility of cyclohexane. The variation in concentration with distance from the tank wall is plotted in Figure 3.9 with the concentration normalised with respect to the concentration values at 9.750 m from the tank wall. In the absence of bund walls, little recirculation occurred resulting in steady and sustained dilution of the current as it travelled away from the tank wall. Figure 3.9 shows that the dilution process is very similar for the two substances as would be expected. This suggests that in the absence of confinement (caused either by bunds or by multiple releases as was the case in Buncefield), rapid dilution will initially continue for some distance from the tank, considerably reducing the concentration relative to that at the foot of the tank. In such cases long-range confinement of the vapour cloud caused by changes in site elevation may be especially important.



**Figure 3.9 Cyclohexane and toluene concentration (Tests 3 and 4)**

### 3.4.5 Effect of bunds on concentration

In all tests in which a bund was introduced, (Tests 1, 2, 5 and 6) the rate of dilution within the bund is greatly reduced by recirculation that occurs from either the sidewalls or the sidewalls and front bund. In the unbunded cases (Figure 3.9) the concentration fell by a factor of about 3, between 4 m and 10 m from the tank wall. In the sloping bund cases the rate of dilution is only 10-30% (Figure 3.10). It appears that the concentration in the primary current falls rapidly to a level corresponding to the concentration in the bund and then is fairly stable – since entrainment simply introduces material with a similar concentration.



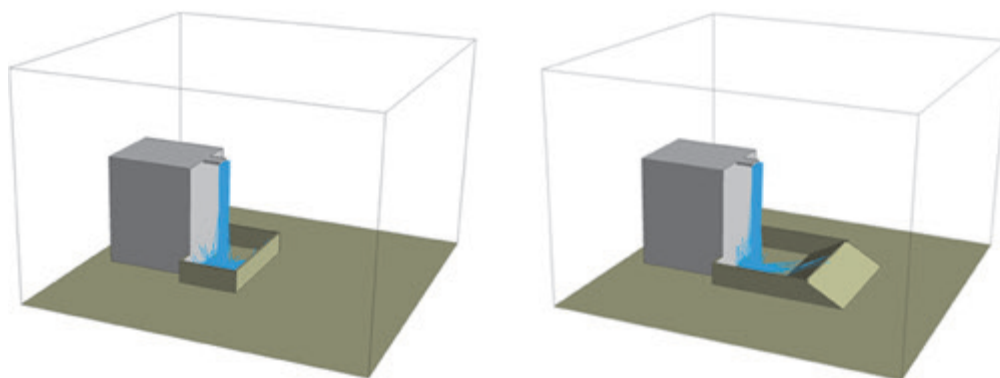
**Figure 3.10 Vapour current dilution in banded and unbanded tests**

### 3.4.6 Concentration in the butane test

Butane concentrations derived from measurements on liquid samples taken at the foot of the cascade and in the sump were found to be 4.4% (w/w) and 4.0% (w/w) respectively. Based on approximate thermodynamic analysis, it can be shown that the butane content of the vapour phase at the base of the cascade is approximately 85% of the saturated level for the residual liquid phase. This strongly suggests that the butane vaporisation process reaches a state that is quite close to equilibrium. Given the likely uncertainties in determining the distribution of spilled liquid in a real overflow and hence the air entrainment rate, it is appropriate in practical risk assessment to calculate the rate of vaporisation based on an equilibrium assumption.

## 3.5 Modelling of Vapour Cloud Development using CFD

A CFD model developed and validated for unbunded overflows [8] was used to model the banded tests in the present programme. Modelling is performed using the general purpose CFD code, CFX 12.1. The model geometry is shown in Figure 3.11. The flow of air and vapour is modelled using an Eulerian approach which involves a computational mesh that is fixed in space through which the gases flow. Momentum, mass and energy conservation equations are solved in each mesh cell to find the velocity, temperature, pressure and concentration distributions. The spray of droplets is modelled using a Lagrangian approach. The paths of discrete computational particles are tracked through the flow domain from their injection point until they hit a solid surface, escape the domain or evaporate completely. Each modelled fluid particle represents a large number of droplets with given mean size and transport properties.



**Figure 3.11 Typical computational geometry**

The exchange of momentum, mass and heat between the Eulerian phase and Lagrangian particles is two-way. For momentum, particles falling through the air are subjected to drag forces, and their trajectories can be affected by turbulent perturbations in the air. The air is also affected by the drag of the droplets and is entrained into the spray. Two-way coupling is important in determining evaporation rates, where the vapour concentration in the gas phase affects the rate of evaporation from the droplets and vice versa. Droplet evaporation leads to a temperature decrease which affects the saturation vapour pressure and hence the calculated evaporation rate. Coupling between the two phases is achieved by



introducing source terms derived from the Lagrangian solution into the Eulerian transport equations. The overall CFD solution is obtained by iterating between the Eulerian and Lagrangian models. The tank walls and ground are treated as solid walls using a simple restitution-coefficient based model.

The CFD predictions of liquid temperatures for both the 10 m bund cases (vertical and sloping) are very close to the experimental values. In the other cases the CFD predicts slightly low temperatures *i.e.* the extent of vaporization at the foot of the cascade is slightly overestimated.

It is not possible to model the splashing process and flow in the impact zone in a fundamental way. Unless compensated for, the additional vaporisation that occurs would be underestimated. To compensate for this, some droplets were re-injected using a process described in [8]. Adopting this approach, the total amount of additional vaporization is well represented. However, the distribution of temperatures and concentrations close to the ground near the impact zone are not. This does not necessarily undermine the usefulness of CFD so long as the properties of the wider vapour cloud accumulating in and spilling out of the bund are reasonably well predicted.

The concentrations in the bund and in the flow outside the bund are reasonably well predicted, with the calculated values being a little higher than the measurements, suggesting that droplet re-injection was somewhat overdone. Refinement of the splashing model could probably improve the level of agreement but the CFD model does appear to reasonably reproduce the dilution processes that determine the concentration in the bund and in the outflow.

### **3.6 Simplified Method for Estimating Vapour Cloud Characteristics**

The work carried out on liquid fuel spills prior to this project<sup>8</sup> enabled a simplified method to be developed for calculating the rate at which the volume of a vapour cloud increases during an overfilling incident (the VCA method). The analysis also gives the concentration of hydrocarbons in the cloud and provides some guidance on the extent of cloud spread in relatively flat sites with the kind of obstructions that would be normal in and around a fuel depot tank farm. Parameters were given for use in this method which were representative of the winter grade gasoline involved in the Buncefield incident.

The results of the experiments in this project support the assumption made in the VCA method that calculation of the equilibrium state provides a reasonably reliable means of estimating the degree of vaporization in the cascade and impact process.

The VCA method was applied to the tests performed in this project. This showed that the rate of vaporization and the volume flow of vapour are reliably predicted by the VCA method. The tests also supported the assumption in the VCA method that, in addition to vaporization in the cascade and impact zone, a further 2% of the total liquid flow rate goes to form a fine spray in the vapour current away from impact.



It is of interest to compare the current results and the VCA method with preliminary guidance given in the PSLG report ([www.hse.gov.uk/comah/buncefield/fuel-storage-sites.pdf](http://www.hse.gov.uk/comah/buncefield/fuel-storage-sites.pdf)) on safety in fuel storage sites.

**Table 3.3 Comparison of the PSLG and VCA methods**

	PSLG method	VCA method
Release rate	115 kg/s	115 kg/s
Air entrainment in cascade	124 kg/s	108 kg/s
Hydrocarbons at tank foot	14.2 % w/w	15.3 w/w
Final concentration in cloud	14.2 %w/w	8.4 % w/w (0.11 kg/m <sup>3</sup> )
Cloud growth	96 m <sup>3</sup> /s	199 m <sup>3</sup> /s

The PSLG method, which was focussed on the analysis of which liquids were "in scope" *i.e.* could produce a flammable cloud (of whatever volume), did not include dilution of the vapour current after the impact point. This led to over predictions of fuel concentrations and under-prediction of cloud volume. In this context the PSLG recommendations were based on the best available evidence at the time. Generally the current experiments and modelling results and VCA method (which is based on these results) predict lower fuel concentrations in the accumulating cloud but this cloud has a somewhat larger volume. The implication is that the current work shows that lower flashpoints (or higher vapour pressures) are required for a liquid to be "in scope" *i.e.* capable of forming an extensive flammable cloud. The work has allowed more accurate cloud concentration and volume prediction than was possible with the PSLG method. The VCA method is also suitable for the calculation of cloud volumes; if the PSLG method was used for this purpose neglecting near-field entrainment would lead to under predicting the cloud volume.

To allow wider application of the VCA method, thermodynamic analysis was performed for a group of solvents and petrochemical mixtures that are commonly found in chemical and petrochemical processing facilities in the UK and the parameters necessary to extend the method to these substances were derived<sup>11</sup>.



## **4 EFFECT OF MIXED DIAMETER OBJECTS ON EXPLOSION CHARACTERISTICS**

### **4.1 Objectives**

The purpose of the work reported in this section was to investigate

- (a) whether small-diameter cylindrical obstacles (pipes) are less effective in generating explosion overpressure than bigger-diameter obstacles, and
- (b) the extent to which combinations of different diameter obstacles have can generate greater overpressures than uniform arrays of obstacles.

The relevance of this work is (a) as a first step in understanding the role of mixed diameter obstacles in overpressure generation as a precursor to the more complex obstacle combinations associated with vegetation and (b) to provide well controlled experimental data on the effect of obstacle combinations which can be used for explosion model validation and development.

### **4.2 Key Findings**

1. No difference was found in the effectiveness of cylindrical obstacles to generate explosion overpressure based on obstacle diameter as long as the area blockage is the same. The range of diameters studied was 4 mm – 104 mm.
2. However, an increase in explosion overpressure was observed when obstacles of different diameters were mixed (keeping the area blockage constant). Depending on the combination of obstacles, the increase in pressure compared to a “single diameter” scenario ranged from 11% to 21%.
3. The data generated is useful for the development of gas explosion models.

### **4.3 Description of the Test Programme**

The tests were performed by Gexcon and the final report is reproduced in Volume 2 of this Publication<sup>10</sup>.

#### **4.3.1 Explosion test rig**

The tests were performed in a 1210 × 1220 × 6100 mm explosion vessel having a volume of 9.0 m<sup>3</sup>. The vessel is vented through one of its short (1210 × 1220) ends – all other faces are closed. The roof of the vessel is covered with plexi-glass to allow filming of the explosion propagation inside the vessel from above. Figure 4.1 shows a view of the vessel taken from the open end with a mix of different diameter obstacles in place.



**Figure 4.1** Test rig – view from open end showing a mix of different diameter pipes

The open end of the vessel was covered with a thin plastic film, held in place using a pneumatic system, in order to keep the gas inside the vessel during gas filling. This plastic film was released 1 second prior to ignition.

All tests were performed using a stoichiometric propane/air mixture with a concentration of 4.2-4.3% by volume, ignited by a high voltage electric spark located 100 mm from the back (closed) wall of the vessel at the centre of this wall (*i.e.* 600 mm from the vessel floor and mid-way between the two long walls).

#### **4.3.2 Congestion**

In order to generate turbulence and flame acceleration, 4 rows of pipes were placed inside the vessel at 2, 3, 4 and 5 m from the closed end of the vessel. The pipes used were in one of three diameter sizes (4, 20 and 104 mm).

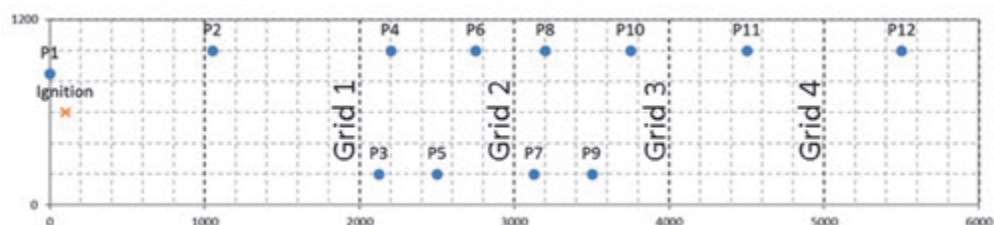
The congestion arrangement in the first test used a series of the largest diameter obstacles (104 mm) selected to achieve an average overpressure of around 1 bar in the middle third along the length of the vessel. In the second and third tests, 20 and 4 mm diameter pipes respectively were used and the number of pipes per row was chosen to achieve an average overpressure in the middle third of the vessel within 20% of the overpressure measured in the first test. Subsequent tests used combinations of 2 or 3 different diameter sizes.

#### **4.3.3 Instrumentation**

##### **Overpressure measurements**

The overpressure generated within the test vessel during the explosion tests was measured using 12 piezo-electric pressure transducers. Figure 4.2 shows the positions of the transducers on plan. Of these, P1 was installed 330 mm above the vessel floor whereas all the other transducers were at vessel floor level.

The external overpressure (in front of the vent opening) was measure using three “skimmer-plate” pressure transducers mounted with their sensitive area perpendicular to the vent area. These were positioned centrally relative to the open end (*i.e.* at an elevation 600 mm from the vessel floor and mid-way between the long wall) at distances of 2.0, 3.0 and 4.0 m from the open end.



**Figure 4.2** Positions in plan of the internal pressure transducers

















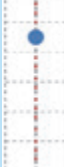
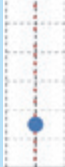







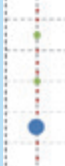


### Video records

All tests were recorded using a high-speed (1200 fps) digital SLR camera. Flame propagation was recorded through the plexi-glass. Two cameras were installed above the vessel, each covering half the length of the vessel. A fast acting LED light-box unit was fired in parallel with the ignition source to indicate the time of ignition on the video camera and to allow flame propagation relative to the time of ignition to be measured. The light box on the recordings was triggered at the same time as the data logger and thus occurred a few milliseconds before ignition. This gave a good visible indication on the video recordings just before the explosion was initiated. Flame propagation analysis and flame speed estimates were made from these high-speed video recordings. A secondary high-speed (240 fps) camera was also used to film the tests.

### 4.3.4 Tests

The test programme comprised scenarios with 7 obstacle arrangements. These are summarised in Table 4.1. Grid 1, 2, 3 and 4 are at 2 m, 3 m, 4 m and 5 m respectively from the closed end of the vessel and the grid diagrams shown in Table 4.1 are vertical cross-sections at the grid positions showing a section through the vertical arrangement of pipes at each grid.

**Table 4.1 Test configurations**

Test No.	Description	Congestion configuration				Area blockage (%)
		Grid 1	Grid 2	Grid 3	Grid 4	
5-7	8 No. 104 mm diameter pipes (2 on each grid line) to give a pressure in the region of 1 bar					17% at each of grids 1-4
5-8	20 No. 20 mm diameter pipes (5 on each grid line) to give a pressure within 20% of test 5-7					8% at each of grids 1-4
5-11	112 No. 4 mm diameter pipes (28 on each grid line) to give a pressure within 20% of test 5-7					11% at each of grids 1-4
5-12	Combination of 10 No. 20 mm diameter pipes and 56 No. 4 mm diameter pipes					8% at grids 1 & 3 10% at grids 2 & 4
5-14	Combination of 4 No. 104 mm diameter pipes and 56 No. 4 mm diameter pipes					17% at each of grids 1-4
5-15	Combination of 4 No. 104 mm diameter pipes and 10 No. 20 mm diameter pipes					12% at grids 1 & 3 14% at grids 2 & 4
5-16	Combination of 3 No. 104 mm diameter pipes, 8 No. 20 mm diameter pipes and 40 No. 4 mm diameter pipes					15% at grids 1-3 7% at grids 4

## 4.4 Summary of Experimental Observations

Maximum and minimum peak pressure measurements both inside and outside the vessel are summarised in Table 4.2. Also given in the table are the average peak pressure values for internal pressure transducers located in the middle third of the vessel along its length. Items in brackets denote the transducer number of the measurement given.

**Table 4.2 Summary of minimum, maximum and average peak pressures**

Test No.	Peak overpressure (mbar)				
	Inside the vessel			Outside the vessel	
	$P_{min}$	$P_{max}$	Av (mid 1/3)	$P_{min}$	$P_{max}$
5-7	912 (P9)	1221 (P2)	1008	371 (SP3)	602 (SP1)
5-8	784 (P10)	910 (P1)	822	315 (SP3)	465 (SP1)
5-11	681 (P12)	974 (P2)	799	287 (SP3)	443 (SP1)
5-12	858 (P8)	1103 (P2)	899	265 (SP3)	536 (SP1)
5-14	937 (P12)	1103 (P2)	1043	390 (SP3)	589 (SP1)
5-15	908 (P11)	1352 (P1)	1064	406 (SP3)	638 (SP1)
5-16	971 (P12)	1326 (P2)	1061	400 (SP3)	616 (SP1)

$P_{min}$  is the minimum recorded peak pressure in mbar

$P_{max}$  is the maximum recorded peak pressure in ms

Av (mid 1/3) is the average peak pressure measured by all transducers located in the middle third of the vessel along its length (*i.e.* P3 – P10)

A summary of all internal peak overpressure measurements at all transducers in the tests is shown in Figure 4.3.

#### 4.4.1 Repeatability

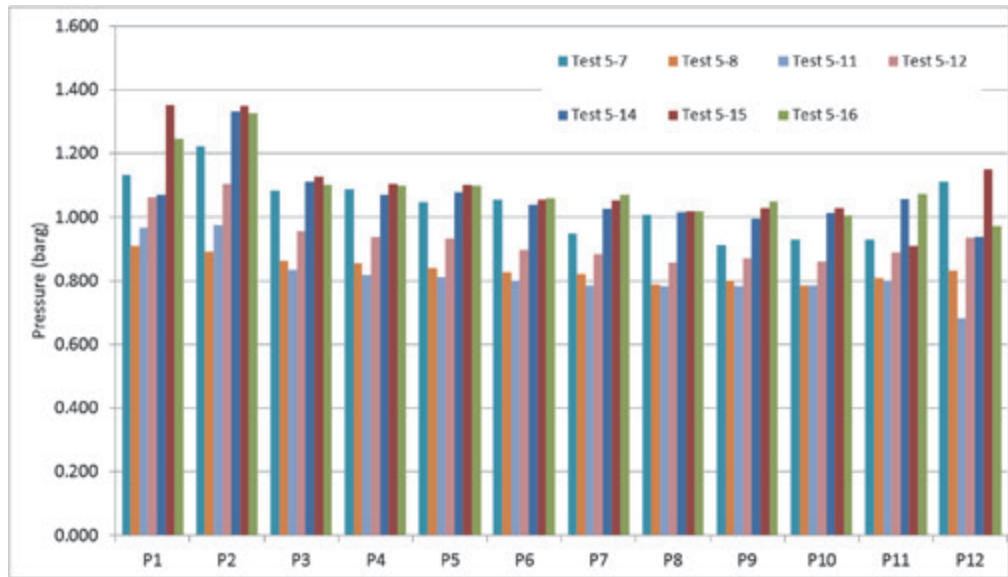
Test 5-7 was repeated twice (Test 5-5 and Test 5-6) and the results are shown in Table 4.3 for the average in the central part of the vessel (transducers P3 – P10).

**Table 4.3 Pressure measurements in the central part of the rig**

Test 5-7 (mbar)	Test 5-6 (mbar)	Test 5-5 (mbar)	Average (mbar)	Standard deviation	Error (95% confidence)
1008	1173	940	1040	$\pm 0.119$	$\pm 23$
1008		940	974	$\pm 0.039$	$\pm 8$

When averaging the results from all 3 tests, the error in these measurements is 23% (for a 95% confidence margin). Closer scrutiny of the pressure traces for Test 5-6 showed that there was a significant noise component occurring with a period of 50 Hz; one of these coincided with the peak overpressure. Removing the peak pressure for Test 5-6 from the average values used in Table 4.3 decreases measurement error to 8%. The source of the signal noise was located and removed from the system, improving the quality of the measured data in all subsequent tests and the repeatability of the tests was deemed to be satisfactory.





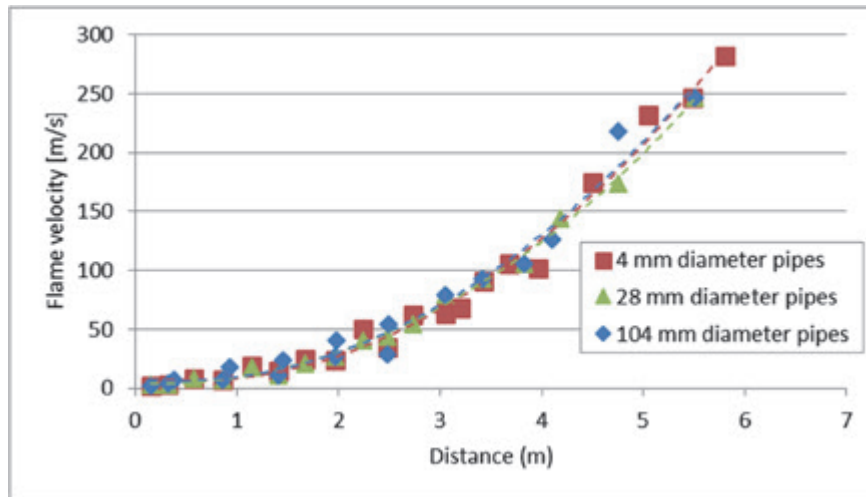
**Figure 4.3 Summary of internal peak overpressure measurements**

#### **4.4.2 Effect of pipe diameter size**

The main factor that causes pressure increase in these tests is the generation of turbulence induced by the obstacles in the vessel due to the flow ahead of the flame as the explosion propagates towards the vent opening. As more obstructions are added, the cross-section of the vessel will be increasingly blocked and thus the effective venting area decreases. As the explosion pressure is generated and increases in the vessel, the reduced venting area increase flow velocities and thereby enhances the explosion pressure in the vessel. It is expected that the turbulence generated in the wake of the obstacles reaches a maximum above which further flame folding and flame propagation enhancement ceases and begins to decrease.

The flame velocity was found to be similar for all 3 “single diameter” tests (5-7, 5-8 and 5-11) as shown in Figure 4.4. The 104 mm diameter pipes (Test 5-7) resulted in flame velocities that were very slightly higher than the 20 mm and 4 mm tests, and corresponds well with the peak overpressure which was slightly higher in Test 5-7. The flame velocity in Test 5-8 was very marginally lower than in Test 5-11. Average peak pressures in the middle third of the vessel were similar in both tests.

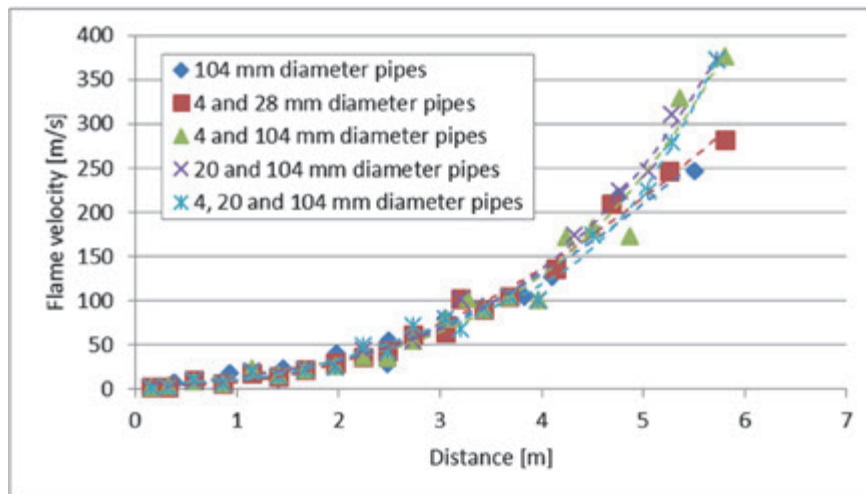




**Figure 4.4** Flame velocity profile for the “single diameter” tests

#### 4.4.3 Effect of combinations of pipe diameters

Figure 4.5 shows the flame velocity profile for all mixed diameter tests together with the flame velocity from the 104 mm diameter pipes only. The peak or exit flame velocity also remained roughly the same when mixing the small and medium obstructions. However, a more significant increase in peak flame velocity was observed when the large (104 mm diameter pipes) were added to the mix. This increase appears to start around the third grid at 4 metres.



**Figure 4.5** Flame velocity profile for the large and mixed diameter pipes

Table 4.4 shows that in all mixed diameter tests an increase in the peak explosion pressure was observed compared with the “single diameter” tests. For the test with combined 4 mm and 20 mm diameter pipes, the pressure increased by approximately 11%. This is a minor increase within the experimental error band or repeatability of the results. In all other cases, however, the increase in peak pressure was somewhat greater, with pressure increases of 15% and 16% in the tests which used two diameter pipes and 21% for the test with a mix of three diameter pipes. Since the area blockage is similar and the flame velocities were higher in these tests, the enhanced explosion propagation, whilst moderate, is most likely caused by the mixing of different diameter pipes.

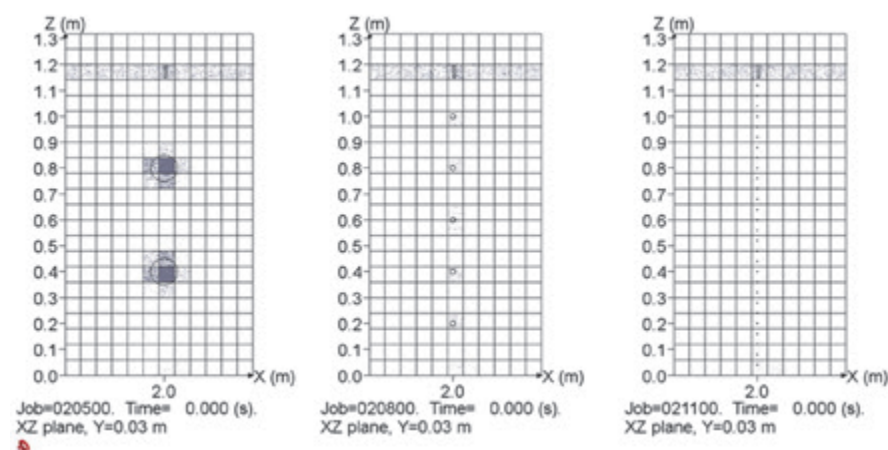
**Table 4.4 Increase in overpressure over single diameter cases**

Pipe diameter	Average of “single diameter” cases (mbar)	Average for the mixed diameter case (mbar)	Percentage increase
4 mm & 20 mm	0.810	0.899	11 %
4 mm & 104 mm	0.904	1.043	15 %
20 mm & 104 mm	0.915	1.064	16 %
4 mm, 20 mm & 104 mm	0.876	1.061	21 %

#### 4.4.4 Implications for CFD modelling of gas explosions

Sub-grid turbulence generation in CFD models is based on the area and volume blockage ratio of a control volume defined by volume and area porosity. This geometry representation and its coupling with the turbulence model is what characterises the use of the distributed porosity concept in CFD models like FLACS. The geometric length scale of obstruction sub-grids is therefore not explicitly taken into account in the simulated turbulence field.

Figure 4.6 illustrates the resolution of the different obstructions in FLACS based on the simulation grid used to model the tests. The turbulence production from the 20 mm and 4 mm pipes is wholly represented by the sub-grid model, while the 104 mm pipes are partly handled by the k-epsilon turbulence model since these are larger than the grid size. This approach is known to be somewhat grid dependent – the turbulence production of an on-grid object will not necessarily correspond exactly to that of an identical object represented sub-grid.

**Figure 4.6 Representation of pipes in test 5-7 (left), 5-8 (middle) and 5-11 (right)**

Simulation of the tests using FLACS showed that maximum overpressures across all configurations were predicted within approximately 30% of the experimental overpressures. Although a limited data set, a slight tendency towards over-prediction of the effect of the 20 mm and 4 mm pipes was observed compared with the effect of the 104 mm pipes. It is known that the characteristic dimension of sub-grid obstacles might play a larger role than what is currently applied in FLACS, so some subtle effects might be lost in the sub-grid modelling. Handling some obstructions as partially on-grid obstacles while others are handled as purely sub-grid obstacles can be a challenge when simulating flame propagation and explosions. The representation of sub-grid versus on-grid obstructions in FLACS is the subject of ongoing development.

## **5 EFFECT OF VEGETATION CONGESTION ON EXPLOSION CHARACTERISTICS**

### **5.1 Objectives**

Work which followed the Buncefield incident supported the proposition that vegetation can cause flame acceleration to velocities of several hundred m/s leading to high overpressures and the possibility of a transition to detonation<sup>12,7</sup>. The main objectives of this work are therefore:

- (a) To study the parameters which influence flame acceleration in vegetation (comprising a hedge or a row of trees), namely the length, width, density and type of vegetation.
- (b) To show whether and in what circumstances a transition from deflagration to detonation can be caused by vegetation.
- (c) To document the experimental data such that it can be used by others to validate existing (or develop new) techniques for modelling vapour cloud explosions of this type and the effects of vegetation on the explosion characteristics. This will require characterisation of vegetation in a form suitable for use by modellers (e.g. number density of branches).

A series of medium scale semi-confined tests and large scale unconfined tests were performed.

### **5.2 Key Findings**

- 1. When an unconfined vapour cloud is ignited, the presence of vegetation accelerates the flame. The resulting flame velocity depends on the density (area and volume blockage) and the width of vegetation present.
- 2. In the tests conducted, flame acceleration occurs within a short distance of travel through vegetation (10 – 20 m). Beyond this, and depending on the characteristics of the vegetation, the flame either settles to a steady limiting speed or a transition to detonation occurs. A transition to detonation occurred in two tests with 4.5 m wide rows of vegetation and different vegetation density.
- 3. The conditions that can give rise to a transition to detonation could not be determined within the limited number of tests performed and the high variability of vegetation. However, detonations only occurred in two of the four 4.5 m wide vegetation tests.
- 4. A test using 2 m wide very dense vegetation produced a flame speed of around 150 m/s and no transition to detonation. The limiting flame speed can be quite sensitive to the precise conditions.
- 5. Different types of vegetation resulted in the generation of similar explosion overpressures where area blockage ratios were similar.

6. Foliage (in the form of leaves or needles) and small diameter twigs ( $< 3$  mm) when present significantly increased flame acceleration and explosion overpressure. In a semi-confined test in which the foliage and twigs were systematically removed, the overpressure reduced by a factor of 2.5 compared with the intact trees.
7. For practical reasons, the vegetation used in the tests was the result of cutting trees and assembling them in the test rig to form a hedge. The branch distribution in a naturally growing hedge is likely to differ from one that is “constructed” in the way described. It was not possible within the scope of the project to quantify this difference.
8. The vegetation was characterised by selecting a number of trees from each batch, cutting these into their constituent parts, and measuring the lengths and diameters of these parts. This data, along with the test results, are documented in detail and can be used for model validation and development.
9. Some modelling of the unconfined vegetation tests was performed during the project. Whilst overpressures and the possibility of detonation were predicted, the rapid flame acceleration within the first 10 – 20 m followed by either a relatively steady flame speed or a transition to detonation was less well predicted.

### **5.3 Description of the Medium Scale Test Programme**

The medium scale tests were performed by Gexcon. A copy of the full final report is reproduced in Volume 2<sup>10</sup>.

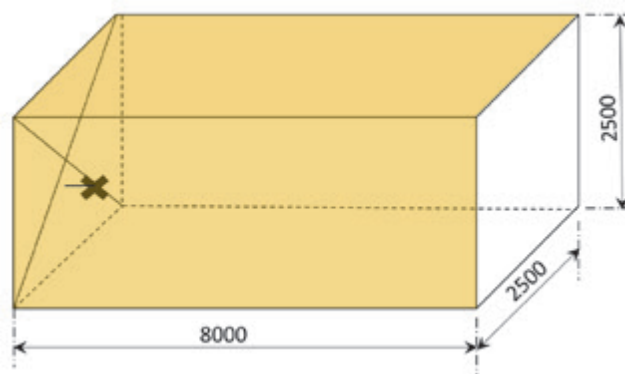
#### **5.3.1 Explosion test rig**

The medium scale tests were performed in a 50 m<sup>3</sup> explosion test rig (8.0 m long, 2.5 m high and 2.5 m wide). Internally, the rig had an array of beams at mid-height which form part of the structure of the rig; otherwise, vegetation (or piping) was used to provide the obstructions in the tests. The test rig is shown in Figure 5.1 with one of the long walls removed. In most tests, a plexi-glass wall was used in this position to enable the flame propagation to be recorded on high speed video. In all tests, all but one of the short ends of the test rig were closed, hence the explosion was directed from one closed end to the opposite open end. In all tests, the ignition point was located 0.26 m in from the closed end of the rig, halfway along the closed end and at a height of 1.10 m above the module floor. A schematic of the test rig showing the boundary conditions and location of the ignition point is shown in Figure 5.2.

The tests were performed using a stoichiometric (4.2% v/v) propane/air mixture with one exception where a lean mix (3.0% v/v) was used. The vent area (the open end of the test rig) was covered with thin plastic film to keep the explosive gas mixture inside the module during gas cloud preparation. The plastic film was clamped in place using a pneumatic retaining system and was released just prior to ignition to allow it to be easily brushed aside by the ensuing explosion.



**Figure 5.1** Test rig shown without one of its long walls in place



**Figure 5.2** Schematic of the test rig showing dimensions, boundary conditions and ignition location (x - denotes the location of the ignition point)

### 5.3.2 Congestion

Three types of vegetation were studied in the medium scale tests. These were Norway spruce, silver birch and Thuja (Figure 5.3). In addition, tests were performed using tree trunks and smooth pipes of a similar diameter to assess whether the surface roughness of the trunks has an effect on the explosion.



(a) Norway spruce



(b) Silver birch



(c) Thuja

**Figure 5.3** Vegetation types used in the medium scale tests



Each of the three types of trees was characterised through detailed measurements of a number of typical trees. Average figures are shown in Table 5.1. For details of the vegetation measurements, reference should be made to Volume 2<sup>10</sup>.

**Table 5.1 Average characteristics of typical trees used in the tests**

Tree type	No. of branches <sup>1</sup> of diameter		Trunk diameter (mm)		Tree volume (litres)		Volume blockage (%) <sup>2</sup>
	<10 mm	≥10 mm	Top	Bottom	Branches	Branches & trunk	
Norway spruce	39	27	42	90	8.7	18.1	0.42
Silver birch <sup>3</sup>	38	16	15-20	43	5.7	7.6	0.28
Thuja <sup>4</sup>	90		3-5	30	—	7.0	5.38

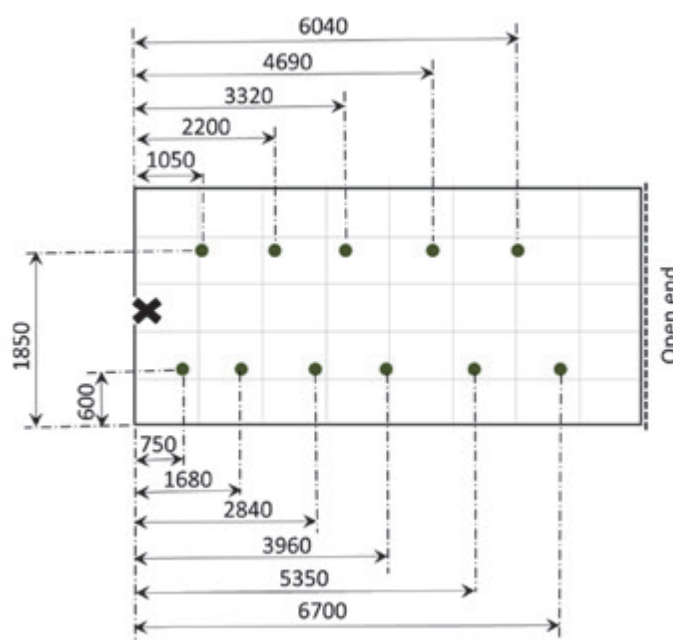
1 This corresponds to branches emanating from the main trunk

2 Volume blockage is calculated as the percentage ratio of the volume of the solid part of the tree to the volume of an envelope of the tree (calculated to be 4.35 m<sup>3</sup> for a spruce tree, 2.75 m<sup>3</sup> for a birch tree and 0.13 m<sup>3</sup> for a Thuja bush of the sizes used in the tests)

3 The numbers relate to two trees installed at each location

4 Each Thuja bush consisted of typically 3-4 main trunks

The obstacles (trees or pipes) were installed at fixed locations within the test rig as shown in Figure 5.4. In some tests, obstacles were installed at all the positions shown whereas only a subset of obstacles were installed in other tests (see Table 5.3). In the case of the Thuja, a hedge was created along the middle of the rig. The hedge comprised either a single or a double row of Thuja bushes.



**Figure 5.4 Plan of fixed obstacle positions**

In some tests the birch trees were trimmed to remove their smallest branches and leaves. This congestion thinning was performed systematically in three stages. At the first stage, sub-branches and twigs with a diameter smaller than approximately 2-3 mm were removed; in the second stage, branches with a diameter in the range 4-8 mm were also removed. In the third stage, only the tree

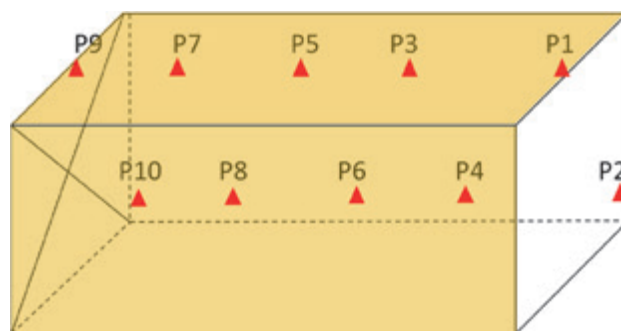
trunks were retained. Note that the term “sub-branches” here refers to those parts of the tree emanating from branches rather than from the main trunk, whereas “branches” refers to those parts emanating directly from the main trunk. The result of this trimming on volume blockage is shown in Table 5.2.

Several tests were performed in which only the main tree trunks were used as obstructions. For these tests, the trees were stripped of all the branches and twigs to leave only the basic rough tree trunks. For comparison with the tree trunk tests, tests were also performed with smooth aluminium pipes with a diameter of 70 mm and a height similar to that of the silver birch trees (2.4 m).

### 5.3.3 Instrumentation

#### Overpressure measurements

The overpressure generated within the test vessel during the explosion tests was measured using 10 piezo-electric pressure transducers (Figure 5.5). Five were mounted along the centre of the roof (P1, P3, P5, P7 and P9) and five along the back long wall 0.48 m above the test rig floor (P2, P4, P6, P8 and P10). The external overpressure (in front of the vent opening) was measured using five “skimmer-plate” pressure transducers mounted such that the sensitive area of the transducer was perpendicular to the vent area. These were positioned centrally relative to the open end at distances of 2.5, 5.0, 7.5, 10.0 and 12.5 m from the open end.






**Figure 5.5** Positions of pressure transducers

#### Video records

All tests were recorded using a high-speed (1200 fps) digital SLR camera. A fast acting LED light-box unit was fired in parallel with the ignition source to indicate the time of ignition on the video camera to allow flame propagation relative to the time of ignition to be measured. The light box on the recordings was triggered at the same time as the data logger and thus occurred a few milliseconds before ignition. This gave a good visible indication on the video recordings just before the explosion was initiated. A secondary high-speed (300 fps) camera was used for observing the movement of the vegetation inside the module. All tests were also recorded using a standard (25 fps) SVHS video camera.

**Table 5.2 Effect of trimming on volume blockage**

Trimming stage	Volume (litres)	Volume blockage (%)	Illustration
No trimming (as cut)	7.6	0.28	
Stage 1 (sub-branches <2-3 mm removed)	4.8	0.17	
Stage 2 (branches 4-8 mm removed)	3.6	0.13	
Tree trunks only	1.9	0.07	

### 5.3.4 Test programme

A total of 16 tests were performed during this work – two were reference tests with an empty module, three were performed with spruce trees, 7 with birch

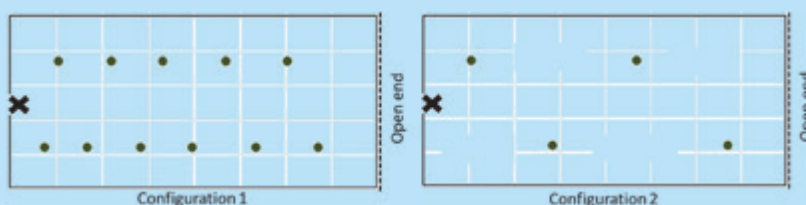


trees, two with pipes and two with hedges of Thuja trees. All tests except one of the spruce tree tests were performed with a homogeneous nominally 4.2 %v/v propane-air mixture filling the entire module. The “high congestion” spruce tree test with 11 trees was performed with a lean propane concentration of 3.0 %v/v to ensure that excessive overpressures, which were feared could damage the test rig, were avoided. A summary of the test programme is given in Table 5.3.

**Table 5.3 Summary of test programme**

Test No.	Gas concentration	Congestion type	Congestion configuration	Volume blockage ratio (%) <sup>1</sup>
3.1-1	4.12	None	n/a	0
3.1-12	4.20	None	n/a	0
3.1-2	3.01	Norway spruce	11 trees – Configuration 1	0.4
3.1-3	4.11	Norway spruce	4 trees – Configuration 2	0.14
3.1-15	4.25	Norway spruce (Trunks only)	11 trees – Configuration 1	0.21
3.1-4	4.08	Silver birch	4 trees – Configuration 2	0.21
3.1-5	4.28	Silver birch (Trim stage 1)	4 trees – Configuration 2	0.04
3.1-13	4.14	Silver birch (Trim stage 1)	4 trees – Configuration 2	0.04
3.1-7	4.18	Silver birch (Trim stage 2)	4 trees – Configuration 2	0.029
3.1-8	4.16	Silver birch (Trim stage 2)	4 trees – Configuration 2	0.029
3.1-9	4.23	Silver birch (Trim stage 2)	4 trees – Configuration 2	0.029
3.1-10	4.27	Silver birch (Trunks only)	4 trees – Configuration 2	
3.1-14	4.25	Pipes	11 pipes – Configuration 1	
3.1-11	4.21	Pipes	4 pipes – Configuration 2	
3.1-18	4.22	Thuja	42 trees in a double-width row along the centre of the rig	0.59
3.1-16	4.21	Thuja	21 trees in a single row along the centre of the rig	0.29

<sup>1</sup> Relative to the volume of the rig (50 m<sup>3</sup>)

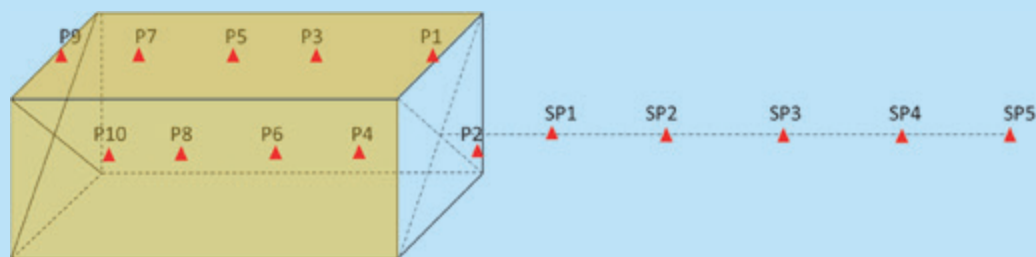


### 5.3.5 Summary of experimental observations

Maximum and minimum peak pressure measurements both inside and outside the rig (as well as the corresponding pressure pulse duration for the maximum and minimum pressures) are summarised in Table 5.4. Also given in the table are the average peak pressure values for all internal and external pressure transducers.

**Table 5.4 Summary of minimum, maximum and average peak pressures**

Test No.	Overpressure characteristics (mbar, ms)									
	Inside the rig					Outside the rig				
	$P_{min}$	$T$	$P_{max}$	$T$	$Av$	$P_{min}$	$T$	$P_{max}$	$T$	$Av$
3.1-1	206 (P8)	78.7	405 (P1)	68.3	318	115 (SP5)	20.1	241 (SP1)	41.0	177
3.1-12	198 (P2)	28.2	307 (P3)	71.0	246	102 (SP5)	24.8	216 (SP1)	40.5	147
3.1-2	1021 (P5)	60.0	1530 (P9)	60.9	1236	256 (SP5)	11.9	636 (SP1)	19.0	435
3.1-3	1222 (P4)	41.0	2836 (P2)	13.0	1671	365 (SP5)	9.5	861 (SP1)	17.4	577
3.1-15	581 (P4)	61.9	843 (P3)	58.0	639	176 (SP5)	19.2	378 (SP1)	25.0	263
3.1-4	1181 (P5)	49.2	2779 (P1)	0.4	1584	430 (SP5)	n/a	883 (SP1)	17.4	609
3.1-5	496 (P6)	65.5	726 (P2)	21.2	600	192 (SP5)	19.7	411 (SP1)	25.3	294
3.1-13	635 (P9)	71.6	888 (P1)	31.1	718	215 (SP5)	18.8	431 (SP1)	24.5	319
3.1-7	390 (P5)	81.9	530 (P1)	7.9	430	154 (SP5)	21.5	309 (SP1)	29.0	224
3.1-8	300 (P2)	15.4	430 (P10)	71.5	374	140 (SP5)	21.8	342 (SP1)	29.2	215
3.1-9	429 (P5)	75.8	674 (P3)	51.6	485	146 (SP5)	20.9	338 (SP1)	29.3	226
3.1-10	277 (P2)	16.5	347 (P7)	96.8	321	121 (SP5)	22.6	264 (SP1)	34.5	178
3.1-14	561 (P5)	71.5	756 (P3)	55.1	642	186 (SP5)	18.8	378 (SP1)	27.4	267
3.1-11	270 (P5)	91.7	349 (P7)	90.3	315	110 (SP5)	23.6	230 (SP1)	34.2	163
3.1-18	1234 (P5)	51.5	2705 (P1)	0.5	1765	427 (SP5)	—	1034 (SP1)	17.9	718
3.1-16	582 (P1)	51.6	756 (P2)	41.9	662	254 (SP5)	17.7	481 (SP1)	29.0	335



$P_{min}$  is the minimum recorded peak pressure in mbar

$P_{max}$  is the maximum recorded peak pressure in ms

$T$  is the pressure pulse duration in ms

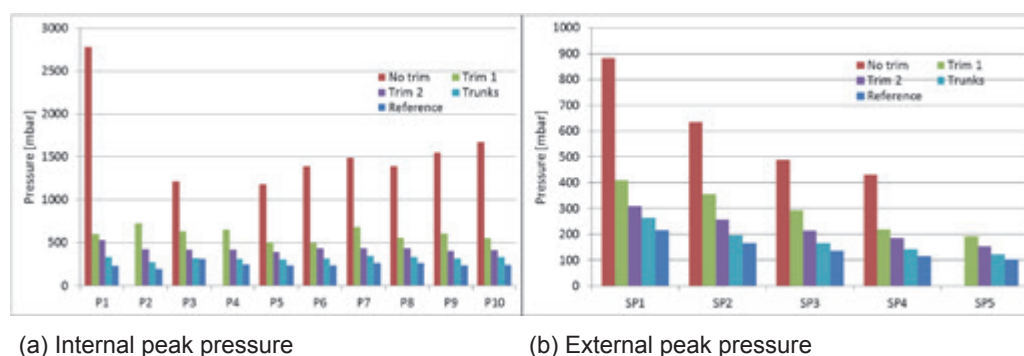
$Av$  is the average peak pressure of all transducers either inside or outside the rig in mbar

### Repeatability

The repeatability of the tests was found to be satisfactory with peak explosion pressures, both inside and outside the test rig, being within approximately 5% of each other for tests performed under similar or identical conditions (e.g. tests 3.1-7, 3.1-8 and 3.1-9). This is especially the case for the pressure results measured outside the rig and in the inner half of the rig. High frequency content in the pressure signals measured inside the rig near the vent opening gave slightly “spikey” pressure curves with peak values in the range of 10% of each other for similar test conditions. Variability of around 5-10% for peak pressure values is deemed satisfactory due to the random nature of the vegetation used for congestion.

### Effect of systematic “thinning” of vegetation

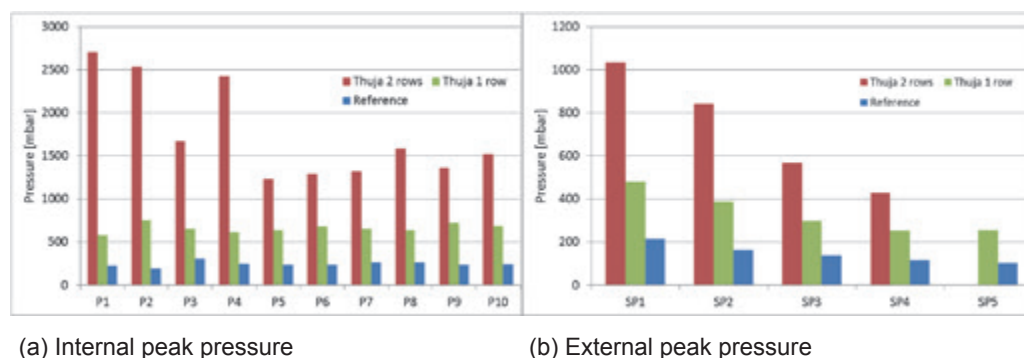
A series of birch tree tests was performed in which the trees were systematically thinned by trimming branches of certain diameter. The stages of thinning were described in Table 5.2. A comparison of the effect of this thinning is shown in Figure 5.6. Using the “as cut” trees (no trim), the overpressure reached approximately 1.5 bar inside the rig (approx. 6 times the reference test with no obstacles). Short duration peaks in excess of 2.5 bar were obtained near the vent. Trim 1 (which removed branches <2-3 mm and the majority of leaves) reduced the pressure from 1.5 bar to around 0.6 bar inside the rig (2-3 times the reference test). Vegetation thinning from the trim 1 to trim 2 (twigs and branches 4-8 mm removed) produced approximately double the pressure in the reference test. The “trunks” test increased the overpressures by about 30-40% compared to the reference test.



**Figure 5.6** Effect of systematically reducing vegetation density

### Thuja hedges

The significant effect on overpressure of doubling the width of the Thuja hedge from one to two rows is illustrated in Figure 5.7. A double row hedge causes an increase of 5-12 times in internal pressure magnitude relative to the reference test whereas the single row hedge causes an increase of 2-4 times.

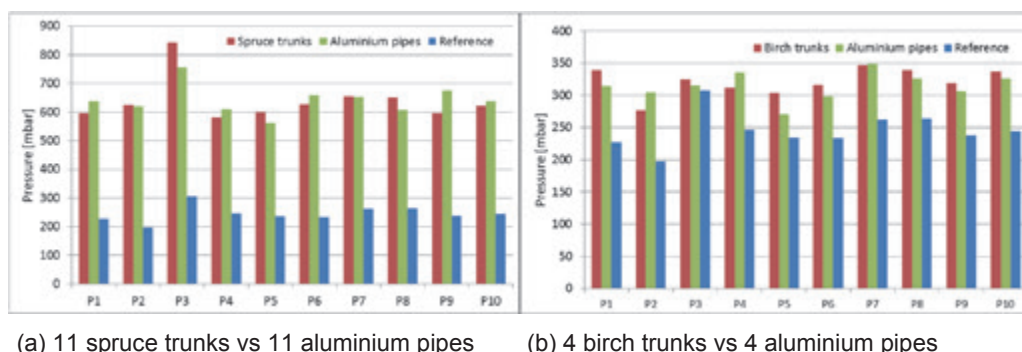


**Figure 5.7** Effect of doubling the width of a Thuja hedge

### Effect of surface roughness of trunks

Comparative tests using tree trunks and smooth pipes were performed to assess the effect of the surface roughness of the tree trunks on the explosion. One test with 11 spruce trunks and one with 4 birch trunks were performed. Corresponding tests with the same numbers of smooth aluminium pipes (of comparable size and giving similar blockage properties) were also performed. Considering the repeatability of the tests, similar numbers of pipes and trunks

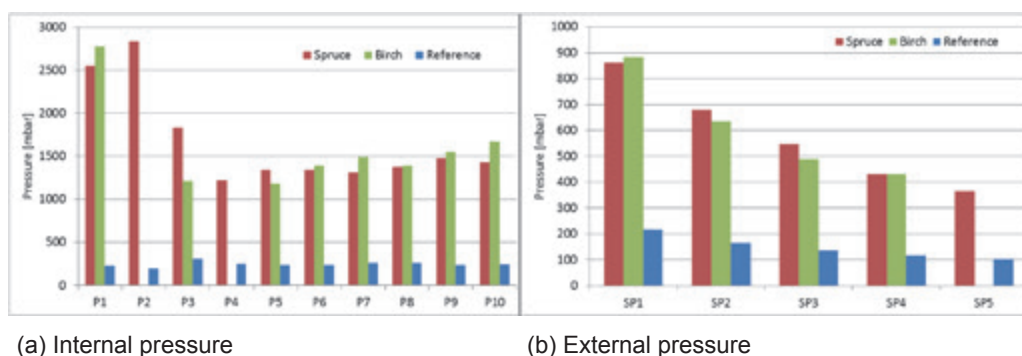
yielded virtually identical results (see Figure 5.8 for the internal pressures); this implies that the effect of surface roughness is secondary.



**Figure 5.8 Effect of surface roughness**

### Effect of varying vegetation type

Comparative tests using 4 spruce and 4 birch trees were also performed. The maximum internal pressures obtained in these tests are shown in Figure 5.9. The tests showed that there was little influence of tree type providing the number and position of the trees is the same. Although the volume blockage ratio of the birch trees was smaller than that of the spruce trees, area blockage is thought to be comparable for the two tree types. However, the area blockage offered by the different types of vegetation could not be measured.



**Figure 5.9 Effect of vegetation type on overpressure generation**

## 5.4 Description of the Large Scale Test Programme

The detonation tests were performed by DNV GL. The full report on this test programme is reproduced in Volume 2<sup>10</sup> to this report.

### 5.4.1 Test facility and procedures

The facility consisted of two 100 m long parallel concrete tracks, each 1.0 m wide for supporting a steel angle frame constructed of 50 × 50 × 6 mm steel angles spanning between the concrete tracks (of dimensions as required for each experiment). The two concrete tracks were cast 4.5 m apart (between the centreline of each track) and the area between the tracks was covered in pea-gravel. The tracks terminate with a 30 m × 10 m concrete slab. Figure 5.10 shows the experimental set up; the concrete slab is visible (closest to the camera) and one of the tracks and steel angle frame can also be seen.



**Figure 5.10 Test set-up (Test 3.2-1)**

To support the trees within the vapour cloud, two methods were used. In Test 3.2-1, a set of 300 8" pipes, 1 m long were installed in the ground to provide holes into which to insert the Norway spruce trees. After this test, it was decided that a much higher density of trees would be required within the vapour cloud and a set of 3 mm steel fencing wire grid was installed at 1 m (or 0.5 m) spacing at a height of 1.0 m from the ground.

A gas injection, recirculation and sampling system, instrument and control cabling and recording equipment and control cabin also formed part of the test set-up for this work. The gas recirculation system comprised 600 mm diameter flap valves, a fan and polythene tubing (visible on the left side in Figure 5.10). To contain the gas mixture within the test rig, a 500 micron polythene sheet of a suitable size was pulled over the steel angle framework prior to each experiment. To avoid any potential effects of confinement due to the polythene sheet, a low energy detonating cord was installed along the outside of the polythene at a height nominally between 1.0 m and 1.5 m from ground level. This cord was detonated immediately prior to the ignition of the gas so as to release the polythene sheet without disturbing the vapour cloud. All tests were performed with a nominally stoichiometric mix of propane/air mixture and the ignition point was located within the row of trees, 1 m from the end, on the longitudinal centreline just above ground level.



Operational checks of all instrumentation and control equipment were performed followed by sealing of the enclosure. The enclosure was then filled with a homogenous propane/air mixture at the required concentration by remote operation of the gas fill valves, recirculation flap valves and fan. Prior to initiation of the spark generator, the recirculation system was isolated from the test rig and purged with air.

#### **5.4.2 Instrumentation and measurements**

##### **Gas analysis**

Samples were drawn from four sample positions in the test rig. Real-time gas concentration measurements were made using infra-red gas analysers calibrated prior to each test using a “zero gas” (nitrogen) and a certified calibration gas (4.2% v/v propane in nitrogen). The operation of the sampling system was checked prior to each test by attaching a sample bag containing the calibration gas to the end of each sample line.

##### **Overpressures**

High frequency response piezo-electric pressure transducers were used to measure the pressures generated by the explosions. Measurements of overpressure made at floor level were performed by mounting the transducer within nylon mounts fixed into metal boxes. The measuring face of the transducer was positioned so that it was level with the face of the mount that was 75 mm in diameter and protruded 5 mm above the metal box. Where possible, these metal boxes were installed so that their top face was flush with the pea-gravel floor of the test rig.

Free-field pressures were measured on the major axis of the rig at a height of 1.5 m above ground, oriented so that the sensing face of the transducer was parallel to the expected direction of travel of the blast wave.

##### **Flame position**

Flame arrival time was measured using an array of ionisation probes located at positions within the vapour cloud.

##### **Video records**

Video footage from each test was recorded using both high speed and normal speed digital video cameras.

#### **5.4.3 Test programme**

The test programme consisted of 8 vapour cloud explosions all conducted using nominally stoichiometric propane air mixtures. In all cases, the ignition of the vapour cloud was by a spark generator. Congestion in the form of trees was installed into the test rig according to pre-agreed layouts and density. The tests are summarised in Table 5.5 and involved changes to the density of trees and width of the congested region formed by the trees. In all cases, the height of the cloud/trees was 3 m.

**Table 5.5 Summary of test programme**

Test	Cloud Dimensions (L × W × H m)	Congested Region Dimensions (L × W × H m)	Congestion Types	Congestion Density
3.2-1	120 × 4.5 × 3	100 × 4.5 × 3	Norway spruce	0.33 trees/m <sup>2</sup> (new trees)
3.2-2	51 × 4.5 × 3	27 × 4.5 × 3	Alders	3 trees/m <sup>2</sup> (new trees)
			Norway spruce trunks	2 trunks/m <sup>2</sup> in central 3 m of alder congestion
			Alders	2 trees/m <sup>2</sup> (reused from Test 3.2-2)
3.2-3	51 × 4.5 × 3	30 × 4.5 × 3	8" Diameter fence posts	15 along the centreline, spaced 2 m apart
3.2-4	51 × 4.5 × 3	30 × 4.5 × 3	Alders	1.5 trees/m <sup>2</sup> (new trees)
3.2-5	51 × 4.5 × 3	20 × 1 × 3	Alders	3 trees/m <sup>2</sup> (new trees)
		25 × 2 × 3		
3.2-6	51 × 4.5 × 3	45 × 3 × 3	Alders	3 trees/m <sup>2</sup> (trees from Test 3.2-5 plus additional trees to increase width of congested region)
3.2-7	51 × 4.5 × 3	45 × 3 × 3	Alders	3 trees/m <sup>2</sup> (repeat of Test 3.2-6)
3.2-8	51 × 4.5 × 3	45 × 2 × 3	Alders and silver birch	6.5 trees/m <sup>2</sup> (trees from Test 3.2-7 plus additional trees to increase density)

#### 5.4.4 Congestion

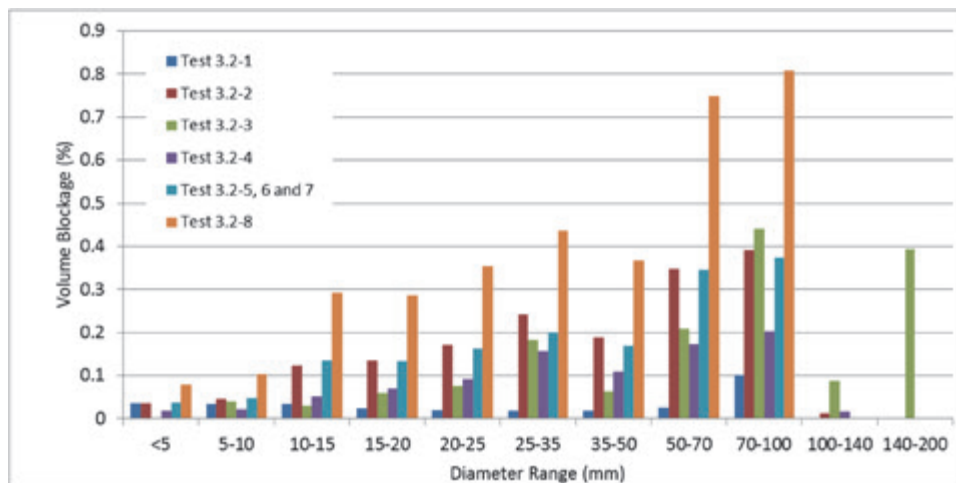
Congestion density was set on a nominal number of trees/m<sup>2</sup>. In order to assess the level of congestion provided by the trees used in each experiment, a set of characterisation analyses were performed. However, as might be expected, there was some variability in the shape and number of branches from one tree to another. Therefore, whilst the analyses began by sampling a small number of trees, the difficulties associated with the interpretation of the results meant that a greater number of trees were analysed in the subsequent tests. The characterisation method used in each test is summarised in Table 5.6.

As the characterisation work proceeded, it became apparent that the limited nature of the characterisation of Test 3.2-2 (Table 5.6) misrepresented the volume blockage for this test. The figures for Test 3.2-2 have therefore been re-calculated from a weighted average of the data obtained from the characterisation of Test 3.2-4 and 3.2-5 where a total of 33 alder trees were fully characterised. Figure 5.11 shows a comparison of all the volume blockage distributions calculated for the test programme based on the characterisations described above (as corrected for Test 3.2-2). Whilst volume blockage on its own is not a suitable means of characterising congestion, a distribution of volume blockage by diameter range allows other congestion characterisation parameters, such as area blockage per metre, to be calculated. This is also shown in Table 5.6. For the purposes of this calculation, tree trunks are in a vertical orientation whilst most branches are angled upwards at an angle of about 45° (from examination of the pictures of the trees). The branches can then be angled in any horizontal orientation. Assuming an even distribution, the projected area of the branches is reduced by a factor of 0.859. The two figures for area blockage are shown in Table 5.6 denoted as “full” and “projected” where the latter allows for the horizontal distribution of the branches.

**Table 5.6 Tree characterisation for each test**

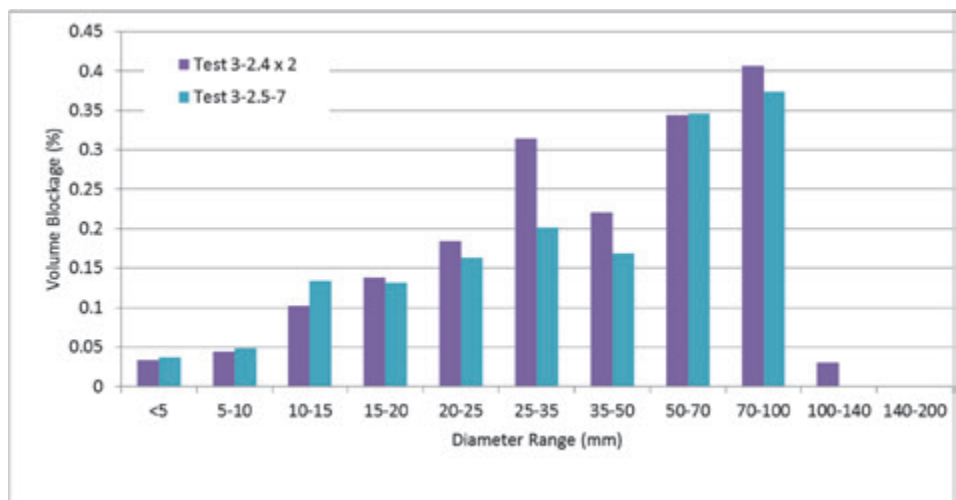
Test	Method	Volume blockage %	Area blockage (m <sup>2</sup> /m <sup>3</sup> )	
			Full	Projected
3.2-1	Two trees were analysed for volume blockage. Every branch was dipped into a water displacement vessel. The diameter at the butt, the length of the branch and its water displacement were recorded. Five branches were cut into their constituent parts and measured to give a distribution of constituent part diameter versus volume for the branch. An ideal tree was thus modelled to provide volume blockage determined by its displacement.	0.308	0.332	0.285
3.2-2	A single tree from the batch was separated into the trunk and branches. Nine of the branches were cut into their constituent parts and each part measured for diameter and length. A model was then devised to estimate the volume blockage of each branch based on the diameter at the trunk and the length. The total volume blockage for the tree was estimated using this model and extrapolated to estimate the volume blockage distribution within the test rig based on the number of trees/m <sup>2</sup> of the rig and the average diameter of the Norway spruce trunks added.	2.536	1.032	0.888
3.2-3	Test 3.2-3 made use of the existing trees already installed in the test rig during Test 3.2-2. Prior to the conduct of Test 3.2-3, the results from the Test 3.2-2 analysis was used to estimate the volume blockage in this reduced congestion test. Fifteen 8" diameter posts were also added to the congestion. Post-test, two 1 m wide strips of trees were removed from the test rig and analysed by cutting into their constituent parts and measuring diameter and length. The resulting volume blockage distribution was found to be lower in the lower diameter range than that initially estimated for Test 3.2-3 based on the Test 3.2-2 analysis.	1.580	0.429	0.373
3.2-4	This test was conducted using a new batch of trees. Two trees were fully characterised (all constituent parts measured for diameter and length). Given that the experiment resulted in a detonation of the vapour cloud, a further twelve trees were removed from the least damaged portion of the test rig and fully characterised.	0.909	0.446	0.384
3.2-5	This test was conducted using a new batch of trees. Twenty-one trees were fully characterised from the batch (all constituent parts measured for diameter and length).	1.603	0.860	0.740
3.2-6	No further characterisation was conducted. Some alder trees were added to the trees already in the rig from Test 3.2-5 to change the width of the congested region from 1 or 2 m to 3 m.	1.603	0.860	0.740
3.2-7	This was a direct repeat of Test 3.2-6, so no additional characterisation was performed.	1.603	0.860	0.740
3.2-8	The trees from Test 3.2-7 were condensed into a 2 m wide congested region. A further one hundred and forty alder trees and forty silver birch were added. A set of ten silver birch trees were fully characterised and gave a similar volume blockage to the alder when installed to a cutting plan which involved removing some of the trunk if greater than 70 mm in diameter and taller than 4 m.	3.474	1.863	1.602





**Figure 5.11 Comparison of congestion volume blockage for all tests**

The variable nature of trees means that some uncertainty in the characterisation remains. This is illustrated by comparing the volume blockage distribution of Test 3.2-4 (1.5 trees/m<sup>2</sup>) with that for Tests 3.2-5 – 3.2-7 (3.0 trees/m<sup>2</sup>). The comparison is shown in Figure 5.12 and is made by doubling the figures for Test 3.2-4 to make the number of trees/m<sup>2</sup> the same. It can be seen that whilst there is close agreement in some diameter ranges there are discrepancies, particularly in the 25-35 mm range. The overall volume blockage for 3 trees/m<sup>2</sup> was 1.82% based a doubling of the Test 3.2-4 characterisation compared to 1.60% based on the Tests 3.2-5 – 3.2-7 characterisation.



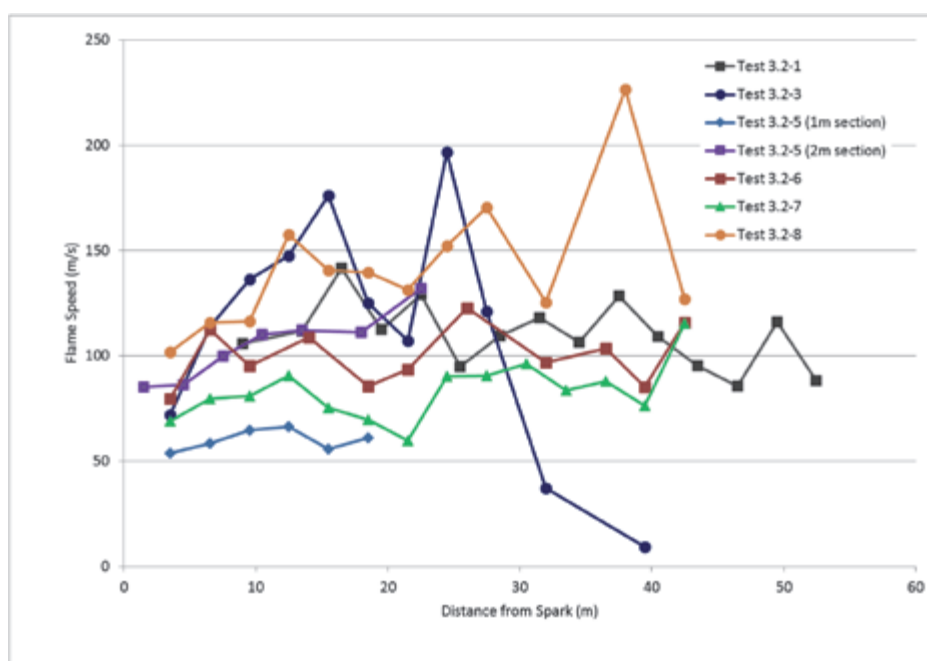
**Figure 5.12 Comparison of 2 × Test 3.2-4 with Tests 3.2-5 - 3.2-7**

#### 5.4.5 Summary of experimental observations

In two out of the eight tests performed, a transition to detonation occurred within a short distance of the ignition point (Test 3.2-2 and Test 3.2-4). Both tests comprised a 4.5 m width of alder trees arranged at densities of 3 trees/m<sup>2</sup> and 1.5 trees/m<sup>2</sup> respectively. Transition to detonation occurred within a short distance from the ignition point (15 – 20 m). The transition to detonation occurred at flame speed in excess of 600 m/s. If a flame entered a region of densely packed trees and bushes already travelling at some speed, then the distance to detonation

will be less (if the mixture is near stoichiometric in concentration). This is supported by earlier tests with open clouds and pipework congestion<sup>13</sup>. These earlier experiments showed that flame acceleration to high flame speeds was possible with propane and cyclohexane-air mixtures and that once flame speeds of 200-300 ms<sup>-1</sup> had been achieved, continued flame acceleration could lead to DDT within a distance of a few metres, typically at flame speeds in excess of 600 ms<sup>-1</sup>.

In all other tests, the maximum flame speed remained much lower, ranging from 60 m/s (for 1 m width of trees in Test 3.2-5) to 200 m/s (for 4.5 m width of trees in Test 3.2-3) and was reached within a short distance from the ignition point (< 20 m). The flame speed profile in all 6 tests that did not detonate is shown in Figure 5.13. For Test 3.2-1, the flame speed is shown for the first 52 m; speed generally declined beyond this. For Test 3.2-5, the speed is plotted in 2 sections for the 1 m width and the 2 m width with the distance for the latter measured from the point at which the width increases from 1 m to 2 m rather than from the ignition point. A summary of the maximum flame speeds from all the tests is given in Table 5.7.



**Figure 5.13 Flame speed in the 6 tests which did not detonate**

It is notable that the maximum flame speed in Test 3.2-1 was around 140 m/s even though this test had volume and area blockage ratios of no more than 20% and 40% respectively of Tests 3.2-5 – 7. This is most likely attributable to the presence of foliage in the form of “needles” of the Norway spruce trees. However, the area blockage contribution of the needles has not been included in the calculation and would be extremely difficult to quantify. Its contribution to turbulence generation would depend on the density of needles present and the interaction of those needles with the blast wind.

**Table 5.7 Maximum flame speed and distance to reach maximum speed**

Test	Max flame speed (m/s)	Approximate distance to max speed (m)
3.2-1	140	16
3.2-2	1800	15
3.2-3	150 - 200	17 - 24
3.2-4	1800	20
3.2-5	60	15
	110	12 <sup>§</sup>
3.2-6	100	10
3.2-7	80	12
3.2-8	150	15

§ measured from the point where the width is increased from 1 m to 2 m

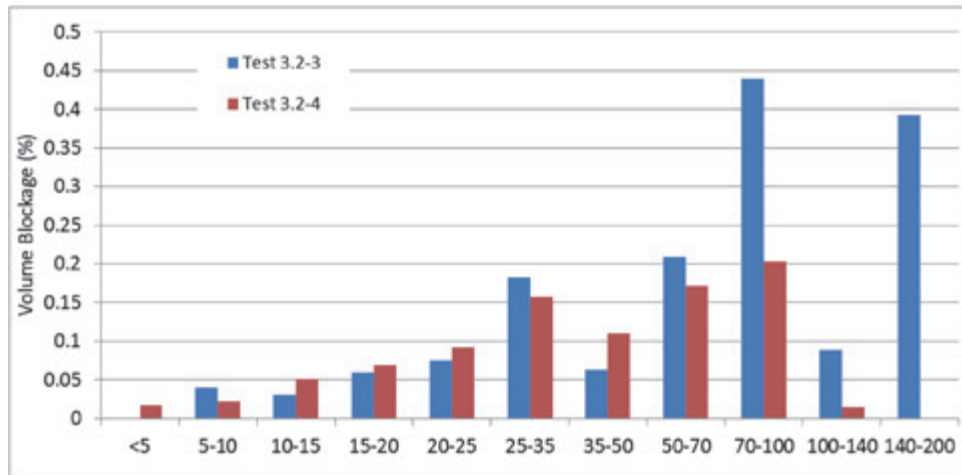
The results of Test 3.2-3 and Test 3.2-4 is surprising relative to one another. The two tests had identical geometry, but Test 3.2-3 had nominally more congestion than Test 3.2-4 as shown in Table 5.8 and a higher overall volume blockage ratio (1.508 vs 0.909). Yet a transition to detonation occurred in Test 3.2-4 and flame speed remained within around 200 m/s in Test 3.2-3.

**Table 5.8 Comparison of Test 3.2-3 and 3.2-4 configurations**

Test	Cloud Dimensions (L × W × H m)	Congested Region Dimensions (L × W × H m)	Congestion Types	Congestion Density
3.2-3	51 × 4.5 × 3	30 × 4.5 × 3	Alders 8" Diameter fence posts	2 trees/m <sup>2</sup> (reused from Test 3.2-2) 15 along the centreline, spaced 2 m apart
3.2-4	51 × 4.5 × 3	30 × 4.5 × 3	Alders	1.5 trees/m <sup>2</sup> (new trees)

The trees used in Test 3.2-3 had already been in a detonation and many of the smaller branches had been broken in the detonation. New trees were used in Test 3.2-4 and these also had some leaves. The trees were installed in a checkerboard fashion with alternately one tree then two trees being installed per square metre. A comparison of the characterised congestion for these two tests is shown in Figure 5.14. Whilst Test 3.2-3 has significantly more large diameter congestion, Test 3.2-4 is more congested in the sub 25 mm categories. Whilst no direct comparison exists with the medium scale tests, it is worth noting that the trimming of the smallest diameter branches (2-3 mm and most leaves) in those tests led to a very significant reduction in overpressures (see Figure 5.6). It is not known whether the checkerboard layout of trees in Test 3.2-4 resulted in the increased flame speeds. If so, this would have implications for naturally growing tree lines which are likely to be uneven.

It is also clear that the limiting flame speed can be quite sensitive to the precise conditions.



**Figure 5.14 Comparison of congestion in Tests 3.2-3 and 3.2-4 (note that the 5-10 mm band for Test 3.2-3 also included all twigs <5mm)**

In Test 3.2-7, (which was a repeat of Test 3.2-6), the maximum flame speed was 80 m/s compared with a maximum speed of 100 m/s in Test 3.2-6. The foliage on the new trees in Test 3.2-6 was burnt off and some of the branches were charred. Again, the results suggest that the experiments are relatively sensitive to small changes in experimental conditions. Flame speeds in the 2 m section of Test 3.2-5 were similar if not slightly greater than in Test 3.2-6. The trees in Test 3.2-5 also had foliage on them and the presence of foliage seems to consistently result in higher flame speeds. This may be attributable to the contribution which foliage makes to area blockage. However the limited results, large number of variables and the fact that area blockage could not be measured means that it is difficult to be conclusive on this point.

In Test 3.2-8, very high density of trees was used to investigate whether a transition to detonation can occur in 2 m width of vegetation. The density used was arguably greater than what might occur naturally. Using 6.5 trees/m<sup>2</sup> gave a volume blockage of 3.5%, more than twice that in any other test. Maximum flame speed remained at around 150 m/s.

It could be argued that, with increasing congestion, a level of congestion could be reached that is so great as to resist forward expansion, potentially reducing flame acceleration. The fact that the flame speeds in Test 3.2-8 were greater than those in the 2 m width section in Test 3.2-5, suggests that this point of reducing flame acceleration has not been achieved, though this is not definitive. Significantly higher volume blockages have been used in other explosion studies, with the effect of increasing flame speeds; however, these experiments were generally not in high aspect ratio configurations.

## 6 CHARACTERISTICS OF LARGE FLAT VAPOUR CLOUD DETONATIONS

### 6.1 Objectives

The objectives of the vapour cloud detonation work are:

- a) To study at a realistic scale the characteristics of detonating shallow vapour clouds and their effect on objects both within and outside the cloud.
- b) To characterise the overpressure field (within and outside the cloud) from a detonating shallow vapour cloud as a function of cloud geometry.
- c) To improve the understanding of forensic evidence left after an incident involving a vapour cloud explosion.

The work is a combination of analytical studies of a range of vapour cloud geometries and ignition locations, and large scale tests with varying cloud aspect ratios as well as tests on clouds of diminishing height.

### 6.2 Key Findings

1. Explosions involving large shallow unconfined vapour clouds can cause very high overpressures.
2. Small variations in fuel concentration from stoichiometric were found to have little effect on the detonation overpressures within the cloud and blast pressure outside the cloud. Rich mixes were found to result in an increase in impulse of the blast wave due to after-burning.
3. The location of ignition point within the cloud was also found to have little effect on the overpressures outside the cloud. The impulse on the side nearer the ignition point was found to increase.
4. The overpressure outside the cloud diminishes rapidly with distance from the edge of the cloud.
5. Very good correlation has been found between maximum overpressure outside the cloud and the ratio of cloud height to distance from the edge of the cloud. Based on this, the following simple expression has been derived which enables the maximum overpressure to be estimated and is applicable to clouds with a radius  $\geq 50$  m:

$$P = 6.571 \times \left(\frac{H}{\Delta R}\right)^{0.975} \text{ where } P \text{ is the overpressure (bar) at distance } \Delta R \text{ (m) from the edge of a pancake shaped cloud of height } H \text{ (m).}$$

6. For smaller clouds (<50 m radius), either the Multi-Energy Method or TNT Equivalence can be used.
7. The approach based on (5) and (6) above appears robust within the limitations of the tests and simulations performed.
8. The above method, used in conjunction with the VCA method, can be used to estimate overpressure at a given location for a given overspill scenario.

9. A detonation can propagate through relatively thin ( $< 200$  mm) detonable layers and paths in a large propane/air vapour cloud. Hence, once detonation is initiated, the remainder of such a cloud will most likely detonate.
10. Overpressures in excess of 3 bar were found to cause significant damage to cars. Only minor damage occurred when the pressure was  $\leq 1$  bar.
11. A 20 ft ISO container sustained minor creasing to its wall facing the detonation when subjected to an overpressure of 420 mbar. The container sustained significant damage to its wall and roof when the pressure was increased to 2 bar in a subsequent test by moving the container closer to the vapour cloud. At this load level the container was also shifted along the ground by around 3 m by the explosion.
12. Oil drums were found to sustain damage at an overpressure level  $> 2$  bar and the damage was pronounced at 3 bar. Instrument boxes sustained very little damage at overpressures  $< 1$  bar; significant distortion to the front and sides occurred at an overpressure of 3 bar.

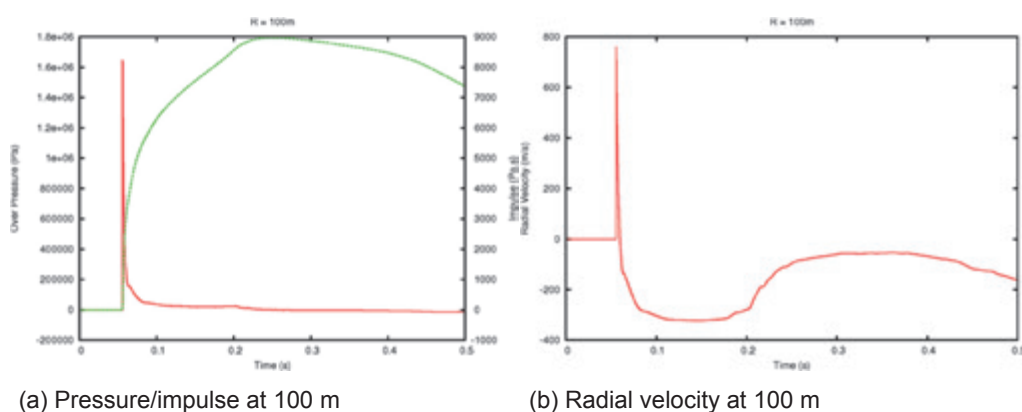
## 6.3 Analytical Study

Analytical simulations of the detonation of propane/air gas clouds were performed using the EDEN Hydrocode<sup>14</sup>. A range of scenarios were analysed in 2D and 3D to study the effect of variations in cloud geometry, stoichiometry and the load and impulse that would act on a range of objects at varying distances from the edge of the cloud. The full report on this work is reproduced in Volume 2<sup>10</sup> to this report.

### 6.3.1 Shallow circular propane/air clouds ignited at their centre

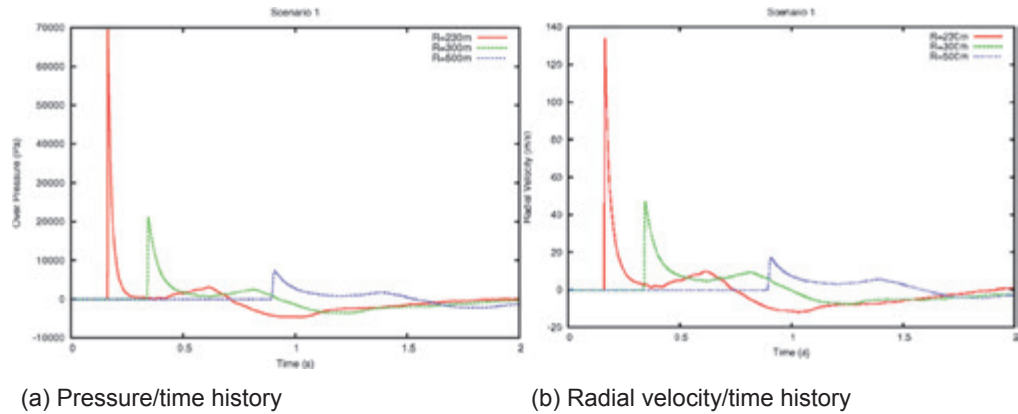
Initial studies were performed to provide a better understanding of the pressure/impulse and radial velocity both within and outside a circular shallow cloud ignited at its centre. Due to the axisymmetry of this geometry, the analyses are performed using 2D models.

Figure 6.1 shows the results for 200 m radius, 3 m deep cloud ignited at its centre (scenario 1). Within the vapour cloud after a short positive velocity the cloud experiences a prolonged negative velocity phase.



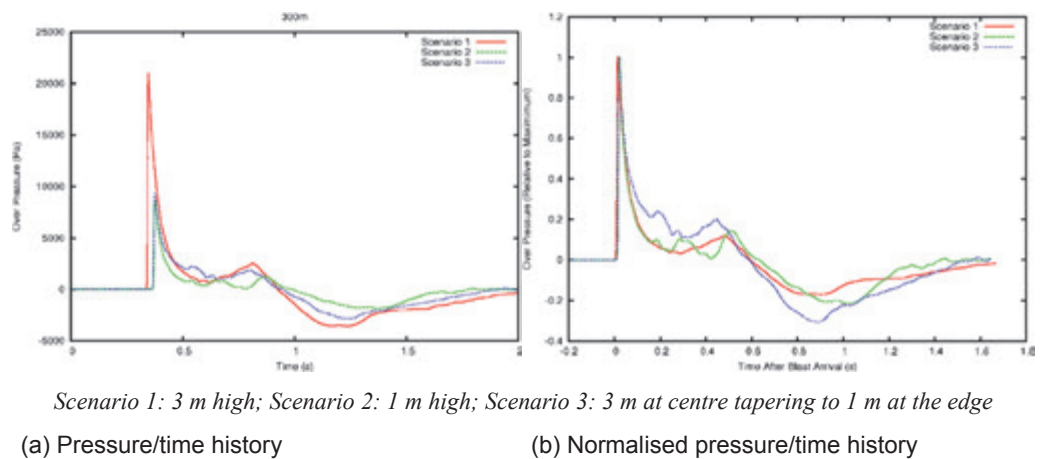
**Figure 6.1** Pressure/impulse and radial velocity at elevation 1.5 m within the cloud

The pressure, impulse and radial velocity were investigated at various distances outside the cloud (30 m, 100 m and 200 m from the cloud edge) to examine how these compare with the features of the detonation within the cloud. Figure 6.2 (a) shows that after a sustained period of positive over-pressure all of the time histories show a negative phase. A detonation of a 200 m radius vapour cloud therefore produces significant periods of negative over-pressure at distances up to 300 m from its edge. The corresponding radial velocity time histories at various distances from the edge of the cloud show in Figure 6.2 (b) the negative radial velocities (flow directed towards the centre of the cloud) coinciding with the period of negative over-pressure.



**Figure 6.2 Detonation characteristics outside the cloud**

The effect of reducing the cloud height from 3 m to 1 m (scenario 2) and of tapering the height from 3 m at the centre to 1 m at the edge (scenario 3) were also investigated for the same cloud radius of 200 m. Resulting pressure/time histories at a distance of 100 m from the edge of the cloud are compared in Figure 6.3 (a). Similar peak pressures were obtained in scenarios 2 and 3 and these were significantly lower than in scenario 1, but both the positive and negative over-pressure phases occur over very similar timescales in all three cases.



**Figure 6.3 Pressure time histories for different geometries of a 200 m radius cloud**

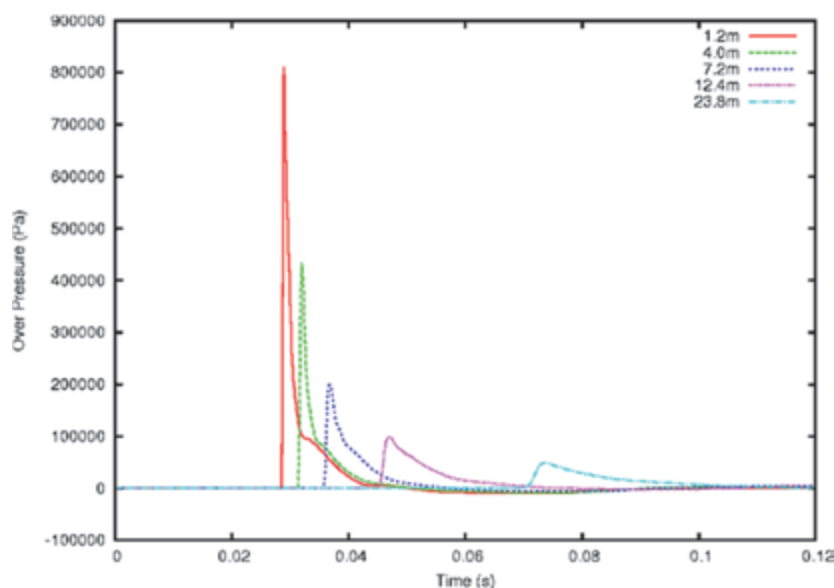
In Figure 6.3(b) each pressure/time profile is normalised using the peak pressure value for that scenario and the profiles are aligned so that blast arrival time is the same for all three scenarios. This shows that in the tapering cloud detonation



there is a more significant positive “tail” and a greater magnitude negative phase than the constant depth clouds. The peak impulse in the three scenarios was found to be directly proportional to the cloud volume.

When the radius of the cloud in scenario 2 was reduced from 200 to 100 m (scenario 4), the corresponding peak pressures outside the cloud reduced and the duration of the negative overpressure phase became much smaller.

A further cloud geometry with a radius of 50 m and height 2 m was also considered. The pressure time history at a range of distances from the cloud edge is shown in Figure 6.4 at an elevation of 1 m (mid-way through the cloud depth). Cloud volume was found to have a direct effect on the magnitude of overpressure at a given distance outside the cloud.



**Figure 6.4 Pressure time history at different distances from the cloud edge**

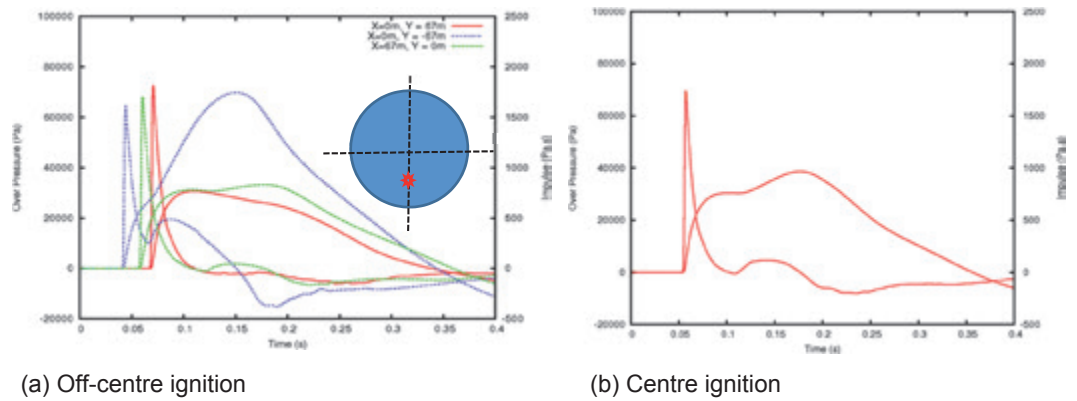
### 6.3.2 Effect of fuel concentration

The effect of fuel stoichiometry was also investigated in the 200 m radius 3 m high cloud. Two cases of a rich propane air mix (6.8% and 5.5% propane by volume) and one lean mix (3.2% propane by volume) were considered. At a distance of 100 m from the edge of the cloud, the peak pressure generated by both rich mixes is the same as for the stoichiometric mix whereas the lean mix results in a peak pressure that is 10% lower. The pressure time histories are otherwise similar in all cases. The additional afterburning in the fuel rich cases, however, resulted in significant increases in the peak impulses.

### 6.3.3 Effect of off-centre ignition

The effect of moving the ignition point away from the centre was investigated by igniting the 50 m radius 2 m high cloud halfway between the centre and the edge of the cloud. The pressure and impulse were monitored at a distance 17 m from the cloud edge (67 m from the centre). The off-centre ignition had little effect on the peak pressure but resulted in a significant increase in impulse on the side of the cloud closest to the ignition point as shown in Figure 6.5(a). The pressure and impulse for a central ignition are shown in Figure 6.5(b) for comparison.



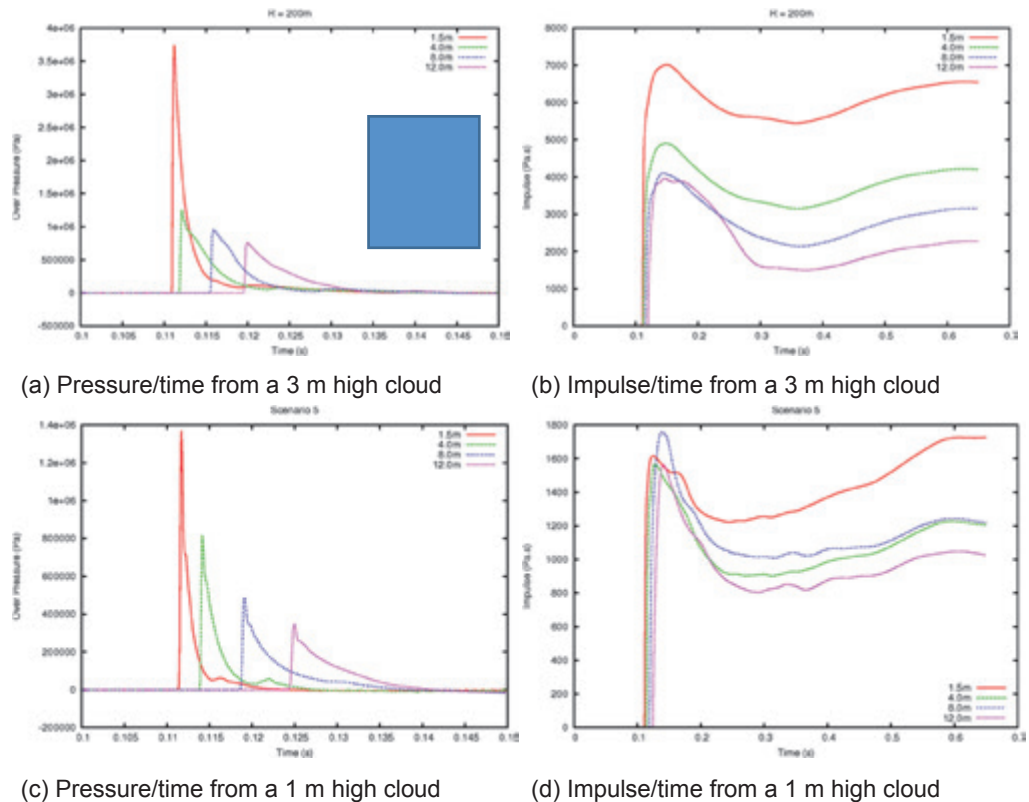


**Figure 6.5 Pressure and impulse (50 radius, 2 m high propane/air cloud)**

### 6.3.4 Loading on rigid objects within and outside the cloud

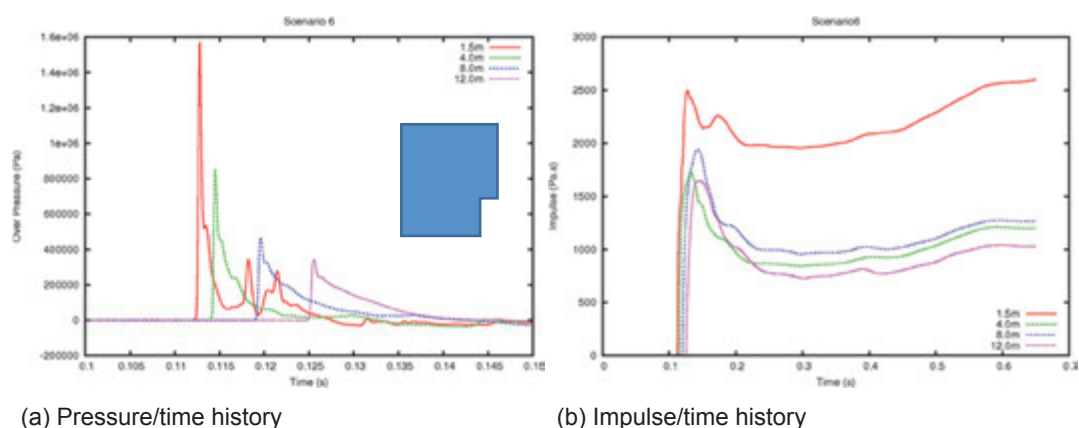
The loading on a range of rigid objects located both within and outside the cloud was studied using both 2 and 3D analysis. A rigid object (13 m high and 13 m deep) was placed at the edge of both the 3 m high and the 1 m high clouds. The pressure and impulse time profiles at different elevations on the face of the object are shown in Figure 6.6. It can be seen that, once at elevations above the cloud, the peak overpressure diminishes rapidly with height.

In the case of the 3 m high cloud, there is not much difference in peak impulse at 8 m and 12 m elevations. For the 1 m high cloud, the peak impulse values are all similar at elevations between 1.5 m and 12 m.



**Figure 6.6 Pressure and impulse time histories for a 1 m high 200 m radius cloud detonation interacting with a rigid 13 m x 13 m rectangular object**

The shape of the rigid object is also important as illustrated in Figure 6.7 where a small cut-out has been introduced at the base of the object to represent a walkway outside a building. The pressure profiles show multiple reflections as a result of this and a rise in the peak pressure at 1.5 m elevation (*i.e.* within the height of the cut-out). The impulse at this elevation is amplified by a factor of 50%. At 12 m elevation, the effect of the cut-out is negligible and the pressure and impulse profiles and magnitudes are the same for the rigid rectangular object.



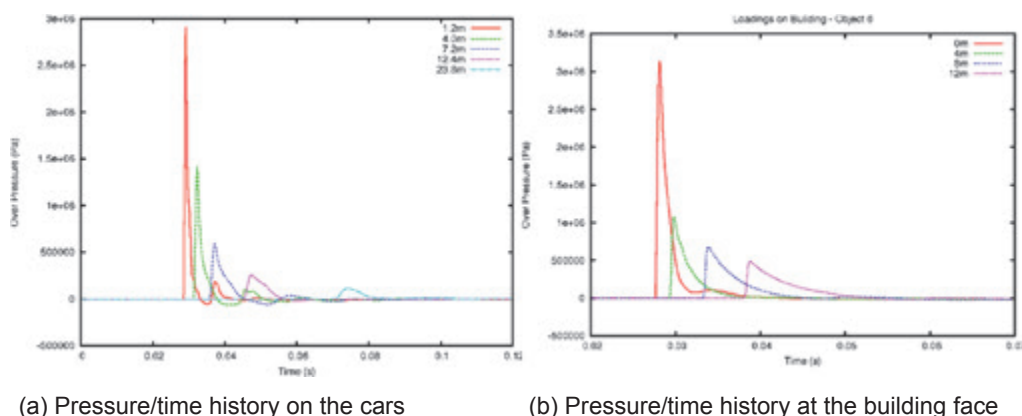
**Figure 6.7 Pressure and impulse time histories for a 1 m high 200 m radius cloud detonation interacting with the rigid shaped object shown**

Further analysis of loading on objects was performed with a stoichiometric propane air cloud of 50 m radius and 2 m height. The objects used are summarised in Table 6.1. Sizes chosen were such that the object sizes were representative of cars, tanks, buildings and large instrument boxes. The objects, all treated as rigid, were placed such that the blast impacts normal to the face of the obstacle in each case. Calculations of reflected loading at 7 cars (5 outside and 2 within the cloud), 2 bulk tanks (1 at the cloud edge and 1 within the cloud), 1 building at the cloud edge and 2 boxes within the cloud were performed.

**Table 6.1 Objects used in the 3D analysis**

	Object and location details						
	Car (4.4 × 1.8 × 1.6 m)						
Object Number	1	2	3	4	5	9	10
Distance from cloud edge (m)	1.2	4.0	7.2	12.4	23.8	CC	CE
Free field peak pressure at location (bar)	8	4	2	1.0	0.5		
	Building (13 × 13 × 13 m)						
Object Number	6						
Distance from cloud edge (m)	0.0						
	Bulk tank (5 m radius × 8 m high)						
Object Number	7	8					
Distance from cloud edge (m)	CC	0.0					
	Box (1 × 1 × 1 m)						
Object Number	11	12					
Distance from cloud edge (m)	CC	CE					
CC – object within cloud close to the centre CE – object within cloud close to the edge							

The reflected pressure/time histories at the 5 “cars” outside the cloud and at different heights on the elevation of the building are shown in Figure 6.8 (a) and (b) respectively.



**Figure 6.8 Reflected pressure/time history (50 radius, 2 m high propane/air cloud)**

The reflected peak pressure at the face of each of the two boxes was similar. However, the peak impulse at the face of the box close to the centre of the cloud was found to be double that at the edge of the cloud.

## 6.4 Description of the Large Scale Detonation Test Programme

The detonation tests were performed by DNV GL. The full report is reproduced in Volume 2<sup>10</sup> to this report.

### 6.4.1 Test facility and procedure

The test facility comprised a 30 m × 10 m concrete slab with a central instrument duct, a steel framed polythene sheeted test enclosure to contain the gas mixture and a gas recirculation system comprising 600 mm diameter flap valves, a fan and polythene tubing (Figure 6.9). The test enclosure was specifically modified for each test to suit the test geometry. Operational checks of all instrumentation and control equipment are performed followed by installation of the explosive initiation charge and sealing of the enclosure. The enclosure is then filled with a homogenous propane/air mixture at the required concentration by remote operation of the gas fill valves, recirculation flap valves and fan. Prior to initiation of the explosive charge, the recirculation system was isolated from the test rig and purged with air.

To commence the test, a sequence timer is initiated, triggering the high speed cameras, data acquisition systems and the small (200 g) high explosive charge used to initiate the detonation of the gas cloud.



(a) External view of test enclosure

(b) Gas re-circulation loop

**Figure 6.9 Detonation enclosure and gas filling system**

## 6.4.2 Instrumentation and measurement

### Gas analysis

Samples were drawn from four sample positions in the test rig. Real-time gas concentration measurements were made using infra-red gas analysers calibrated prior to each test using a “zero gas” (nitrogen) and a certified calibration gas (4.2% v/v propane in nitrogen). The operation of the sampling system was checked prior to each test by attaching a sample bag containing the calibration gas to the end of each sample line.

### Overpressures

High frequency response piezo-electric pressure transducers were used to measure the pressures generated by the explosions. Free-field pressures were measured at a height of 1.5 m above ground, oriented so that the sensing face of the transducer was parallel to the expected direction of travel of the blast wave. Pressure measurements were made inside the cloud, along both major and minor axes of the test enclosure and at 45° to the main axes.

### Flame position

Flame arrival time was measured using an array of ionisation probes located at positions within the vapour cloud.

### Video records

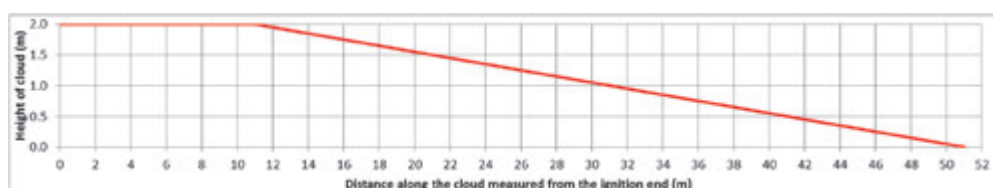
Video footage from each test was recorded using both high speed and normal speed digital video cameras.

## 6.4.3 Test Programme

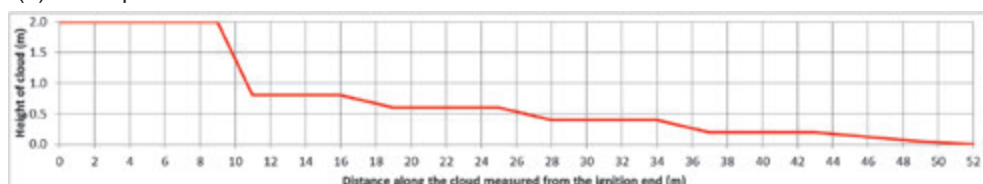
The programme consisted of 6 tests summarised in Table 6.2, all conducted using nominally stoichiometric propane/air mixtures. Detonation of the vapour cloud was initiated using a small explosive charge in all 6 tests.

**Table 6.2 Summary of large scale detonation tests**

Test	Geometry (m)			Purpose
	Length	Width	Height	
4.2-1	30	10	3	To study the effect of a gas cloud detonation on objects within the cloud and to provide information on the decay of pressure with distance from the cloud.
4.2-2	30	10	4	To study the effects of the aspect ratio of the vapour cloud on the pressure field generated away from the cloud and the effect on objects of interest placed outside of the vapour cloud.
4.2-3	30	4	4	
4.2-4	30	10	2	
4.2-5	51	4.5	See	To study the effects of the height above ground of the vapour cloud on detonation propagation and the external pressure field.
4.2-6	52	4.5	Figure 6.10 for cloud height	



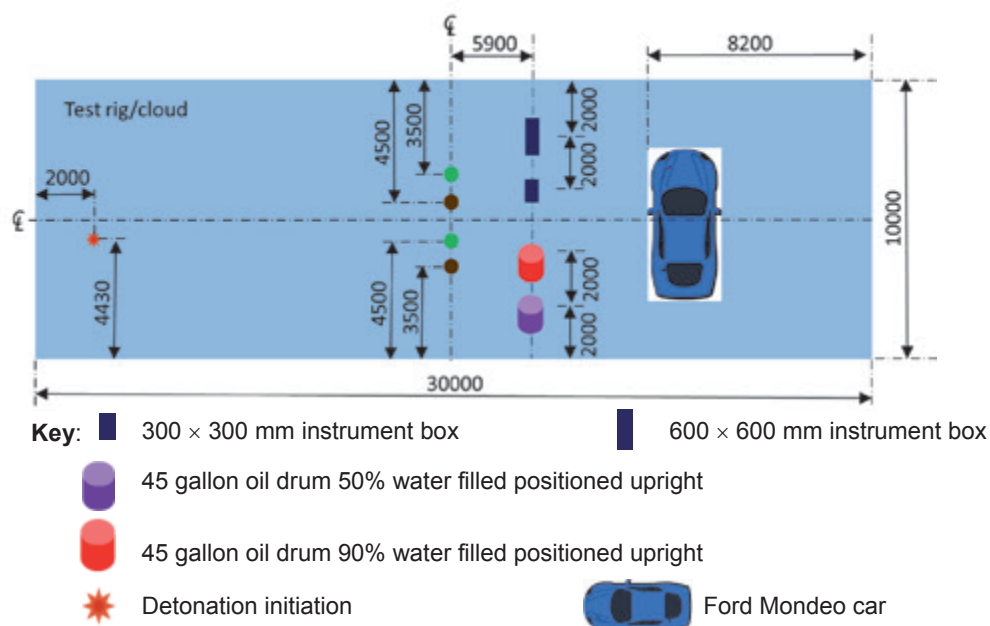
(a) Cloud profile for test 4.2-5



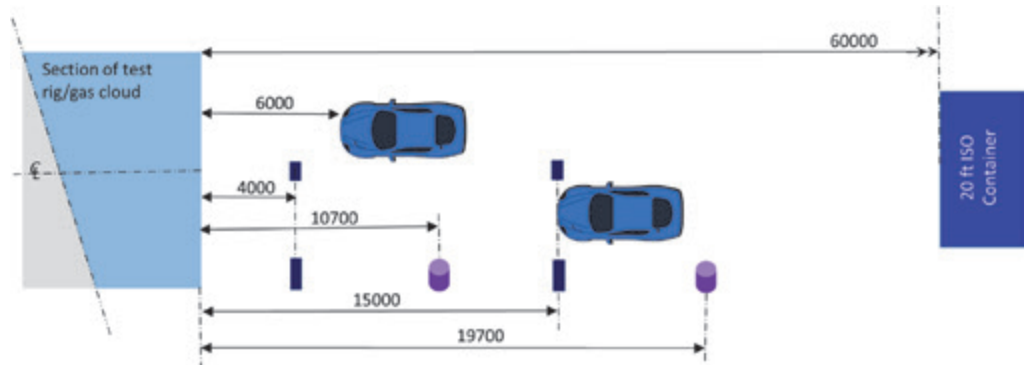
(b) Cloud profile for test 4.2-6

**Figure 6.10 Cloud profiles for tapered detonation tests (4.2-5 and 4.2-6)**

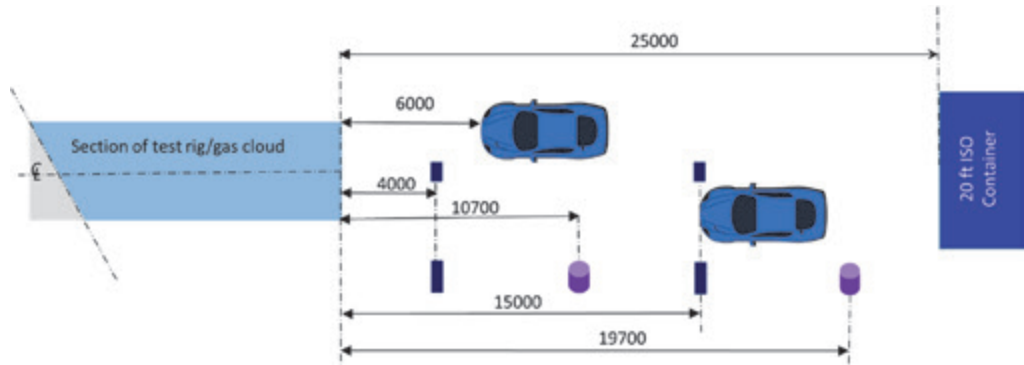
The layout of obstacles in Test 4.2-1 is shown in Figure 6.11 and in tests 4.2-2 – 4.2-5 in Figure 6.12. No obstacles were used in test 4.2-6.



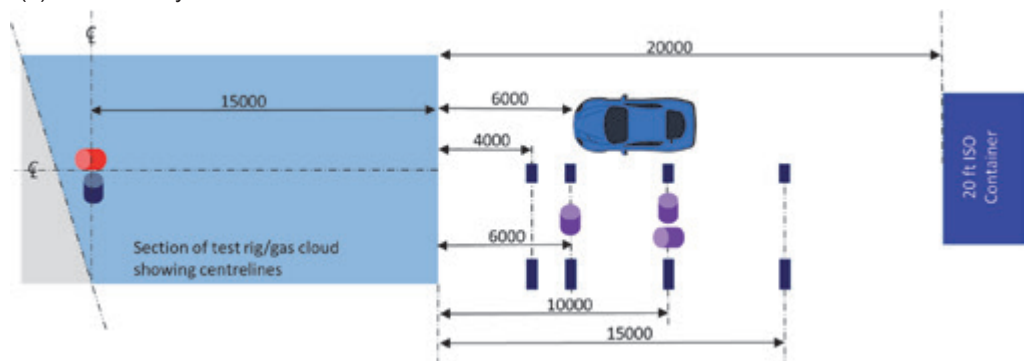
**Figure 6.11 Obstacle locations**



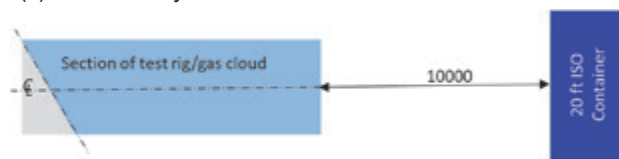
(a) Obstacle layout for test 4.2-2



(b) Obstacle layout for test 4.2-3



(c) Obstacle layout for test 4.2-4



(d) Obstacle layout for test 4.2-5

**Key:**

- |                           |   |  |                             |
|---------------------------|---|--|-----------------------------|
|                           | 45 gallon oil drum positioned upright     |  | 600 x 600 mm instrument box |
|                           | 45 gallon oil drum positioned on its side |  | 300 x 300 mm instrument box |
| Colour code for oil drums |   |  |                             |
|                           | Oil drum empty                            |  | Ford Mondeo car             |
|                           | Oil drum 50% water filled                 |  |                             |
|                           | Oil drum 90% water filled                 |  |                             |

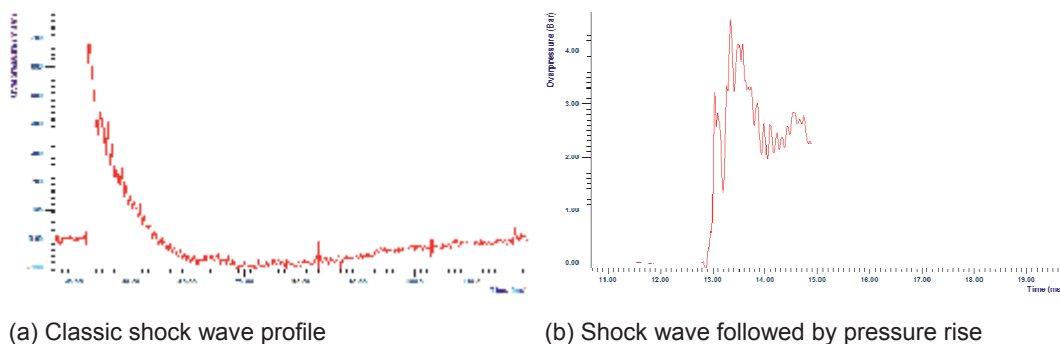
**Figure 6.12 Obstacle locations for tests 4.2-1 – 4.2-5**



## 6.4.4 Overpressure characteristics

### Definition of peak overpressure

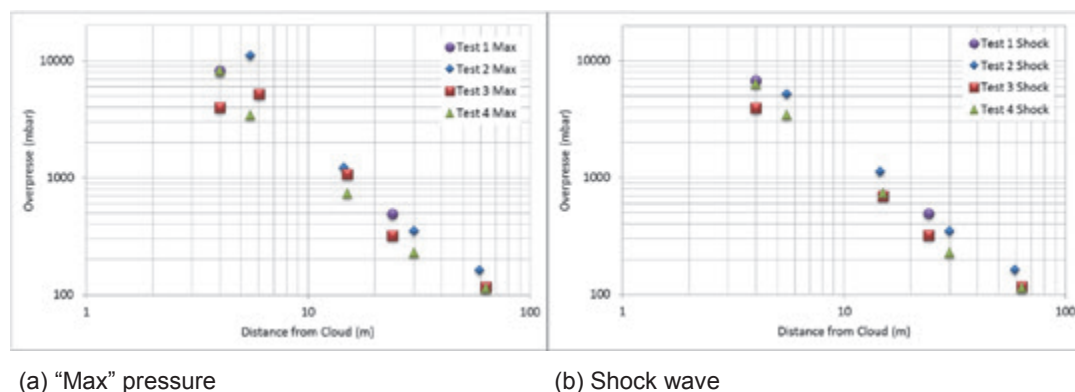
In most instances, overpressure profiles recorded were a classic shock wave as in Figure 6.13(a). In these cases, the initial shock provides the maximum pressure recorded in the profile. However, for some pressure profiles, particularly those measured close to the test rig where the high pressures resulted in rapid failure of the transducer or cable, the profile exhibits multiple peaks. An example is shown in Figure 6.13(b) (expanded to show clearly the pressure trace during the first few milliseconds) which has an initial shock of around 3 bar followed by a second pressure rise to well over 4 bar. As the transducer or cable was in the process of failing, it is not certain that this second peak corresponds to a measurement of real pressure. As a consequence, where there is a significant difference between the maximum overpressure recorded in the pressure pulse and the pressure of the initial shock, both values have been quoted. These pressures are referred to as the ‘Max’ and the ‘Shock’ overpressures respectively.



**Figure 6.13** Pressure profiles

### Pressure decay outside the cloud

The pressure decay outside the cloud is best studied using transducer data along the major axis of the rig where the largest number of external pressure measurements were taken. Measurements from transducers in the immediate vicinity of cars or the ISO container were excluded as these were affected by reflections off these large objects. It can be seen from Figure 6.14 that the clouds with larger volume result in higher pressure at a distance from the cloud.



**Figure 6.14** Pressure decay on the major axis

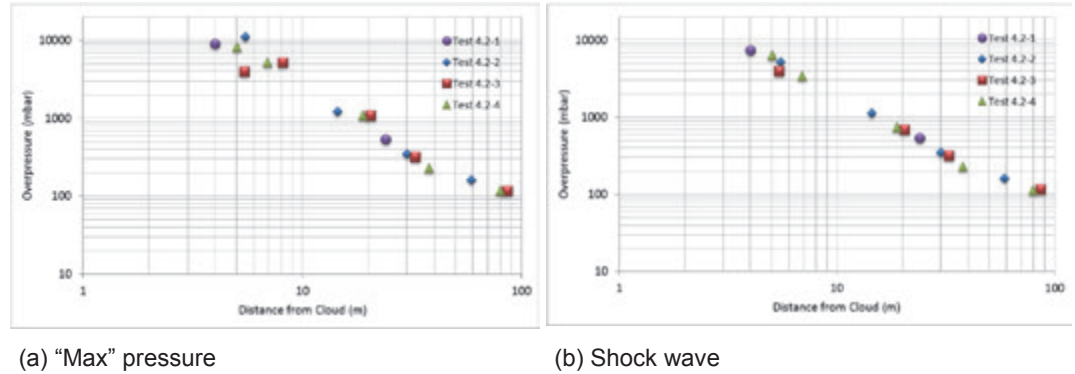
The overpressure at distance is dependent on the cube root of the energy in the cloud, which is effectively a dependency on the cube root of the cloud volume



for a given fuel and concentration. This is illustrated by normalising the distances to measurement point to Test 4.2-2 (which has the largest cloud volume). All distances to measurement points are therefore multiplied by:

$$\sqrt[3]{\frac{V_{Test\ 4.2-2}}{V_{Test\ 4.2-i}}}$$

When the distances are normalised in this way, the data lies on a single straight line, and the relationship holds up to relatively close distance (4 m) to the edge of the cloud (Figure 6.15).



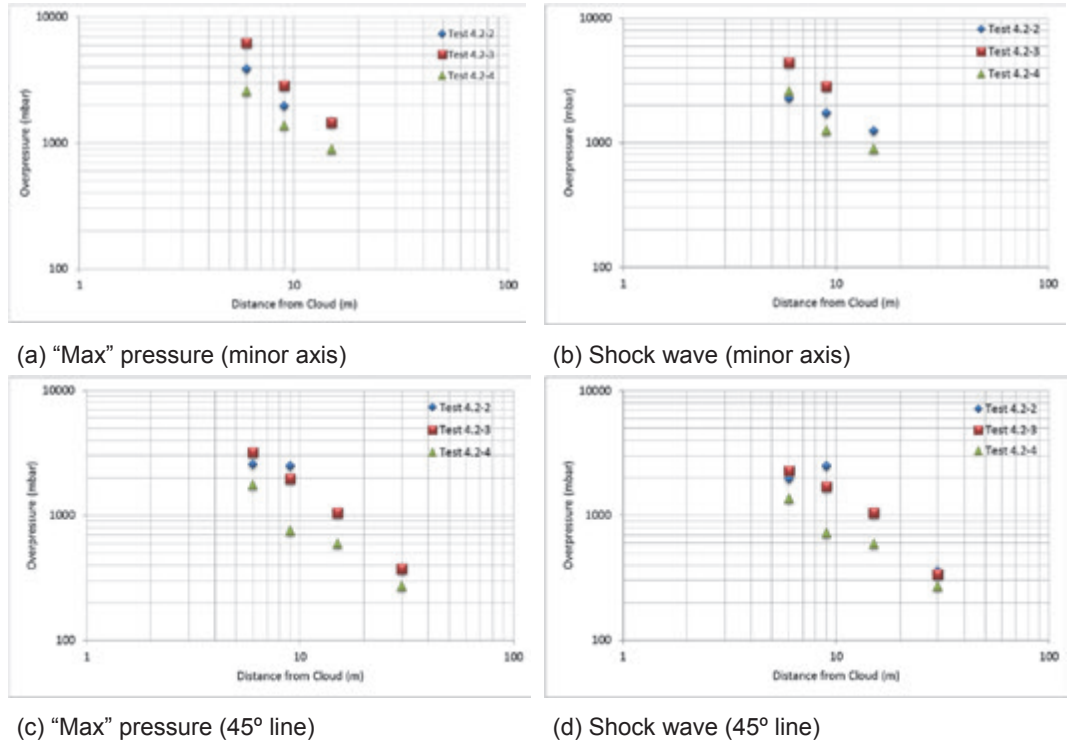
**Figure 6.15 Pressure decay on the major axis normalized to Test 2 cloud volume**

Examination of the pressure decay on the minor axis of the test rig and on a line at 45° (*i.e.* between the major and minor axes) shows that close to the test rig, the overpressures on the major axis are significantly greater than those on the minor axis and the 45° line. At a distance of 15 m from the test rig, the overpressures on the major and minor axes are similar whereas the overpressure on the 45° line is only 2/3 that on the major axes at the same distance. At 30 m from the test rig, the 45° line overpressures are similar to the major axis overpressures. Therefore, directionality effects are negligible at distances of 30 m or more from the cloud edge.

### Effect of cloud aspect ratio

In order to provide an assessment of the effect of aspect ratio, the external pressures have been ‘normalised’ using the largest volume test (Test 4.2-2) by multiplying the pressures by the cube root of the ratio of the Test 4.2-2 volume to the volume of the cloud for the test being considered (in the same way as in the assessment of overpressure decay above). As can be seen from Figure 6.15, aspect ratio does not appear to have an effect on pressure decay on the major axis. On the minor axis (Figure 6.16(a) and (b)), pressures are greatest for the highest aspect ratio test (4.2-3) and Test 4.2-2 has resulted in greater pressures than Test 4.2-4; these tests have the same aspect ratio and plan dimensions, but 4.2-2 has twice the height as 4.2-4. Pressures have not converged at a distance of 15 m.

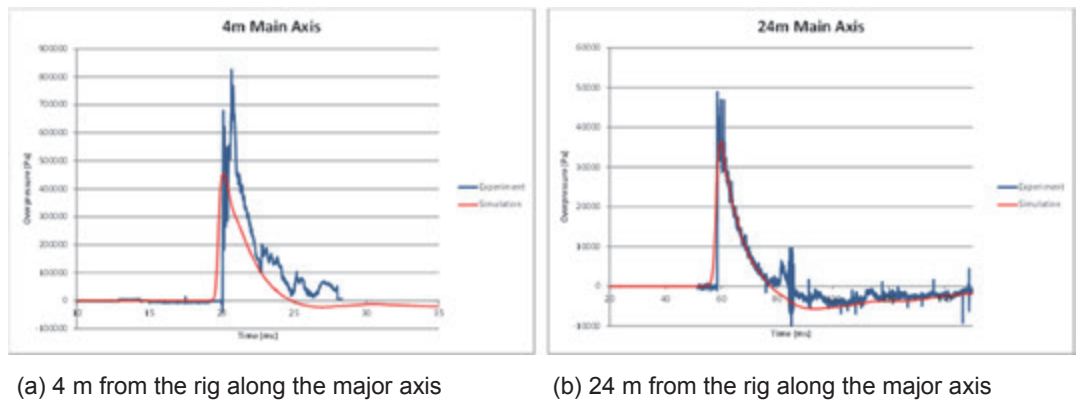
On a 45° line (Figure 6.16(c) and (d)), Tests 4.2-2 and 4.2-3 are similar while Test 4.2-4 is significantly lower up to a distance of 30 m, where the pressures from the three tests start to converge.



**Figure 6.16 Comparison of normalised pressure on the minor axis and 45 ° line**

### Comparison of Test 1 with analytical predictions

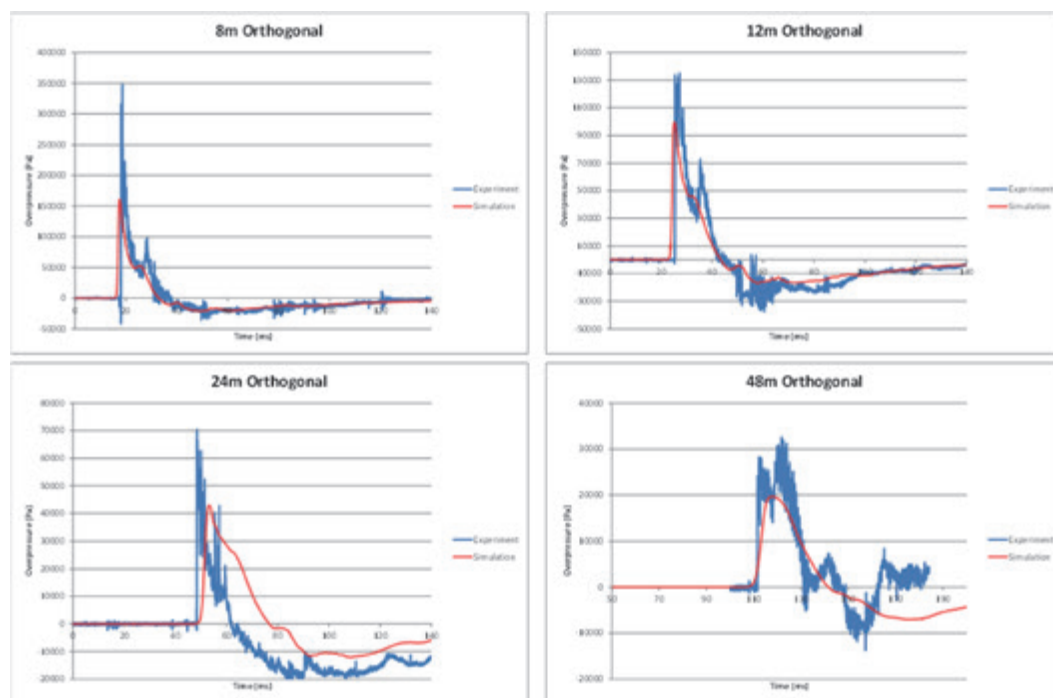
Test 1 was simulated using Fluid Gravity's Hydrocode<sup>14</sup>. A comparison between the predicted and measured overpressure-time profiles at two measurement positions on the major axis of the rig is shown in Figure 6.17. The profile at 24 m distance is predicted well by the simulation while a significant discrepancy exists for the 4 m distance due to the magnitude of the second peak after the initial shock. This suggests that the latter is a symptom of imminent failure of the transducer rather than a real physical effect. When a 1 ms moving average is applied to the overpressure measurements at this location, agreement between the experimental results and simulation are much improved with peak overpressure just below 400 mbar.



**Figure 6.17 Comparison of simulated and experimental profiles (major axis)**

Comparison of the overpressure-time profiles on the minor (orthogonal) axis (Figure 6.18) at the measurement positions (8, 12, 24 and 48 m) show that the overall shape and duration of the pressure wave is predicted by the simulation, including the negative phase of the profile. However, the peak overpressure is

less well predicted due to very short duration shocks that are not resolved by the simulation.



**Figure 6.18 Comparison of simulated and experimental profiles (minor axis)**

There is therefore reasonable agreement between the experimental and simulation results for both the positive and negative phases. Differences are due to short duration pressure spikes and some instrumentation issues.

#### 6.4.5 Simple methods of overpressure prediction

Given the lack of directionality, it is reasonable to test whether the pressures in the far field could be estimated by simple methods such as the TNO Multi-Energy Method (MEM)<sup>15</sup> and TNT equivalence<sup>16</sup> or other simple correlation techniques.

##### Multi-Energy Method

The lack of directionality found in the tests allows the vapour cloud to be simplified as a hemispherical cloud with equivalent volume. The explosion strength curve 10 is used in the assessment as this relates to a detonation. The overpressure at a given measurement point is calculated using the distance from the centre of the equivalent hemispherical cloud. A comparison of the MEM and measured overpressures in the far field is given in Table 6.3. Generally reasonable agreement between MEM predictions and the measured data is found, with the largest differences being associated either with points closer to the test rig or in the highest aspect ratio test (Test 4.2-3).

**Table 6.3 Comparison of MEM and far field measurements**

Test	Distance from edge of test rig	Rig axis	Equivalent hemispherical cloud		MEM prediction (mbar)	Measured (shock) (mbar)	Difference %
			Radius (m)	Distance from centre (m)			
4.2-1	24	Minor	7.55	29.0	401	704	-43.0
	48	Minor	7.55	53.0	183	242	-24.4
	24	Major	7.55	39.0	275	491	-44.0
4.2-2	30	Major	8.31	45.0	258	349	-26.1
	59	Major	8.31	74.0	131	162	-19.1
4.2-3	24	Major	6.12	39.0	212	320	-33.8
	63.4	Major	6.12	78.4	81	117	-30.8
4.2-4	30	Major	6.59	45.0	190	228	-16.7
	63.4	Major	6.59	78.4	88	114	-22.8

A comparison between MEM and the results of the simulation of Test 4.2-1 (Table 6.4) shows good agreement on the minor axis of the rig and in the far field on the 45° and major axes. The reason for the better agreement with the simulation is the short duration high pressure spikes in the experimental results.

**Table 6.4 Comparison of MEM and simulation of Test 4.2-1**

Test	Distance from edge of test rig	Rig axis	Equivalent hemispherical cloud		MEM prediction (mbar)	Simulation (mbar)	Difference %
			Radius (m)	Distance from centre (m)			
4.2-1	24.0	Minor	7.55	29.0	401	429	-6.5
	48.0	Minor	7.55	53.0	183	196	-6.6
	48.0	45°	7.55	62.5	145	139	4.3
	24.0	Major	7.55	39.0	275	363	-24.2
	48.0	Major	7.55	74.0	143	158	-9.5

### TNT Equivalence

The TNT mass has been determined by calculating the mass of propane within the cloud (multiplied by ten) and assuming an efficiency of 0.4 in conversion of combustion energy to overpressure. Pressure decay has been calculated from the centre of the vapour cloud, which adds 15 m on the major axis of a 30 m long rig. A comparison between TNT Equivalence predictions and the far field measurements is given in Table 6.5. It can be seen that there is generally reasonable agreement between TNT Equivalence predictions and the measured data. As with the MEM, TNT equivalence also under-predicts (to a lesser extent than MEM) the measured data.

**Table 6.5 Comparison of TNT Equivalence and far field measurements**

Test	Distance from edge of test rig	Major/minor axis	TNT Equivalence		TNT Equiv prediction (mbar)	Measured (shock) (mbar)	Difference %
			TNT mass (kg)	Distance from charge (m)			
4.2-1	24	Minor	302	39	587	704	-16.6
	48	Minor	302	29	201	242	-16.9
	24	Major	302	53	337	491	-31.4
4.2-2	30	Major	403	45	316	349	-9.5
	59	Major	403	74	142	162	-12.3
4.2-3	24	Major	161	39	236	320	-26.3
	63.4	Major	161	78.4	84	117	-28.2
4.2-4	30	Major	202	45	208	228	-8.8
	63.4	Major	202	78.4	95	114	-16.7

### Simple correlation

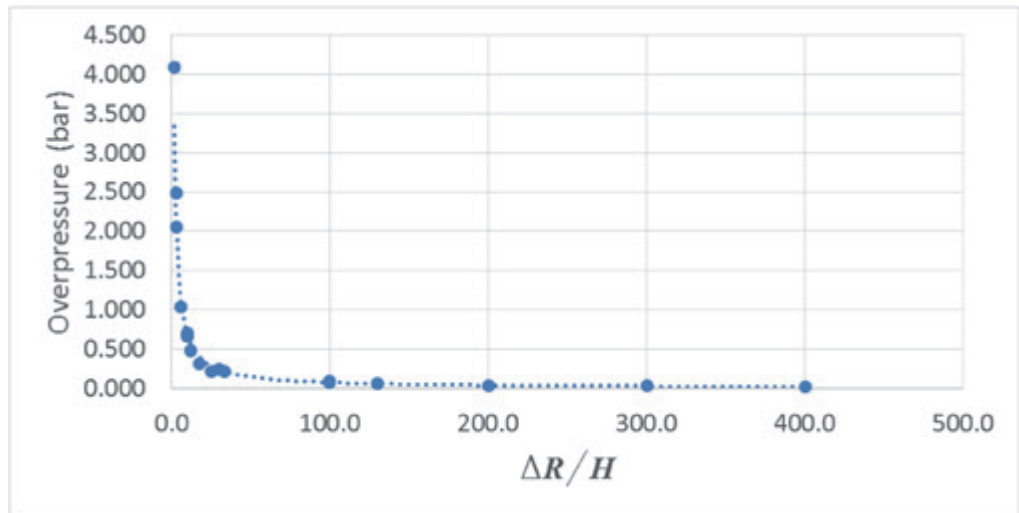
The results of the simulations are shown in

Table 6.9. Figure 6.19 shows the external overpressure ( $P$ ) plotted against distance from the edge of each cloud ( $\Delta R$ ) normalised by cloud height ( $H$ ). For the cloud geometries studied, the results appear to follow a simple power law. This can be seen by representing the same results on a log-log scale (Figure 6.20) which shows the results collapsing onto a single straight line described by:

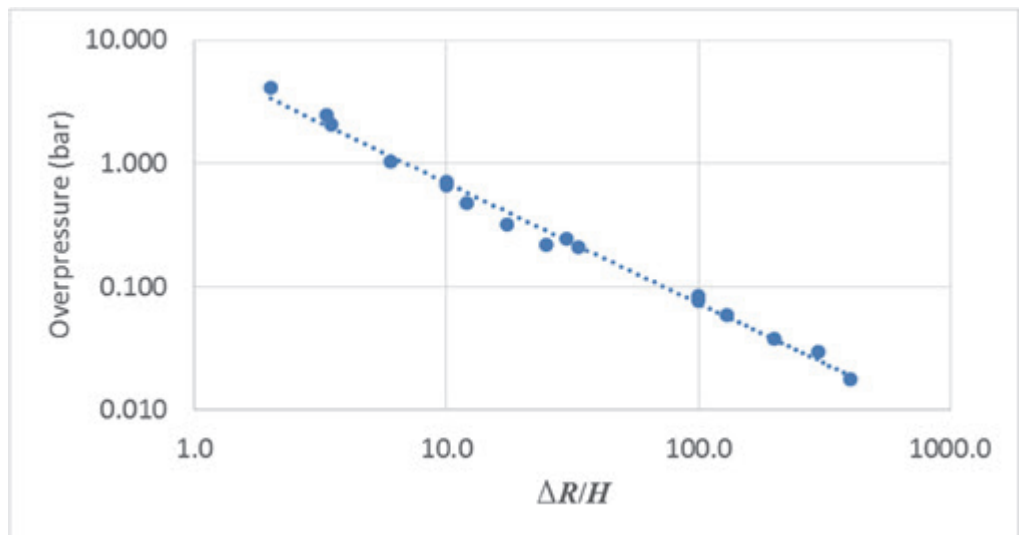
$$P = 6.571 \times \left( \frac{H}{\Delta R} \right)^{0.975}$$

**Table 6.6 Simulation results for cloud geometries studied**

Cloud radius $R$ (m)	Cloud Height $H$ (m)	Distance to edge of cloud $\Delta R$ (m)	$\frac{\Delta R}{H}$	Simulation overpressure (bar)
200	3	10.0	3.3	2.490
		30.0	10.0	0.705
		100.0	33.3	0.210
		300.0	100.0	0.078
200	1	10.0	10.0	0.665
		30.0	30.0	0.245
		100.0	100.0	0.085
		300.0	300.0	0.030
100	1	130.0	130.0	0.059
		200.0	200.0	0.038
		400.0	400.0	0.018
50	2	4.0	2.0	4.090
		7.0	3.5	2.060
		12.0	6.0	1.030
		24.0	12.0	0.478
		35.0	17.5	0.317
		50.0	25.0	0.220



**Figure 6.19** Variation in overpressure against distance from cloud edge (normalised by cloud height)



**Figure 6.20** Variation in overpressure against distance from cloud edge (normalised by cloud height) – represented on a logarithmic scale

A comparison of the simulation results with the above simple correlation model is shown in Table 6.7. It can be seen that the correlation model predicts with good accuracy the simulation results. As this correlation is independent of the cloud volume, it suggests that for large pancake shaped clouds, the volume of the cloud that contributes to the maximum overpressure for any specific cloud height is constant. The shape of the pressure wave (and the total impulse) will depend on the whole cloud.

Comparison of the results of the simulation of Test 4.2-1 with the simple correlation is shown in Table 6.8. The simulation results (rather than the test results) are used in the comparison as (a) the correlation has been derived using the simulation results of the large (50 – 200 m radius) vapour clouds and (b) the test results contain short duration pressure spikes. Table 6.8 shows that the simple correlation overestimates by a large margin (up to 224%) the simulation results of Test 4.2-1.

**Table 6.7 Comparison of simulation results and correlation model**

Cloud radius $R$ (m)	Cloud Height $H$ (m)	Distance to edge of cloud $\Delta R$ (m)	$\frac{\Delta R}{H}$	Overpressure (bar)		Error %
				Simulations	Correlation	
200	3	10.0	3.3	2.490	2.032	-18%
		30.0	10.0	0.705	0.696	-1%
		100.0	33.3	0.210	0.215	2%
		300.0	100.0	0.078	0.074	-5%
200	1	10.0	10.0	0.665	0.696	5%
		30.0	30.0	0.245	0.238	-3%
		100.0	100.0	0.085	0.074	-13%
		300.0	300.0	0.030	0.025	-16%
100	1	130.0	130.0	0.059	0.057	-3%
		200.0	200.0	0.038	0.038	-1%
		400.0	400.0	0.018	0.019	6%
50	2	4.0	2.0	4.090	3.343	-18%
		7.0	3.5	2.060	1.937	-6%
		12.0	6.0	1.030	1.145	11%
		24.0	12.0	0.478	0.583	22%
		35.0	17.5	0.317	0.403	27%
		50.0	25.0	0.220	0.285	29%

**Table 6.8 Comparison of simple correlation and simulation of Test 4.2-1**

Test	Distance from edge of test rig	Rig axis	Simple correlation (mbar)	Simulation (mbar)	Difference %
4.2-1	24.0	Minor	889	429	107
	48.0	Minor	452	196	131
	48.0	45°	452	139	224
	24.0	Major	889	363	145
	48.0	Major	452	158	186

### Conclusions on the calculation of overpressure outside the vapour cloud

The above comparisons have shown that the correlation model (which takes into account the cloud height only) predicts well the maximum external overpressures for the large clouds (Table 6.7) whereas the MEM and TNT Equivalence (which take into account the cloud volume) give better estimates of maximum external overpressures due to small cloud volumes (as was the case in Tests 4.2-1 to 4.2-4 – see Table 6.3, Table 6.4 and Table 6.5). It can also be seen from Table 6.7 that the error band associated with the 50 m radius cloud is greatest when compared to larger radius clouds.

It is concluded that only a limited zone of the cloud can influence the external overpressure. Parts of the cloud outside this “zone of influence” do not have an effect and when the cloud size exceeds the size of the zone of influence, only the cloud height affects the external maximum overpressure. The extent of this zone



of influence is dependent on the speed at which pressure travels through the combustion products in the cloud and the time available to influence the peak overpressure at a particular point. The shock waves associated with a detonation mean that pressure travels at  $\gg 1000$  m/s and the time available for influencing the peak overpressure is at most a few 10's of milliseconds. This suggests that the zone of influence is a few 10's of meters. This would explain why, for the larger clouds (100 – 200 m radius), the external maximum overpressure is volume independent and for the smaller clouds, (as used in the tests), it is cloud volume dependent. At a radius of 50 m, the error associated with the simple (volume independent) correlation increases to 29%.

Whilst this assessment is based on a limited set of cloud geometries, the following methodology is proposed for estimating the maximum external overpressure caused by the detonation of a vapour cloud:

- For clouds with a representative radius of 50 m or more, the correlation model derived above based on cloud height should be applied.
- For smaller clouds, either MEM or TNT Equivalence should be applied using the whole cloud volume.

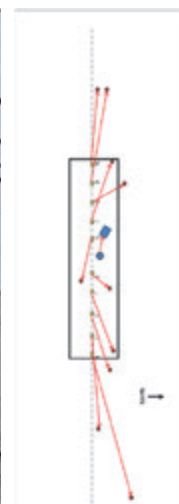
This approach is likely to be conservative for clouds just below the 50m radius size but will gradually become more accurate as the cloud size increases or decreases. It should be remembered, however, that the proposed models are based on a limited set of simulations and application of these models should take into account these limitations.

#### 6.4.6 Displaced items

Short vertical lengths of pipe were used to assess directional effects in Tests 4.2-2 to 4.2-4. The pipes were placed within the cloud (Figure 6.21(a)) and (in Test 4.2-2) additional pipes were just outside. In general, it was found that for the first half of the cloud from the point where the detonation was initiated, the pipes were moved in the reverse direction to the direction of propagation of the detonation whereas in the second half of the cloud, the pipes were moved in the same direction as the detonation (Figure 6.21(b)).



(a) Arrangement of pipes used in Test 4.2-4



(b) Pipe displacement during Test 4.2-4

**Figure 6.21 Displacement of items in the tests**

In addition, in Test 4.2-1 where numerous objects were placed within the cloud (oil drums, instrument boxes, cars), in almost all cases, items were displaced in the 'reverse direction' relative to the direction of propagation of the detonation, even close to the end of the test rig opposite to the point of initiation. The displacement of items is likely to depend on a number of factors, including the inertia of the item and its initial freedom to move. However, the experiments clearly show that there is a net reverse impulse on items well within the cloud and that a 'positive' impulse may result close to the cloud boundary, where the reverse flow will be shorter in duration.

#### **6.4.7 Detonation propagation**

Two tests (4.2-5 and 4.2-6) were conducted to determine the minimum cloud depth that would sustain a detonation. The cloud profile in those tests is shown in Figure 6.10. Due to loss of some high speed video in Test 4.2-5 it has been necessary to use flame ionisation and overpressure data to assess the cloud depth at which the detonation process stopped. This data shows that overpressures were 10 – 11 bar lower than what would be expected in a detonation in the region where the cloud depth was 0.5 – 0.35 m.

In Test 4.2-6, the cloud height was reduced more sharply initially, followed by stepped reduction. High speed video records and ionisation probe data suggest that the detonation was maintained to a point where the cloud had a height of just less than 200 mm. However, accumulation of rain water on the polythene in the shallow section of the test rig depressed the polythene, so it cannot be conclusively stated that the detonation could not propagate in a cloud height of even less than 200 mm. Overpressures in this section of the test rig were variable (3 – 13 bar) suggesting that the detonation may have been failing.

From a practical viewpoint, these experiments have shown that a detonation can travel through a thin cloud layer (probably <200 mm). Therefore, a detonation would be able to propagate through relatively thin detonable layers and paths in a large cloud. However, it should be noted that the tests involved a stoichiometric cloud. At other detonable concentrations, where the cell size will be bigger, the detonation will require larger cloud depths than the stoichiometric case.

Deflagrations can be relatively sensitive to concentration variations; rich or lean concentrations in the congested region can result in flame deceleration and oscillatory pressures rather than the energy being contained within a single pressure pulse. A detonation will continue through any part of the cloud that is within the detonable range. Even in zones within the detonable cloud where concentrations are outside the detonable limits, the detonation can pass either under, over or around the fluctuation from the point of initiation to the boundaries of the detonable cloud. In other words, once detonation is initiated, the remainder of the cloud will to all intents and purposes detonate.

#### **6.4.8 Damage to objects**

##### **Cars**

In Test 4.2-1, a Ford Mondeo car was placed within the cloud. In Tests 4.2-2 – 4 Ford Mondeo cars were placed facing the detonation at either 6 m or 15 m from the edge of the cloud on the major axis. The damage is illustrated in Figure 6.22. Cars located at a distance of 6 m suffered moderately severe damage, experiencing overpressures of over 3 bar. The level of damage reduces

significantly as a result of the rapid decay of pressure from the edge of the cloud, with overpressures of less than 1 bar causing relatively minor damage to cars. Based on the simulations discussed in section 6.3.1, the overpressure drops to 1 bar at a distance of 12.4 m from the edge of a 50 m diameter 2 m high cloud and at a distance of 20 m for the edge of a 200 m diameter 3 m high cloud.



(a) Two views of Ford Mondeo car damaged within the cloud in Test 4.2-1



(b) Test 4.2-2 Car 1 at 6 m – overpressure 11050 mbar (Max), 5191 mbar (shock)



(c) Test 4.2-2 Car 2 at 15 m – overpressure 1211 mbar (Max), 1126 mbar (shock)



(d) Test 4.2-3 Car 1 at 6 m – overpressure 5209 mbar (shock)



(e) Test 4.2-3 Car 2 at 15 m – overpressure 1074 mbar (Max), 693 mbar (shock)



(f) Test 4.2-4 Car 1 at 6 m – overpressure 3428 mbar (shock)

**Figure 6.22 Damage to cars in Tests 4.2-1 – 4**



By way of comparison, Figure 6.23 shows images of cars damaged in some of the recent incidents.



(a) Cars damaged within the cloud in the Buncefield incident, December 2005



(b) Cars damaged close to the cloud boundary in the Buncefield incident, December 2009



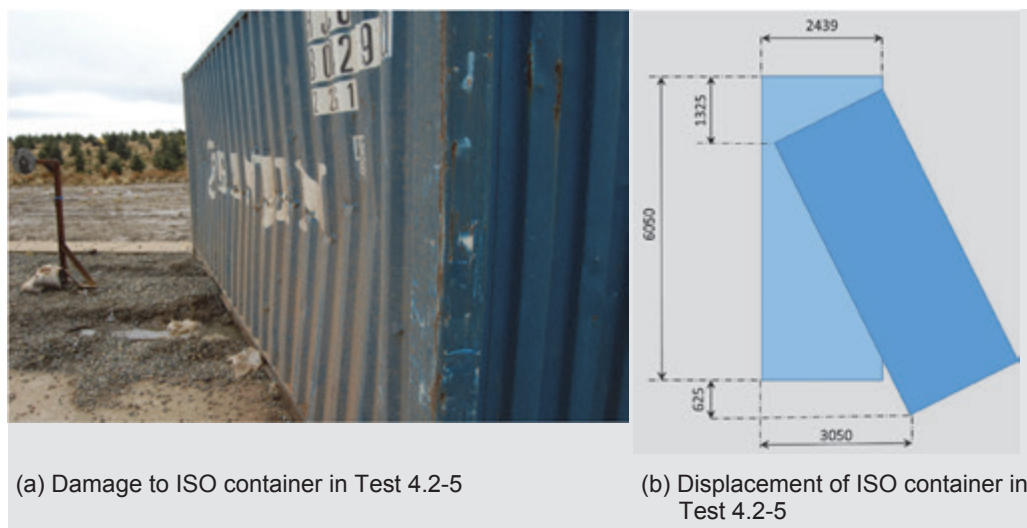
(c) Cars damaged in the IOC Jaipur incident, October 2009 (left) within the cloud and (right) outside the cloud

**Figure 6.23 Damage to cars in past incidents**

### ISO Container

In Tests 4.2-2 to 4.2-5, an ISO container was placed at various locations along the major axis of the test rig in order to subject it to a range of overpressure loadings. No damage was sustained in Tests 4.2-2 (at 60 m from the edge of the cloud) and 4.2-3 (at 25 m from the edge of the cloud), where the incident overpressure was up to 320 mbar. Some minor creasing occurred to the front face in Test 4.2-4 (at 20 m for the edge of the cloud) where the incident overpressure was 426 mbar.

In Test 4.2-5 (at 10 m from the edge of the cloud), the incident overpressure was 2 bar; the degree of creasing on the front face was greater and the container was displaced as shown in Figure 6.24 (b).




**Figure 6.24 Damage to ISO container in Test 4.2-5**

### Oil Drums

Oil drums were placed inside (Tests 4.2-1 and 4.2-4) and outside the cloud (Tests 4.2-2 – 4) the cloud. A combination of empty and partially filled drums were used. They were placed either upright or lying on their side. The results are summarised in Figure 6.25 (drums at similar distance from the edge of the cloud are arranged in columns). It can be seen from the results that incident overpressures in excess of 3 bar cause damage to the oil drums whereas incident overpressures of 2 bar do not. It should be noted however that the drums were located off the major axis whereas the pressure measurements were taken on the major axis (except for Test 4.2-4 where the drums were very close to the major axis). Therefore the drums in Tests 4.2-2 and 4.2-3 were probably exposed to somewhat lower overpressures than those quoted.




 45 gallon oil drum positioned upright

 45 gallon oil drum positioned on its side

 Oil drum empty

 Oil drum 50% water filled

 Oil drum 90% water filled

**Figure 6.25 Damage to oil drums**

By way of comparison, Figure 6.26 shows images of near full oil drums damaged in the IOC Jaipur incidents in October 2009.





**Figure 6.26** Near full oil drums damaged in the IOC Jaipur incident, December 2009

### Instrument boxes

A total of 18 instrument boxes were used in the detonation tests inside the cloud (in Test 4.2-1) and at a range of distances from the cloud (in Tests 4.2-2 – 4). Two box sizes were tested ( $600 \times 600 \times 200$  and  $300 \times 300 \times 200$ ). Figure 6.27 shows the two box types. In all cases, the boxes were supported by steel angle frames bolted to a concrete floor and the box door faced the explosion. In Tests 4.2-2 – 4, the small boxes were located along the major axis of the test rig, whilst the large boxes were placed along a parallel axis to the major axis and at 5 m from it.



(a)  $300 \times 300 \times 200$  mm box



(b)  $600 \times 600 \times 200$  mm box

**Figure 6.27** Instrument boxes used in the detonation tests









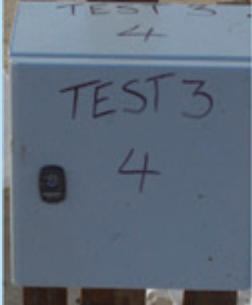

Table 6.9 shows all the boxes used in the tests following the explosion. The incident overpressure at each box is also given. In several cases (particularly at the large box locations), the overpressure is estimated from pressure transducers on the major axis of the rig at the same or similar distance to the box.









It can be seen that when the incident overpressures is 1 bar or less, there is very little damage to the boxes, though the doors may be opened by the pressure wave (probably the rarefaction phase). When the incident pressure exceeds 3 bar, distortion occurs to the front doors and, in most cases, the sides of the box. At incident pressures of over 5.2 bar, the damage to the large box is comparable to the damage to the same box located inside the vapour cloud. In this case (and in the case of the large box in Test 4.2-1 where the box was inside the cloud), failure



of the front door of the box resulted in the pressure wave entering the box and pushing the back face outwards.

**Table 6.9 Damage to instrument boxes in detonation tests**

Test	Distance from cloud edge (mm)	Overpressure (mbar)	Box damage	
			300 × 300 × 200	600 × 600 × 200
4.2-1 900 m <sup>3</sup> cloud	Within the cloud	>10000		
4.2-2 1200 m <sup>3</sup> cloud	4000	>5200 <sup>§</sup>		
	15000	1130 - 1210 <sup>§</sup>		
4.2-3 480 m <sup>3</sup> cloud	4000	Small box 3970 Large box <sup>§</sup> 3310 – 6040		
	15000	690 - 1070 <sup>§</sup>		

Test	Distance from cloud edge (mm)	Overpressure (mbar)	Box damage	
			300 × 300 × 200	600 × 600 × 200
4.2-4 600 m <sup>3</sup> cloud	4000	Small box 6350 – 8220 Large box 1940 – 4340		
	6000	3430 <sup>§</sup>		
	10000	1150 - 2070 <sup>§</sup>		
	15000	740 <sup>§</sup>		
<sup>§</sup> The large box overpressure is estimated on the basis of the major axis transducer at the same or similar distance from the cloud				

By way of comparison, Figure 6.28 shows examples of instrument boxes damaged in previous incidents.



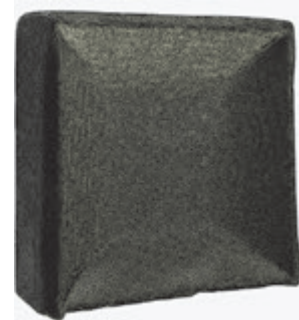
Figure 6.28 Instrument boxes damaged in previous incidents

#### 6.4.9 Digital record of damaged objects

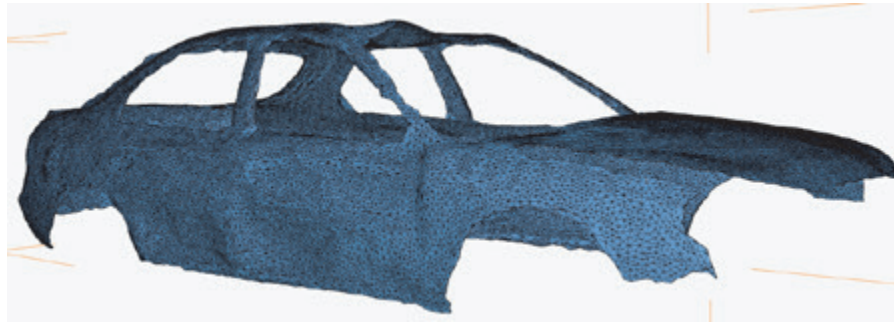
In order to provide a quantitative record of the damage to all the objects used in Tests 4.2-1 – 5, each object was laser scanned and the data processed into digital files that can subsequently be used in further analysis. Examples of the digital scans are shown in Figure 6.29.



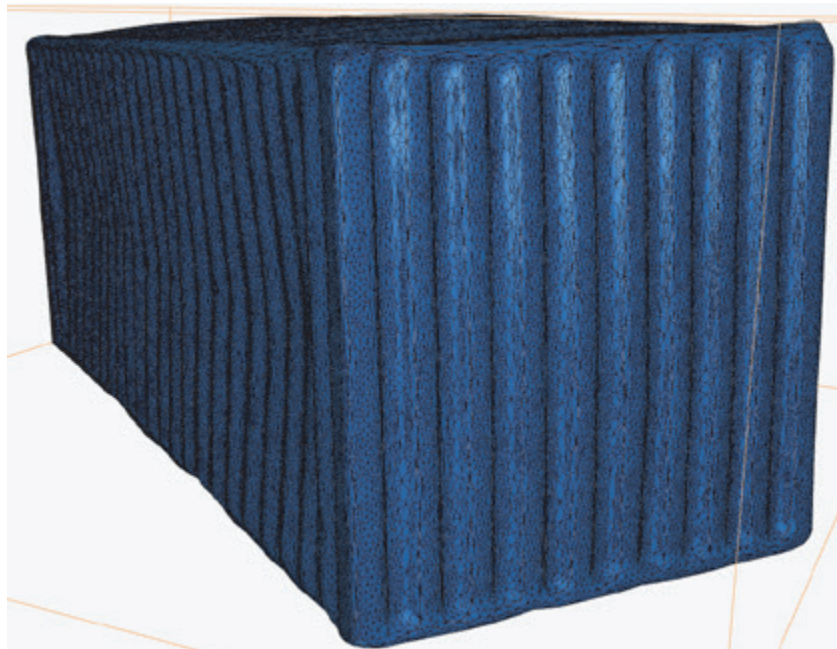
(a) 90% full oil drum on its side inside the gas cloud in Test 4.2-4



(b) Large box at 4 m from the cloud in Test 4.2-3



(c) Ford Mondeo car at 6 m from the edge of the cloud in Test 4.2-3



(d) ISO container at 10 m from the edge of the cloud in Test 4.2-5

**Figure 6.29** Examples of laser scans of objects damaged in the detonation tests

## **7 EXPLOSION RESPONSE OF INSTRUMENT BOXES**

### **7.1 Objectives**

Simple objects on industrial sites, such as instrument boxes and oil drums, can in the event of an accidental explosion serve as good indicators of the explosion overpressure at their positions. Such objects were used to great effect in estimating the overpressure magnitude at Buncefield following the incident in 2005<sup>7</sup>.

In the large scale detonation test programme (see Section 6.4), a series of such objects were located at varying distances from the cloud, as well as some within the cloud. Overpressure measurements were made at or adjacent to the location of these objects.

The objectives of the work reported in this section are:

- (a) To validate finite element models of the instrument boxes using the test data.
- (b) To develop pressure-impulse (PI) diagrams which can be used to provide a rapid assessment of explosion magnitude through an examination of the damage level of instrument boxes.

### **7.2 Key Findings**

1. Alternative methods of finite element analysis with increasing complexity were used to model the instrument boxes in the detonation experiments. Coupled Eulerian-Lagrangian analysis was found to predict the deformation of the boxes very well, particularly where the deformation was severe (following exposure to  $> 3$  bar overpressure). Uncoupled analysis and pure Lagrangian analysis over-estimated the deformations. Therefore, if such analysis is used to estimate overpressure from observations of deformed boxes, the overpressure is likely to be underpredicted.
2. Graphically illustrated pressure-impulse diagrams have been produced for instrument boxes. These can be used to provide a quick estimate of the explosion characteristics in forensic investigations.
3. Further work on modelling simple structural objects subjected to extreme explosion loads has been initiated outside the project as the subject of a PhD thesis and this will be completed and published in 2014.

### **7.3 Analytical Techniques and Numerical Models**

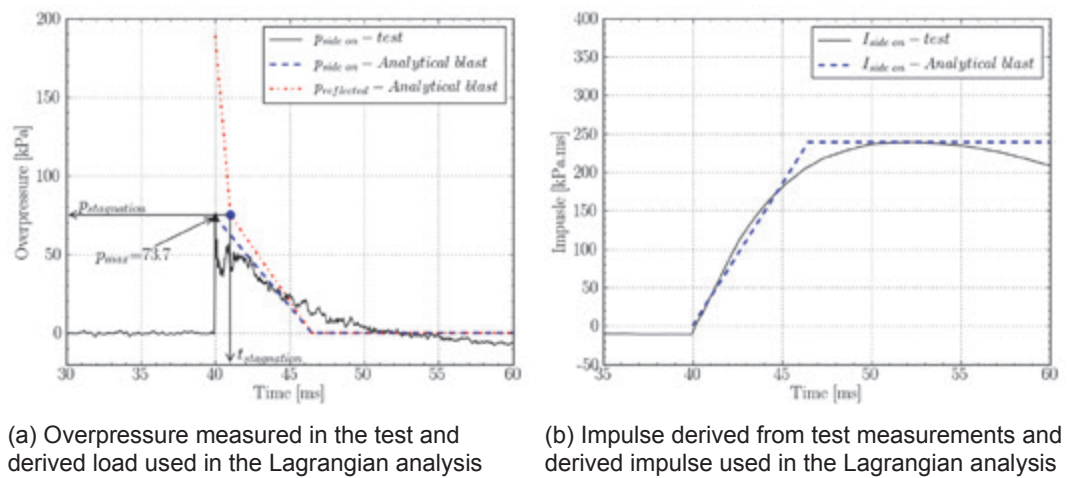
A number of different analytical techniques were compared to determine which and in what circumstances each method worked best. These were Lagrangian, uncoupled Eulerian-Lagrangian and coupled Eulerian-Lagrangian analysis (in increasing order of computational demand). The difference between the three approaches is briefly outlined below.



### 7.3.1 Lagrangian analysis

In a Lagrangian analysis, the box is modelled using shell elements and the blast load is applied directly to the surface of the elements as a uniformly distributed load. The reflected and side on blast loads were derived using an analytical method<sup>17</sup> using the blast wave parameters (peak overpressure and impulse) of the incident blast wave from the tests.

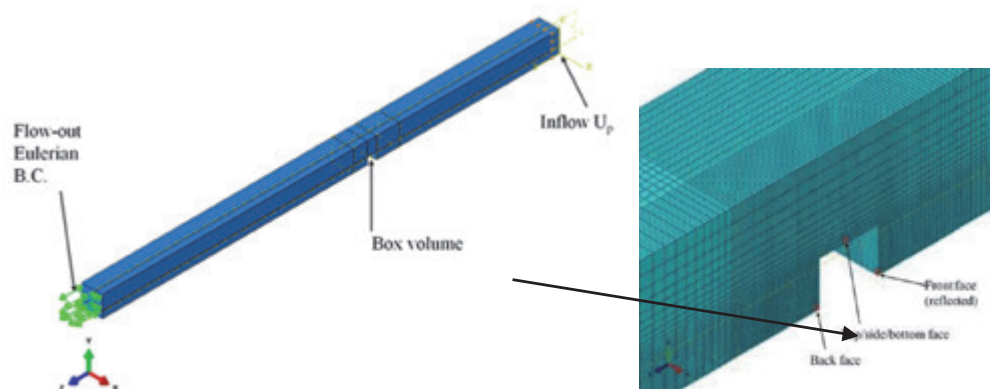
The reflected load is applied to the front face of the box (the door). Given the relatively small dimensions of the boxes, there is negligible pressure decay as the blast wave passes over the boxes. Therefore, the other faces of the box are subjected to loading that closely matches the measured side on pressure. A comparison of the overpressure and impulse measured in the test with the derived values for one of the boxes is shown in Figure 7.1.



**Figure 7.1** Example of loading used in the Lagrangian analysis (shown for a small box at 15 m from the edge of the cloud in Test 4.2-4)

### 7.3.2 Uncoupled Eulerian-Lagrangian analysis

This is a two-step approach. In the first (Eulerian) step, the box is treated as a rigid object and a high intensity blast wave generated by the expanding gases propagates through air from the origin of the explosion towards the box (Figure 7.2). The Eulerian analysis produces the dynamic pressure-time traces acting on all the surfaces of the box.

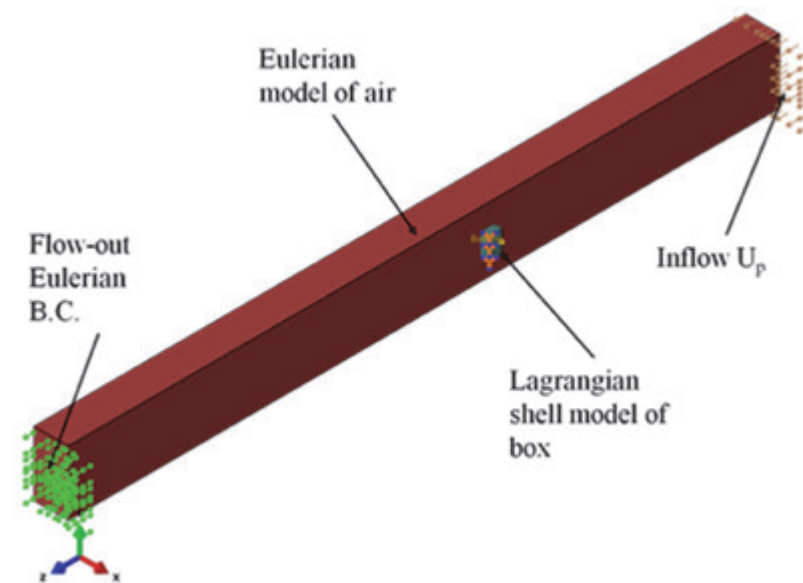


**Figure 7.2** Eulerian model (only  $\frac{1}{4}$  of the model is shown taking account of symmetry)

Once calculated, these pressures are then applied to the box in the second (Lagrangian) step of the analysis. Provided the deformation of the box has negligible influence on the development of the pressure loading on the surfaces of the box, this method is expected to give accurate results.

### 7.3.3 Coupled Eulerian-Lagrangian analysis

Using this approach, the Eulerian and Lagrangian models are combined (Figure 7.3). Interaction between the blast wave and structural deformation is accounted for by the model which allows for contact between the Eulerian and Lagrangian parts. This is the most accurate approach where the interaction of the structure of the box influences the way in which the pressure acts on the surfaces of the box. This is likely to be the case where the pressures are relatively high and the box deformations large. The method is, however, computationally very demanding and as such is not suitable for general use.



**Figure 7.3 Combined Eulerian-Lagrangian model (only ¼ of the model is shown taking account of symmetry)**

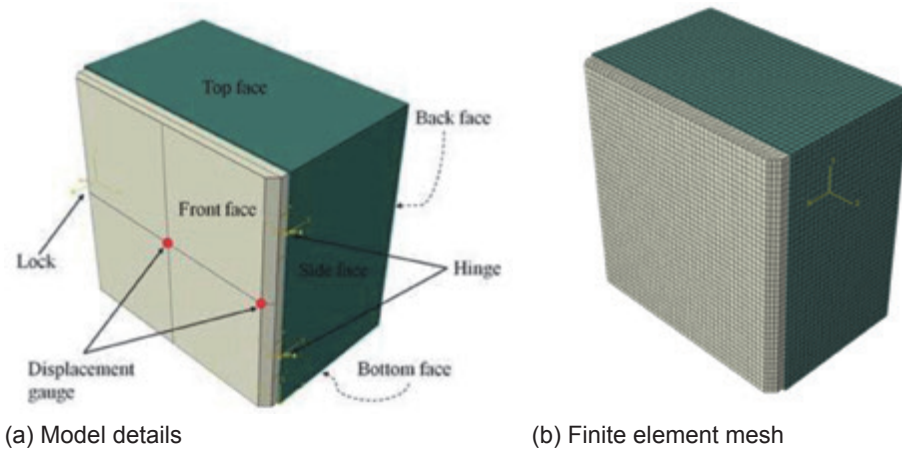
The starting point to both the coupled and uncoupled analyses is to calibrate the model so that it represents the free field incident blast wave. This is done using a one-dimensional Eulerian model and imposing a particle (inflow) velocity at the inlet boundary of the model. A trial and error process (including variation of the particle inflow velocity) is used to determine the correct numerical blast wave with the same peak overpressure and impulse as measured in the tests.

The difference in computational demand can be illustrated by comparing the run-time for a typical blast analysis of one of the boxes. The run times on a high performance computer are 2 minutes, 57 minutes and 15 hours for the Lagrangian, uncoupled and coupled analysis respectively.

### 7.3.4 Instrument box models

The body and door of the boxes were modelled using shell elements. The door hinges and lock were modelled using rotational hinges. A typical model is shown in Figure 7.4. The box is supported horizontally and vertically along its two back vertical edges and around its base perimeter. The boxes are made of galvanised

steel with nominal plate thickness 1.25 mm, average yield stress 279 N/mm<sup>2</sup> and average ultimate stress of 297 N/mm<sup>2</sup>.



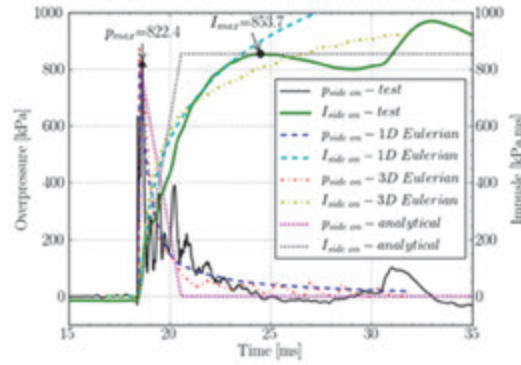
**Figure 7.4 Numerical model for a 300 x 300 x 200 box**

## 7.4 Analysis Results

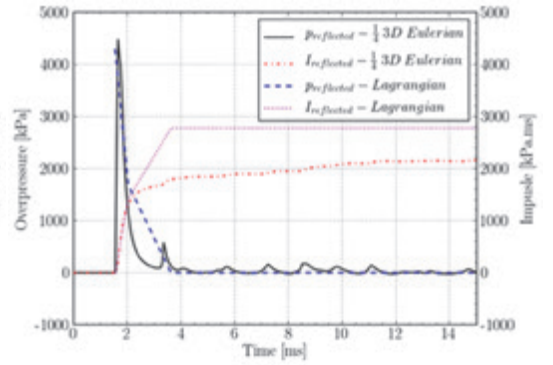
The boxes were analysed using the three analytical methods described above. The methodology is illustrated by reference to the small box in Test 4.2-4 located at a distance of 4 m from the edge of the cloud. The first (calibration) step in both the coupled and uncoupled analyses is illustrated by reference to Figure 7.5(a). It shows the experimental free field overpressure-time trace (and the corresponding impulse), the calibration free field pressure and impulse (using a 1-D analysis) and the free field pressure and impulse generated by the 3-D Eulerian analysis using the parameters derived from the 1-D calibration. In Figure 7.5(b) the reflected overpressure time history and impulse derived from the analytical method<sup>17</sup> are compared with those calculated by the Eulerian analysis. Figure 7.5(c) shows the overpressure time profiles on all box faces calculated in the first step of the uncoupled Eulerian-Lagrangian analysis. These are the loadings sustained by the box in the uncoupled analysis.

Figure 7.5(d) shows the results of the analysis using the displacement at the centre of the door of the box as a reference point. It can be seen that the coupled Eulerian-Lagrangian analysis is in close agreement with the test, while the uncoupled analysis and the Lagrangian analysis overestimate the deflection.

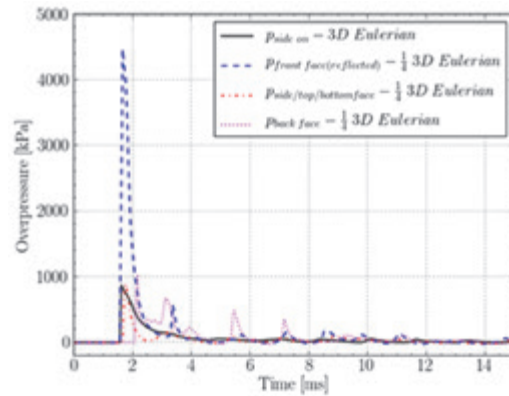




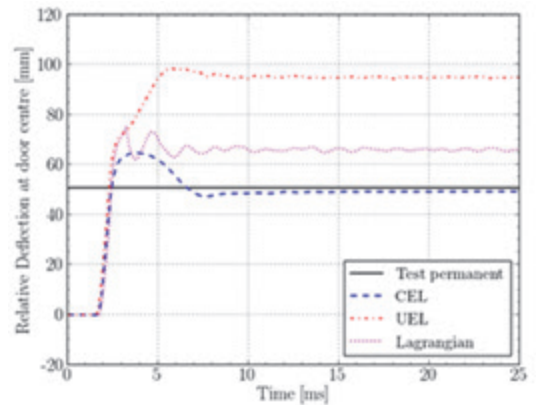
(a) Calibration of inflow velocity and derivation of numerical free field blast wave



(b) Comparison of numerical reflected pressure derived by simplified calculations<sup>17</sup> and using the 3-D Eulerian analysis



(c) Overpressure loading on all the box faces calculated using Eulerian analysis



(d) Box door centre displacement calculated using the three methods compared with the measured permanent deformation in the test

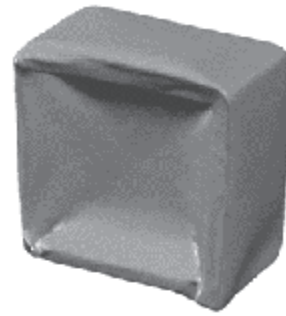
**Figure 7.5 Analysis results for a small box in Test 4.2-4 at 4 m from the cloud edge**

The deformed shape of the box as determined by the three analysis methods is compared with the image of the box after the test and with the laser scan record of the box shown in Figure 7.6.

In the following figures and tables coupled Lagrangian-Eulerian analysis is referred to as “CEL”, uncoupled as “UEL” and pure Lagrangian analysis as “L”.



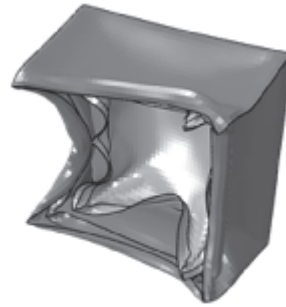
(a) Box after test (prepared for scanning)



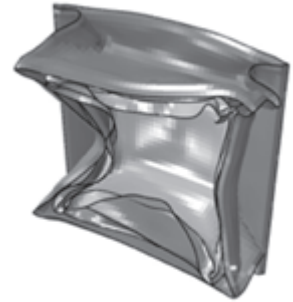
(b) Scanned image of box



(c) CEL



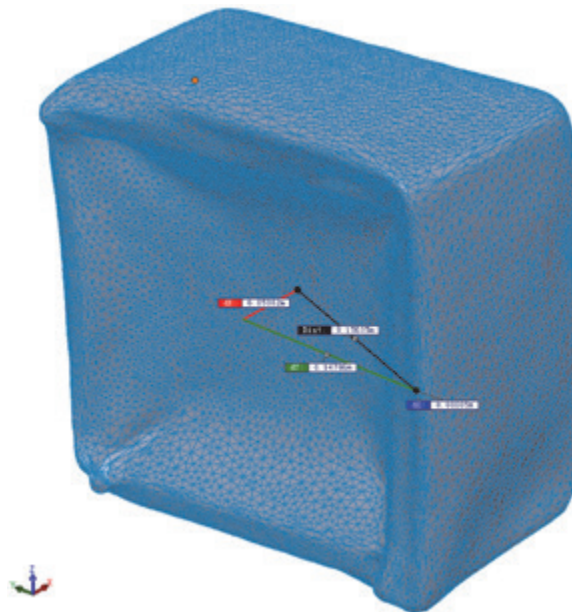
(d) UEL



(e) L

**Figure 7.6 Actual and predicted deformed shapes**

A summary of the results for the boxes is shown in Table 7.1. The numbers below the images are the permanent deformation in mm at the centre of the door of the box. This deflection was measured relative to the middle of the box vertical edge of the box (from the laser scanned record for the tests and from the finite element model in the case of the analyses). This is illustrated in Figure 7.7 for a scanned image of one of the boxes.


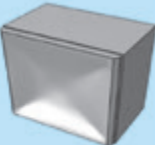
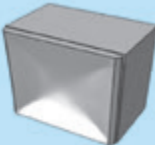
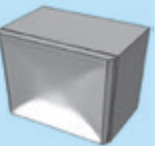
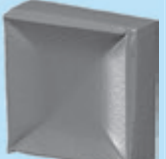
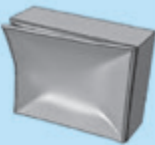
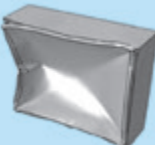

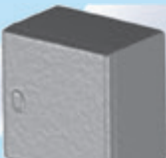
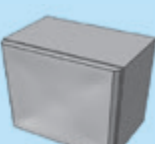
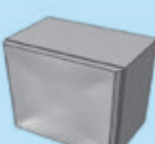
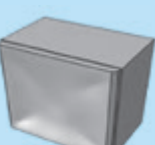

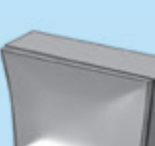
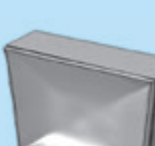
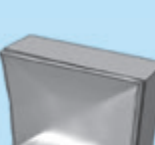




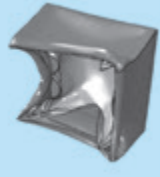

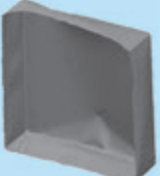
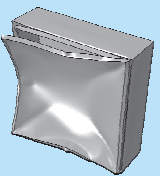
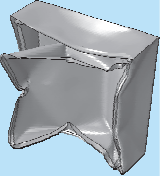
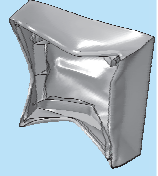


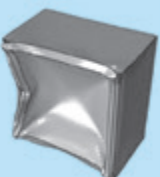


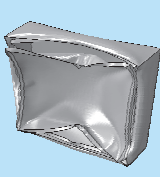
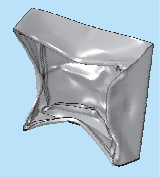


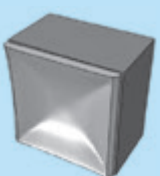
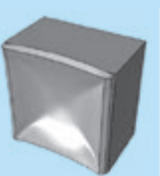
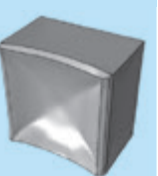
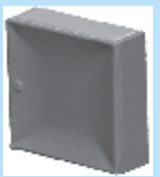
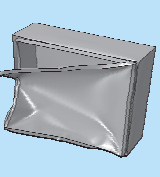
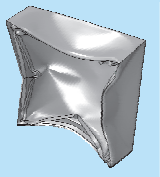
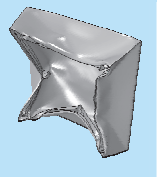

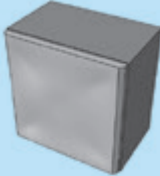
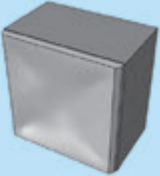
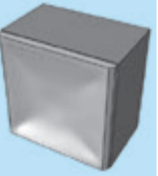

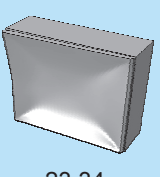
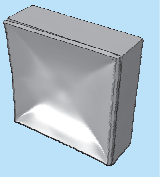
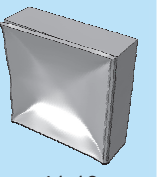
**Figure 7.7 Door centre deformation measurement**

In all but the most severely deformed boxes the side edge remained straight. However, where the side edge deforms, this can give rise to misleading comparisons as illustrated for example in Figure 7.6(e) and is a particular problem in the Lagrangian analysis where application of the incident pressure to the side wall can cause premature buckling of the wall and hence inward movement of the vertical edge.

As a general observation, very good agreement was found between the CEL analysis and the measured deformation for the small boxes. As noted in Section 6.4.8 (Table 6.9), pressure transducers were located on the major axis of the rig alongside the small boxes. The large boxes were located off the major axis and the pressures were estimated. The overpressure values used in the analysis were generally at the upper limit of the estimated range in Table 6.9. Consequently, the calculated deformations in the analysis tend to be higher than those measured in the case of the large boxes.

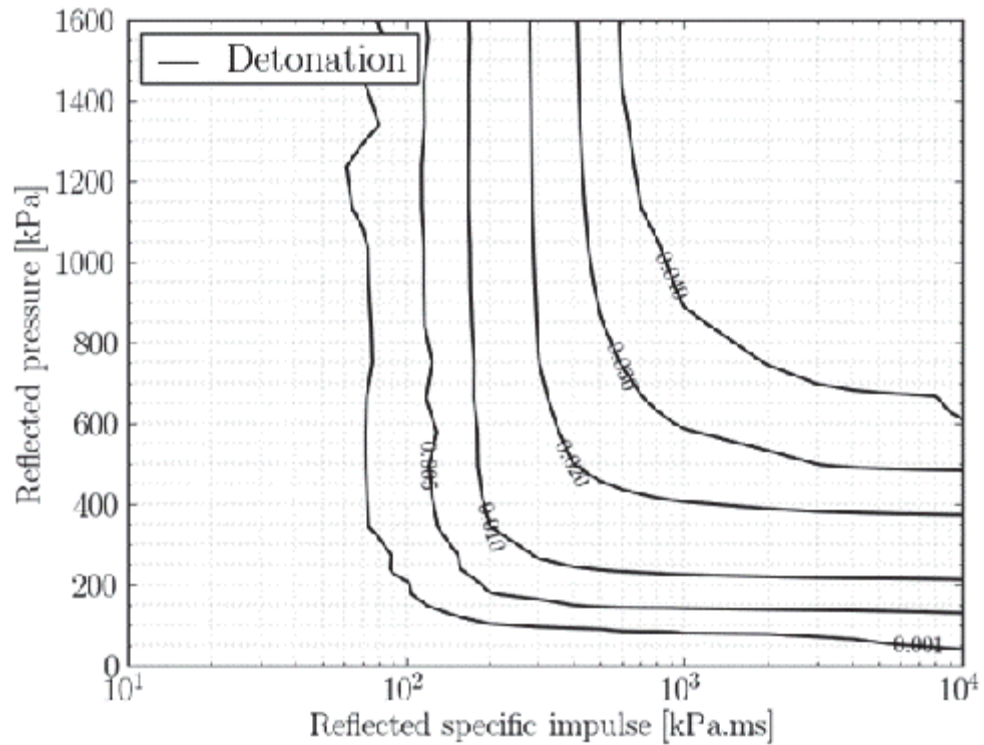
**Table 7.1 Summary of instrument box analysis results**

Test	Box	P (mbar)	Permanent deformation at door centre (mm)			
			Laser scanned box	CEL	UEL	L
4.2-2	Small 15 m	1126	 11.67	 10.53	 13.85	 15.00
	Large 15 m	1126	 59.45	 45.21	 95.32	 98.89
4.2-3	Small 15 m	693	 0.26	 0.53	 4.21	 5.87
	Large 15 m	693	 13.60	 24.92	 40.47	 38.84

Test	Box	P (mbar)	Permanent deformation at door centre (mm)			
			Laser scanned box	CEL	UEL	L
4.2-4	Small 4 m	8224	 50.59	 49.21	 94.89	 65.95
	Large 4 m	4345	 140	 55.21	 105.67	 109.636
	Small 6 m	3428	 32.6	 42.4	 55.4	 54.5
	Large 6 m	3428	 68.00	 100.97	 85.18	 65.71
	Small 10 m	2067	 9.91	 24.28	 32.09	 35.48
	Large 10 m	2067	 34.60	 54.27	 130.68	 83.71
	Small 15 m	737	 1.55	 1.62	 4.62	 6.83
	Large 15 m	737	 -2.00	 23.34	 34.59	 41.19

## 7.5 Pressure-Impulse and Explosion Damage Diagrams

Pressure-impulse diagrams have been constructed for the small instrument boxes using the validated finite element model. A range of the free field incident overpressure of 10 to 400 kPa (100 mbar to 4000 mbar) corresponding to a reflected overpressure range of 20 – 1665 kPa (200 mbar to 16650 mbar) was used. The impulse range covered was from 10 to 10000 kPa.ms (100 mbar.ms to 100000 mbar.ms). The resulting P-I diagram is shown in Figure 7.8 for door centre deformations ranging from 1 mm to 40 mm.



**Figure 7.8 P-I diagram for 300 × 300 × 200 boxes subjected to a detonation**

It should be noted in the above that box sidewall buckling may occur when the incident pressure is greater than 200 kPa (2000 mbar) corresponding to a reflected overpressure of 660 kPa (6600 mbar). When this happens, the relative deformation of the centre of the door to the edge remains in the range of 50 – 60 mm as the whole door moves back into the box. A visual representation of deformed shape under a range of detonation loads is shown in Figure 7.9.



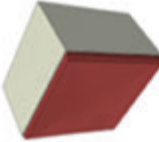

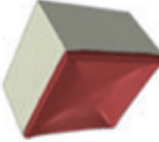
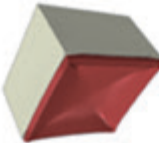
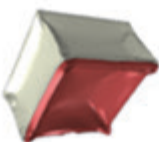




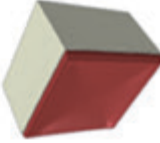
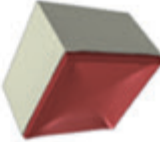
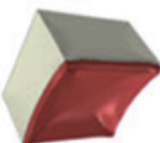
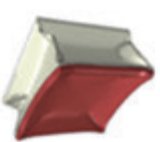



Box200		back support						Reflected(Side-on) residual deflection(m)	
Detonation	Pa.s	125(30)	250(60)	333(80)	416(100)	1027(400)	1659(700)	2300(1000)	8763(4000)
	m	0.006	0.017	0.025	0.030	0.054	0.058	0.057	0.055
	Impulsive 1665 kPa								
	kPa	93(40)	209(80)	344(120)	579(180)	664(200)	1035(280)	1341(340)	1665(400)
	m	0.002	0.010	0.018	0.035	0.052	0.052	0.054	0.056
	Quasi-Static 10000 kPa.ms								

Figure 7.9 Deformed shapes for selected cases (300 × 300 × 200)

## **8 INVESTIGATION OF ALTERNATIVE EXPLOSION MECHANISMS**

### **8.1 Objectives**

Work carried out to understand the characteristics of the vapour cloud at Buncefield concluded that the most likely explanation was that flame acceleration took place along lines of trees and undergrowth at the boundary of the site. This deflagration then underwent a transition to detonation, which propagated through the widespread vapour cloud. However, the possibility remained that the explosion might have involved an alternative mechanism in which forward radiation from the advancing flame can ignite cellulose particulates ahead and close to the flame front. This results in fast flame propagation within an extended range. Still further out from the flame front, particulates and gas are not pre-heated sufficiently to be ignited by adiabatic compression. When the pressure subsides, gas associated with these more distant particles cools and to a temperature well below that required for spontaneous ignition. There is an extended delay until forward radiation brings gas and particles to the temperature required for ignition and the next cycle of rapid combustion can start. The mechanism is an unsteady deflagration accelerated by forward radiation from the flame front and has become known as “episodic deflagration”. The objective of the work reported in this section is to demonstrate at a realistic scale the feasibility of the episodic deflagration mechanism.

### **8.2 Key Findings**

1. Attempts at large scale to initiate episodic deflagrations were not successful after three attempts. A more fundamental investigation was initiated outside the project as the subject of a PhD thesis and this will be completed and published in 2014.

### **8.3 Description of the Test Programme**

This test programme was conducted by DNV GL. Full details are given in Volume 2<sup>10</sup> to this report.

#### **8.3.1 Test facility and procedure**

The test facility comprised a 30 m × 10 m concrete slab with a central instrument duct, a steel framed polythene sheeted test enclosure to contain the gas mixture and a gas recirculation system comprising 600 mm diameter flap valves, a fan and polythene tubing (Figure 8.1(a)).

To conduct a test, the polythene sheet was pulled over the steel angle frame and secured to the concrete plinth around the perimeter. The explosion was started inside an initiation chamber (Figure 8.1(b)) and its purpose was to create an initial confined region designed to provide flow and flame jets over a wide area.

Dust, in the form of carbon black particles was spread widely across the test rig, with the intention that this dust could be picked up by the flow ahead of the flame. Dust was placed on ledges just inside the explosion chamber



(Figure 8.1(b)) such that this would be picked up by the flame and would also provide both a highly radiating flame front combined with flow ahead of the flame. Dust was also spread on the floor of the rig and on elevated trays placed at points inside the test rig designed to increase the potential for dust to be dispersed ahead of the flame. In addition, dust was also dropped from the roof of the rig at the time of ignition in the third test.

Operational checks of all instrumentation and control equipment were performed and the enclosure was then filled with a homogenous propane/air mixture at the required concentration by remote operation of the gas fill valves, recirculation flap valves and fan. Prior to initiation of the explosive charge, the recirculation system was isolated from the test rig and purged with air.

To commence the test, a sequence timer was initiated triggering the high speed cameras, data acquisition systems and the detonating chord (used to split the polythene), immediately followed by the spark to ignite the gas cloud.



(a) External view of test enclosure



(b) Explosion initiation vessel

**Figure 8.1 Episodic deflagration enclosure and explosion initiation vessel**

### 8.3.2 Instrumentation and measurement

#### Gas analysis

Samples were drawn from four sample positions in the test rig. Real-time gas concentration measurements were made using infra-red gas analysers which were calibrated prior to each test using a “zero gas” (nitrogen) and a certified calibration gas (4.2% v/v propane in nitrogen). The operation of the sampling system was checked prior to each test by attaching a sample bag containing the calibration gas to the end of each sample line.

#### Overpressures

High frequency response piezo-electric pressure transducers were used to measure the pressures generated by the explosions. External free-field pressure was measured in one location at a height of 1.5 m above ground oriented so that the sensing face of the transducer was parallel to the direction of travel of the blast wave. A further 5 pressure measurements were made at ground level inside the cloud, along the major axis of the test enclosure.

#### Thermal radiation

The thermal radiation produced during each of the experiments was measured at three locations using wide angle radiometers. Each of the radiometers was calibrated prior to commencement of the experimental programme in a black body furnace.

## Flame position

Flame arrival time was measured using an array of 30 ionisation probes located at positions within the vapour cloud.

## Video records

Video footage from each experiment was recorded using both high speed and normal speed digital video cameras.

### 8.3.3 Test programme

The programme consisted of 3 tests summarised in Table 8.1, all conducted using propane/air mixtures. The tests primarily involved variations in the distribution of particulate matter, different propane concentrations and variations in the locations of instruments.

**Table 8.1 Summary of test programme**

Test	Concentration	Distribution of cellulosic matter
4.1-1	5.8	
4.1-2	4.3	
4.1-3	4.1	
<p>Notes:</p> <p>The drop stretcher in Test 4.1-3 activated just before ignition and dropped particulate matter into the path of the flame.</p> <p>Coordinates of trays and instrumentation are given in Volume 2<sup>10</sup></p>		

## 8.4 Summary of Findings

### 8.4.1 Overpressure generation

The overpressures generated in the experiments were consistent with pressure being generated in the vented confined explosion in the explosion initiation

chamber, which then decayed as it propagated away from the explosion chamber. No other pressure generation was observed. From the context of pressure generation therefore, there was no evidence that would support the proposed episodic explosion mechanism.

#### **8.4.2 Flame propagation**

Video records showed dust being picked up from the trays in advance of the flame. The dust was also clearly carried downstream from the trays prior to flame arrival, but with little apparent vertical displacement. There was no evidence of dust being lifted significantly from the floor of the test rig. The flame was highly luminous close to the floor with a blue laminar flame above this. The high luminosity is associated with the flame interacting with the dust and leaves on the floor. There was no evidence however of dust being picked up from the floor of the test rig and dispersed upwards. There was also no evidence of ignition of particles occurring ahead of the flame. Based on the thermal radiation measurements, the maximum that could be obtained in these experiments was around 690 kW/m<sup>2</sup>.

Consequently, the tests did not provide evidence that support the episodic deflagration mechanism.

## 9 REFERENCES

- 1 Chang J.I. and Cheng-Chung L. ‘A study of storage tank incident’, Journal of loss prevention in the process industries, 2006, 19, pp 51-59.
- 2 CNN World, 26 October 2009  
<http://www.cnn.com/2009/WORLD/americas/10/26/puerto.rico.fire/> (checked on 1 November 2013).
- 3 The Times of India, 30 October 2009,  
<http://timesofindia.indiatimes.com/city/jaipur/12-killed-in-Jaipur-IOC-depot-fire-Army-called/articleshow/5178346.cms> (checked on 1 November 2013)
- 4 Johnson, D. M. Characteristics of the Vapour Cloud Explosion Incident at the IOC Terminal in Jaipur, 29<sup>th</sup> October 2009, DNV GL Report Number 11510, August 2011, [http://www.fabig.com/Files/FABIG/GL\\_Report\\_No.\\_11510.pdf](http://www.fabig.com/Files/FABIG/GL_Report_No._11510.pdf).
- 5 Explosion Mechanism Advisory Group Report, Buncefield Major Incident Investigation Board, Crown copyright, published 08/2007.
- 6 The Buncefield Explosion Mechanism, FABIG Technical Meeting, June 2009, [www.fabig.com](http://www.fabig.com)
- 7 Buncefield Explosion Mechanism Phase 1 (Volumes 1 and 2), Prepared by The Steel Construction Institute, Crown copyright, published 06/2009.  
(<http://www.hse.gov.uk/research/rrhtm/rr718.htm>).
- 8 Health and Safety Executive, Vapour cloud formation – Experiments and modelling, Report RR908 prepared by the Health and Safety Laboratory, HSE Books, 2012.
- 9 Atkinson, G. and Coldrick, S., Work package 2: Vapour cloud formation, Report FP/12/18, Health and Safety Executive, July 2012.
- 10 Dispersion and Explosion Characteristics of Large Vapour Clouds, Volume 2, The Steel Construction Institute, Ascot, UK, December 2013.
- 11 FABIG Technical Note 12, Vapour cloud development in over-filling incidents, April 2013, FABIG ([www.fabig.com](http://www.fabig.com))
- 12 van Wingerden, M. and Wilkins, B. “Experimental Investigation of the Effect of Flexible Obstructions on Flame Propagation in Vapour Cloud Explosions”, Ref. No.: GexCon-08-F44110-RA-1, 31/10/2008.
- 13 Harris, R.J. and Wickens, M.J. “Understanding vapour cloud explosions – an experimental study”, IGE comm. 1408, 1989.
- 14 Cargill, S.B. Modelling of propane/air cloud detonations, CR123/11, November 2011.
- 15 A.C. van den Berg, “The multi-energy method: A framework for vapour cloud explosion blast prediction”, Journal of Hazardous Materials, Volume 12, Issue 1, Dec 1985, Pages 1–10.
- 16 Kingery, C.N. and Bulmarsh, G., “Airblast parameters from TNT Spherical Air Burst and Hemispherical Surface Burst”, Aberdeen Proving Ground, Maryland, Ballistic Research Library, ARBRK-TR-02555, 1984.
- 17 Kinnley G. F. and Graham K.J., Explosive shocks in air, Springer Verlag, 1985.











SCI Membership

Technical Information

Construction Solutions

Communications Technology

SCI Assessment

SCI Ref: ED024

**SCI**

Silwood Park, Ascot, Berkshire. SL5 7QN UK

T: +44 (0)1344 636525

F: +44 (0)1344 636570

E: [reception@steel-sci.com](mailto:reception@steel-sci.com)

[www.steel-sci.com](http://www.steel-sci.com)